DESIGN AND DEVELOPMENT OF NOVEL FLUORESCENCE-BASED DETECTION METHODS FOR BIO-ANALYTES

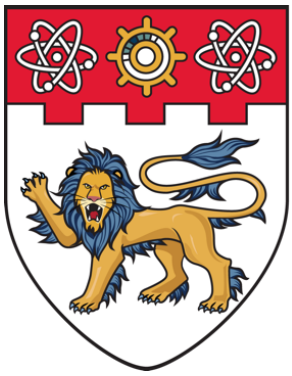

NANYANG TECHNOLOGICAL UNIVERSITY
SINGAPORE

DESIGN AND DEVELOPMENT OF NOVEL FLUORESCENCE-BASED DETECTION METHODS FOR BIO-ANALYTES

NG SHUE MEI

NG SHUE MEI 2019

SCHOOL OF PHYSICAL AND MATHEMATICAL SCIENCES
NANYANG TECHNOLOGICAL UNIVERSITY

2019

DESIGN AND DEVELOPMENT OF NOVEL FLUORESCENCE-BASED DETECTION METHODS FOR BIO-ANALYTES

NG SHUE MEI

School of Physical and Mathematical Sciences

A thesis submitted to the Nanyang Technological University
in partial fulfilment of the requirement for the degree of
Doctor of Philosophy

2019

Statement of Originality

I hereby certify that the work embodied in this thesis is the result of original research done by me except otherwise stated in this thesis. The thesis work has not been submitted for a degree or professional qualification to any other university or institution. I declare that this thesis is written by myself and is free of plagiarism and of sufficient grammatical clarity to be examined. I confirm that the investigations were conducted in accord with the ethics policies and integrity standards of Nanyang Technological University and that the research data are presented honestly and without prejudice.

4/2/2019

Date

Ng Shue Mei

Supervisor Declaration Statement

I have reviewed the content and presentation style of this thesis and declare it of sufficient grammatical clarity to be examined. To the best of my knowledge, the thesis is free of plagiarism and the research and writing are those of the candidate's except as acknowledged in the Author Attribution Statement. I confirm that the investigations were conducted in accord with the ethics policies and integrity standards of Nanyang Technological University and that the research data are presented honestly and without prejudice.

4/2/2019	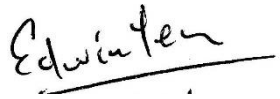
Date	Assoc. Prof. Edwin Yeow

Authorship Attribution Statement

This thesis contains material from 1 paper published in the following peer-reviewed journal where I was the first author.

Chapter 2 is published as Ng, S. M.; Wu, X.; Khyasudeen, F.; Nowakowski, P. J.; Tan, H.-S.; Xing, B.; Yeow, E. K. L. Vancomycin determination by disrupting electron-transfer in a fluorescence turn-on squaraine-anthraquinone triad. *ACS Sens.* **2018**, *3*, 1156-1163. DOI: 10.1021/acssensors.8b00188.

The contributions of the co-authors are as follows:

- Assoc. Prof. Edwin Yeow and Dr. Xiangyang Wu provided the initial project direction, gave critical advice on the experimental results and edited the manuscript drafts.
- Assoc. Prof. Edwin Yeow and I prepared the manuscript drafts.
- Other than the femtosecond-transient absorption spectroscopy measurements, all experiments were carried out by me. Data analysis was performed with the guidance of Assoc. Prof. Edwin Yeow and Dr. Xiangyang Wu.
- Mr. M. Faisal Khyasudeen, Dr. Pawel J. Nowakowski and Assoc. Prof. Howe-Siang Tan assisted in the femtosecond-transient absorption spectroscopy measurements, which included the collection and interpretation of data.
- Purification of the final products on a high performance liquid chromatography instrument was carried out in Assoc. Prof. Bengang Xing's lab.

4/2/2019

Date

Ng Shue Mei

Acknowledgements

I would like to express my gratitude to many people who have given me their help and support in one way or another throughout my four years of research studies.

First of all, I would like to thank Nanyang Technological University for the research scholarship and great opportunity to pursue my graduate studies in such a wonderful environment. I would like to thank the Division of Chemistry and Biological Chemistry (CBC) for the excellent research infrastructure and the devoted staff for their kind assistance that has helped my research experience to be a lot smoother.

I would like to express my heartfelt thanks to my supervisor, Assoc. Prof. Edwin Kok Lee Yeow. I know that sometimes you find it difficult to communicate your point across to me, but thank you for not giving up and still being so patient to teach and guide me. You taught me how to be more open-minded to consider different questions and not to reject it hastily. You also taught me how to look at the bigger picture whenever I am stuck with the details of my work. Thank you for guiding me through the different projects and the whole process of publishing a paper with your expertise and hard work.

I would also like to thank my co-supervisor, Assoc. Prof. Bengang Xing, for your encouragement and advice throughout the four years. I am very grateful to my mentor and colleague, Dr. Xiangyang Wu. You are a very experienced and knowledgeable researcher. Thank you for teaching me many things from my first year of PhD and always guiding me and helping me to solve many problems. You have a lot of ideas and you are persistent to work on those ideas. The way you conduct research taught me how a research life is and should be like.

I would like to thank my collaborators, Assoc. Prof. Howe Siang Tan, Mr. Khyasudeen Muhammad Faisal and Mr. Nowakowski Pawel Jacek for their kind assistance with the femtosecond-transient absorption studies in my first paper.

I would like to thank my group members and friends from other groups, Miss Jin Wang, Dr. Shengtao Lu, Mr. Ming Hu, Dr. Linna Lyu, Dr. Jing Mu, Dr. Junxin Aw, Dr. Xiangzhao Ai, Mr. Zhimin Wang and Miss Lei He, for all the helpful discussions and kind assistance.

I want to give my special thanks to my good friends, Miss Sherli Gan, Miss Yikyie Ng, Miss Naziah Mohamad Latiff, Miss Xinyi Chew, Mr Sebastian Quek Yongshen, Mr Zhizhong Ang and Mr Siuchung Chan, for all the support, encouragement, comfort and joy that you guys have brought to me. It has made my time in the lab more enjoyable and bearable. Thank you for the sincere friendships and understanding that have kept me going for the four years of research studies.

I would like to thank the CBC teaching lab staff, Miss Aihua Seow, Miss Charlene Poo and Miss Yanlin Chan, for being so gracious in letting me use the equipment in the teaching lab. I would also like to thank my thesis advisory committee members, Assoc. Prof. Howe Siang Tan and Assoc. Prof. Cheng Gee Koh, for your encouragement and advice.

Last but not least, I want to express my deepest gratitude to my family. Thank you for taking care of everything in the house so that I can pursue PhD without much burdens. Thank you for sharing my joy as well as many difficult moments for the past four years. Thank you for always trying your best to support me, cheer me up and pray for me. I would not be able to go this far without the constant love, warmth and rest in this family. I would like to thank my brothers and sisters in church for your ceaseless prayers, love, care, support and encouragement throughout the four years.

Table of Contents

Summary

Fluorescence-based detection methods are advantageous because of their high sensitivity, rapidity and simplicity. Furthermore, various fluorescent materials and sensing mechanisms can be used in the rational design of these methods, which also demonstrate the versatility of such methods to be tailored to detect various targets with high sensitivity and selectivity. In Chapter 1, we focused our discussion on two fluorescent materials, organic dyes and upconversion nanoparticles, as well as two commonly applied sensing mechanisms, namely photoinduced electron transfer (PET) and fluorescence resonance energy transfer (FRET). These would be used in the design and development of novel detection methods for a first-line antibiotic vancomycin (Van; Chapters 2 and 3) and an important neurotransmitter epinephrine (EP; Chapter 4). Toward the end of Chapter 1, a comprehensive and detailed discussion on current methods reported for Van detection is included to serve as a bridge for the introduction of our proposed method in Chapters 2 and 3.

In Chapters 2 and 3, two organic PET-based probes were prepared and their ability to sense Van in a fluorescence "turn-on" manner were tested. The first probe consists of a triad made up of a squaraine dye conjugated to two anthraquinone molecules via Van-specific peptide sequences, *i.e.* Lys-D-Ala-D-Ala (Chapter 2). In the absence of Van, an energetically favourable electron transfer from the excited dye to anthraquinone resulted in fluorescence quenching of the triad, which was recovered upon the addition and binding of Van to the -D-Ala-D-Ala ligands. The detection mechanism of the triad was investigated using time-resolved spectroscopy. The second probe consists of the triad made up of a cyanine dye conjugated to two ferrocene moieties via Lys-D-Ala-D-Ala peptides (Chapter 3). In this case, fluorescence quenching in the absence of Van takes place via a hole-transfer process from the excited

dye to ferrocene. An investigation of the influence of linker length between the cyanine dye and ferrocene on the hole-transfer quenching efficiency was also conducted.

In Chapter 4, a novel FRET-based probe utilizing o-phenylenediamine (OPD)-conjugated upconversion nanoparticles was proposed for the detection of EP. The preparation of the conjugated nanoparticles and its application to sense EP are described in this chapter.

List of abbreviations

ACN	Acetonitrile
AQ	Anthraquinone
Boc	tert-Butyloxycarbonyl
Cy5	Cyanine dye 5
DCM	Dichloromethane
DIPEA	*N,N*-diisopropylethylamine
DMF	Dimethylformamide
DMSO	Dimethyl sulfoxide
EDC·HCl	*N*-(3-dimethylaminopropyl)-*N'*-ethylcarbodiimide hydrochloride
EP	Epinephrine
ESI-MS	Electrospray ionization mass spectroscopy
Fc	Ferrocene
Fmoc	Fluorenylmethyloxycarbonyl
FRET	Fluorescence resonance energy transfer
fs-TA	Femtosecond-transient absorption spectroscopy
HBTU	*O*-(Benzotriazol-1-yl)-*N,N,N',N'*-tetramethyluronium hexafluorophosphate
HOMO	Highest occupied molecular orbital
HRMS	High-resolution mass spectrometry
LOD	Limit of detection
Lys-D-Ala-D-Ala	L-lysine-D-alanine-D-alanine
LUMO	Lowest unoccupied molecular orbital
MPS	(3-Mercaptopropyl)trimethoxysilane

OPD	o-Phenylenediamine
PBS	Phosphate buffered saline
PET	Photoinduced electron transfer
^{1}H NMR	Proton nuclear magnetic resonance spectroscopy
HPLC	High performance liquid chromatography
TCSPC	Time-correlated single photon counting
TDM	Therapeutic drug monitoring
TEM	Transmission electron microscopy
TEOS	Tetraethyl orthosilicate
TFA	Trifluoroacetic acid
TIPS	Triisopropylsilane
UCL	Upconversion luminescence
UCNP	Upconversion nanoparticles
UV	Ultraviolet
Van	Vancomycin
Van CDP-1	Vancomycin crystalline degradation product
λ_{abs}	Absorption maximum
λ_{em}	Emission maximum
ΔG_{et}	Change in free energy for an electron-transfer process
ΔG_{ht}	Change in free energy for a hole-transfer process
$\tau(\alpha)$	Fluorescence lifetime (contribution of the lifetime component)
Φ	Quantum yield

Chapter 1 General introduction

1.1 Theory of fluorescence

Fluorescence-based techniques have been widely employed in the design of numerous detection systems due to the simplicity, rapidity, high sensitivity and versatility of such techniques.[1-3] The process of fluorescence (for an organic fluorophore) can be described using the famous Jablonski diagram (Figure 1).[4] In the simplest case involving only the first excited state (S_1), an electron in the ground state (S_0) is first promoted to the S_1 state after photon absorption. It then loses its energy via vibrational relaxation to the lowest energy level in the S_1 state and returns to the ground state by emitting a photon of lower energy (*i.e.* fluorescence) than that of the absorbed photon. As a result, the recorded fluorescence spectrum shows a red-shift to longer wavelengths compared to the absorption spectrum, and the difference between the wavelength of absorption and emission maxima, known as Stokes shift, is a property characteristic for a particular fluorophore (Figure 2). After photon absorption and excitation, the loss of energy can also take place via other non-radiative (*e.g.* internal conversion from higher singlet excited states (*e.g.* S_2) to S_1 state, intersystem crossing from singlet to triplet excited state (T_1)) and radiative (*e.g.* phosphorescence) processes. The typical timescales of the different photophysical processes are also included in Figure 1 and it can be seen that fluorescence occurs in nanoseconds. The fluorescence lifetime is another important property that is commonly studied and/or applied in detection systems.[5]

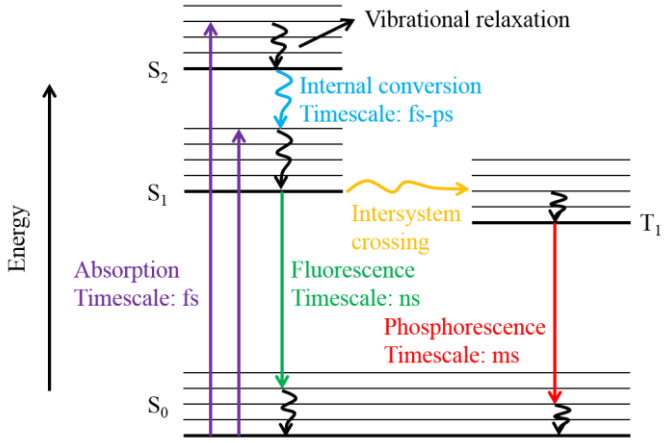

Figure 1. (Simplified) Jablonski diagram showing the different photophysical processes and their typical timescales for an organic fluorophore.

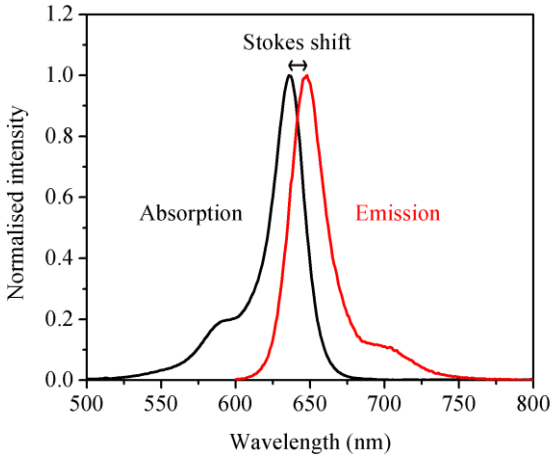

Figure 2. Overlap of normalized absorption and fluorescent spectra showing the Stokes shift between the absorption (λ_{abs}) and emission (λ_{em}) maxima for an organic fluorophore.

To date, many different materials have been explored in the design of fluorescent probes for various analyte(s) and these include organic dyes, fluorescent proteins, quantum dots, upconversion nanoparticles (UCNP), silica nanoparticles, metal-, polymer-, and carbon-based materials.[1, 3-4, 6] The following discussion would be mainly focused on organic dyes and UCNP which were employed in the design of novel

detection systems for two biologically significant molecules, vancomycin (Chapters 2 and 3) and epinephrine (Chapter 4).

1.2 Organic dyes

Organic dyes are molecular probes which have a long history of application as fluorescent labels for detection purposes. Consequently, the synthesis, functionalization and labelling protocols for organic dyes are well-established, for which reproducible (optical) properties can be attained.[7] These offer an advantage over materials such as quantum dots and UCNP, where related studies are still mostly proof-of-concepts. Moreover, such materials have optical properties that are size-dependent, requiring control over size distribution in each batch of synthesized materials.[8] The effect of microenvironment on the optical properties of organic dyes is also better understood and this knowledge not only simplify the analysis but has also been exploited in the design of systems monitoring changes in environmental factors such as pH and polarity.[9-10]

Over the years, dyes with improved properties have been developed to overcome one or more of the problems associated with traditional dyes (*e.g.* fluorescein) such as low water solubility, tendency to aggregate (decreases fluorescence intensity), low photostability and significant background interference arising from the autofluorescence of biological materials.[1] For example, by introducing functional groups such as sulfonate groups, the corresponding dye shows better solubility and aggregates less easily in aqueous environments, presumably due to increased polarity and repulsion of negative charges between neighbouring sulfonate groups. Consequently, higher fluorescence signal and detection sensitivity can be derived.

The cyanine dyes and Alexa dyes are two examples of the more successful classes of dyes developed, for which various commercial products are readily available.

These dyes have absorption and emission spanning the visible and near-infrared (NIR) spectra,[1] thus providing researchers with a wide selection of dye labels to choose from. Those dyes with NIR optical properties also circumvent the problem of poor signal-to-noise ratio due to minimal autofluorescence of biological materials in this biological transparent window (*i.e.* 700-1100 nm).[11] This property has been increasingly exploited in many fields, especially in bioimaging, as NIR wavelengths provide deeper tissue penetration depth while minimizing the damage to the tissue cells due to the low energy of such wavelengths.[12] Commercial products of cyanine dyes and Alexa dyes functionalized with reactive groups such as *N*-hydroxysuccinimide (NHS) ester and maleimide are available, which greatly increase the ease of labelling using established protocols. These dyes also possess other desirable properties including high extinction coefficients (on the order of 10^4-10^5 $M^{-1}cm^{-1}$), high photostability and tolerance to pH changes over a broad range.

Despite the merits, some problems encountered when using organic dyes as fluorescent labels such as non-specific binding and highly sensitive detection with lower fluorescence output remain to be solved. Vigorous validation is also necessary when applying a calibration curve established in buffer solution to real systems.[2]

1.3 UCNP

UCNP are fluorescent nanomaterials comprising of an inorganic host doped with trivalent lanthanide ions (Ln^{3+}).[13] Ln^{3+} possesses $4f^n$ $5d^{0-1}$ inner shell configurations that are well shielded by the outer, complete 5s and 5p shells.[11, 13] This give rise to sharp emission peaks via intra 4f-4f and 4f-5d transitions which exhibit high resistance to photobleaching and photochemical degradation.[4] Contrary to organic dyes and quantum dots which produce emissions by a downconversion process (*i.e.* emitted photon is of

lower energy than the absorbed photon), UCNP emits via an upconversion process involving the sequential absorption of low energy photons facilitated by the ladder-like energy levels of Ln^{3+} to emit photons of higher energy. Consequently, it is possible to excite UCNP with NIR light and obtain (shorter) NIR, visible and ultraviolet (UV) lights which exhibit large anti-Stokes shift (Figure 3).[14] This property, together with the sharp emission peaks, minimizes spectral cross-talk and enables efficient separation of signals (*e.g.* emission from excitation wavelength and among multiple emission peaks).[11, 14] It is therefore possible to perform multiplex detection using UCNP luminescence intensity and also lifetime due to the long lifetime of the nanomaterial in the sub-millisecond range, which allows easy identification from the short-lived luminescence of biological materials.[15] As mentioned earlier, the advantages of NIR excitation are exemplified in the greater penetration depths and lower photodamage to biological tissues, reduced autofluorescence of these materials and less light scattering. Other advantages of UCNP include its biocompatibility and low cytotoxicity in vitro and in vivo as compared to quantum dots.[13] However, the main problem of UCNP is the low efficiency of the upconversion luminescence (UCL) (*i.e.* low quantum yield), for which various methods have been suggested to improve the efficiency.[11]

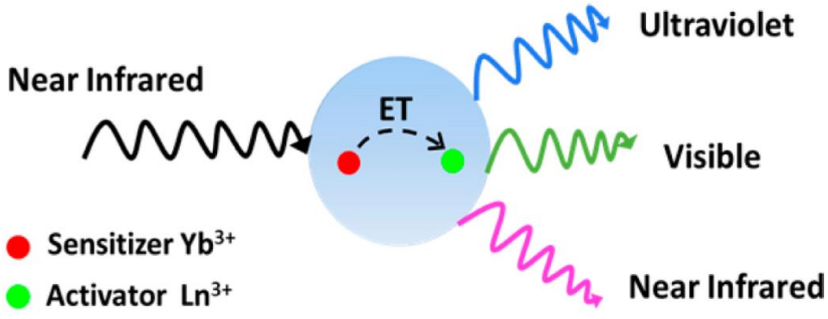

Figure 3. Schematic diagram showing the emission of (shorter) NIR, visible and UV lights upon NIR excitation and transfer of energy from sensitizer to activator within the UCNP. This figure is adopted from reference 14.

$NaYF_4$ (Y = yttrium) doped with ytterbium/thulium ions (Yb/Tm) or ytterbium/erbium ions (Yb/Er) have been reported to be the most efficient UCNP.[16] $NaYF_4$ as the host material provides low lattice phonon energy, which is important to reduce non-radiative loss and increase radiative emission. The transitions between the dopants Yb/Tm or Yb/Er, on the other hand, yield the UCL when excited at a suitable wavelength.[17] Yb^{3+} has a large absorption cross-section at ~980 nm that coincides with the output of commercial NIR laser diodes, thus it is often use as the sensitizer to enhance upconversion efficiency through an energy transfer process to Tm^{3+} or Er^{3+} (also known as the activators; Figure 3). These activator ions possess ladder-like energy levels that facilitate photon absorption and energy transfer in the upconversion process.[14]

1.3.1 Energy transfer upconversion (ETU) mechanism

The ETU mechanism is primarily responsible for the highly efficient upconversion process[18] and will be illustrated with the Yb/Tm dopant system. Figure 4 shows the energy levels of Yb^{3+} and Tm^{3+}.[19] When excited at 980 nm, Yb^{3+} absorbs a photon and is promoted from the ground state $^2F_{7/2}$ to the excited state $^2F_{5/2}$. As it returns to the ground state, the absorbed energy is transferred non-radiatively to Tm^{3+} to promote it to the $^3H_5$ level. It then decays rapidly to the $^3F_4$ level, where a second energy transfer step promotes it to the $^3F_2$ level. This is followed by decay to the $^3H_4$ level, promotion to the $^1G_4$ level and further promotion to the $^1D_2$ level and then the $^1I_6$ level by a third, fourth and fifth energy transfer step, respectively. UCL of varying wavelengths are produced when Tm^{3+} relaxes (radiatively) to different energy levels. For example, the blue UCL at 450 nm and 475 nm are produced by radiative relaxation of Tm^{3+} from $^1D_2 \rightarrow {}^3F_4$ and $^1G_4 \rightarrow {}^3H_6$ (ground state), respectively. The ETU process

is advantageous in that it is independent of the pump power (unlike the photon avalanche (PA) mechanism)[13] and has higher efficiency than the excited state absorption (ESA) mechanism (happens in a single ion).[20] PA and ESA are other upconversion mechanisms,[11] for which detailed discussions would not be included here. Having said that, the efficiency of the ETU process is dependent on the dopant concentration which affects the distance between neighbouring ions. Optimal concentrations of Yb^{3+} and Tm^{3+} which avoid the deleterious concentration quenching effects were found to be 20-30 mol% and 0.2-0.5 mol%, respectively.[17, 21]

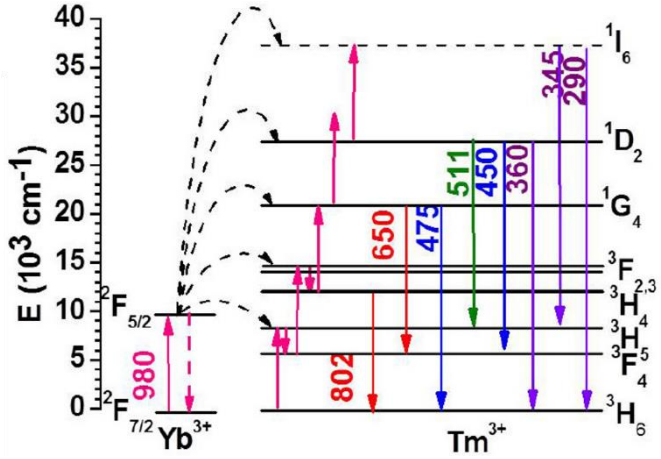

Figure 4. Schematic diagram showing the ETU process for the Yb/Tm dopant system. Assignment of the wavelengths of UCL arising from different Tm^{3+} transitions is also included. This figure is adopted from reference 19.

1.3.2 Synthesis

Various synthetic strategies have been investigated to prepare highly efficient lanthanide-doped UCNP. These include thermal decomposition, co-precipitation, sol-gel processing and hydro(solvo)thermal method.[20] For the co-precipitation and hydro(solvo)thermal method, a post heat treatment step or long reaction time, respectively, is needed to obtain the highly efficient hexagonal phase UCNP (*vs.* the less

efficient cubic phase UCNP which is more easily formed).[17] However, this often yields large size and polydispersed nanoparticles with mixed crystal phases (*i.e.* impure).[22] The sol-gel method has also been reported to have limited control over synthesized particle size.[20] Synthesis of UCNP using the thermal decomposition method, on the other hand, generates highly toxic fluorinated by-products due to decomposition of the metal precursors (*i.e.* metal trifluoroacetates) at high temperatures. Consequently, extra caution has to be exercised to carry out the experiments in well-ventilated fumehoods. Furthermore, this method requires vigorous (*i.e.* anhydrous and oxygen-free) and harsh (*i.e.* high temperature) reaction conditions, and the fast nucleation or growth process tends to produce particles with more defects which is detrimental to the quantum yield.[11]

To avoid the production of hazardous fluorinated compounds, Li *et al.* developed an efficient and user-friendly procedure to synthesize purely hexagonal phase UCNP by first converting all reactive fluoride reactants to small solid-state $NaYF_4$ nuclei at room temperature, followed by increasing the temperature (to 300 ℃) to facilitate further nucleation to form larger nanoparticles by a Ostwald ripening process.[22] Ostwald ripening is the process where larger particles which have a smaller surface-to-volume ratio and are energetically more stable are formed preferentially from smaller particles which are less stable.[11] By controlling the reaction time and temperature, it is possible to obtain purely hexagonal phase UCNP that are monodispersed and have a narrow size distribution. In addition, the Ostwald ripening process allows relatively more time for particle growth which yields nanoparticles with less defects and higher quantum yield compared to the thermal decomposition method.

1.3.3 Properties

The synthesized UCNP are often capped with hydrophobic ligands (*e.g.* oleic acid) which limit its biological application in aqueous environment. Surface modification via different approaches is usually required to improve the hydrophilicity, biocompatibility as well as target-recognition ability of the nanoparticles. This can be achieved by ligand exchange or oxidation or removal, silanization, layer-by-layer assembly and amphiphilic coating. Surface silanization (or silica coating) is most commonly used due to well-established coating protocols, and favourable properties of silica (stable, optically transparent, biocompatible) and silica-coated UCNP (water-dispersible, biocompatible). By using different silane reagents, the nanoparticle surface can be easily decorated with functional groups such as carboxylic acid (-COOH), amine ($-NH_2$) and thiol (-SH), to suit various conjugation chemistries in subsequent steps (*e.g.* formation of an amide bond between a -COOH and $-NH_2$ group or disulfide bond between two SH groups). Furthermore, silica coating procedures for both hydrophobic (*i.e.* reverse microemulsion method) and hydrophilic (*i.e.* Stober method) UCNP are available.[11, 20] The former was used to prepare SH-functionalized UCNP in Chapter 4, for which more details about the procedure can be found in section 4.3.1.

1.4 Design of fluorescent probes and their applications

In the design of fluorescent probes, photoinduced electron transfer (PET) and fluorescence resonance energy transfer (FRET) are two mechanisms commonly applied to modulate fluorescence intensity in the absence and presence of a target.[23]

1.4.1 PET

The PET mechanism is usually employed in the design of fluorescence "turn-on" probes that have a general fluorophore-spacer-receptor architecture.[24] In the case of a simple fluorophore, fluorescence (FL) is produced when an excited electron in the lowest unoccupied molecular orbital (LUMO) returns to the highest occupied molecular orbital (HOMO) via radiative decay (Figure 5A). When conjugated to a receptor (via a spacer) which has a HOMO energy level between the HOMO and LUMO energy levels of the fluorophore, PET can take place upon excitation where an electron is transferred from the HOMO of the receptor to that of the fluorophore, resulting in fluorescence quenching (Figure 5B). In the presence of a target, the binding between the receptor and the target lowers the HOMO energy level of the receptor below that of the fluorophore. Consequently, PET is inhibited and fluorescence is recovered (Figure 5C). A less efficient PET quenching process can also be achieved by increasing the distance between the fluorophore and the receptor, for which the distance-dependency of PET efficiency is proportional to $e^{-\beta d}$ (where d = distance between the HOMO energy levels of the fluorophore and receptor). This translates to a more efficient radiative decay process which yields stronger fluorescence (Figure 5D).[25]

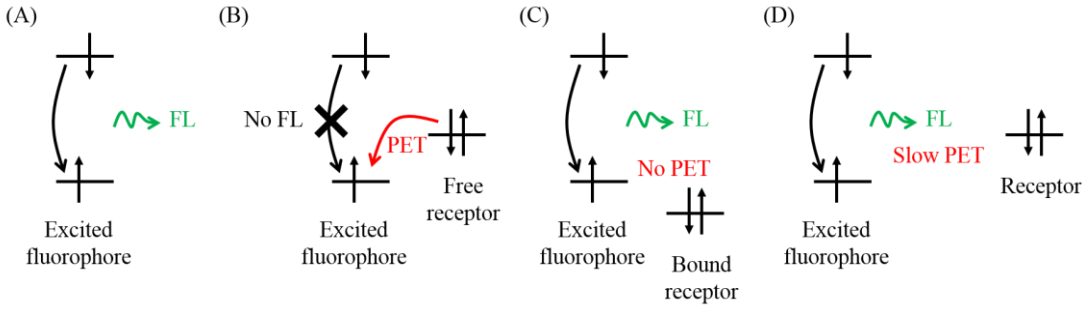

Figure 5. PET mechanism.

Various targets such as ions, small molecules, proteins and DNA have been detected using PET-based probes.[26-29] The probes for small active molecules (*e.g.* thiols) and enzymes are usually designed in a way that makes use of their reactive or catalytic activity, respectively. For those targets that do not exhibit such activity, an alternative design approach is based on conformational change of the probe upon target binding. Sparano *et al.* designed a PET-based probe consisting of the fluorophore 2,7-dichlorofluorescein (DCF) conjugated to two aniline derivatives to sense RNA.[25] In equilibrium and in the absence of RNA, the probe can adopt two conformations, *i.e.* an unfolded state which is fluorescent and a folded state which is non-fluorescent. The folded state of the probe is non-fluorescent owing to PET from the lone pair of electrons on the nitrogen atom to DCF at close proximity. Fluorescence is recovered in the unfolded state of the probe due to less efficient PET at increased distance between the two entities (Figure 6). The latter state is preferentially formed in the presence of RNA which binds to the aniline derivative and causes the probe to adopt an unfolded (or open) conformation. This saw a 13-fold improvement in fluorescence signal at a RNA concentration of 100 μM. The increment was found to be concentration-dependent, thus enabling quantification of RNA using the proposed probe (Figure 7). Other reasons were also suggested to contribute to the enhanced fluorescence upon RNA binding. These include a lower HOMO energy level of the nitrogen atom (*i.e.* quencher), restricted motion of the benzoate group and conformational change of the other, unbound aniline derivative in the probe-RNA complex. The latter was proposed to result in greater distance separation between the unbound aniline derivative and DCF, thus contributing to further fluorescence enhancement.

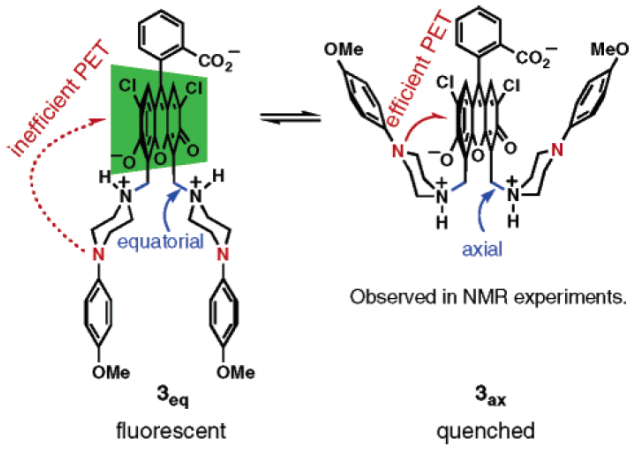

Figure 6. Two conformations adopted by the probe in equilibrium. In the folded state (right), PET from the nitrogen atom to DCF quenches the fluorescence of the probe, which is recovered in the unfolded state (left) due to lower quenching efficiency at increased distance between the two entities. This figure is adopted from reference 25.

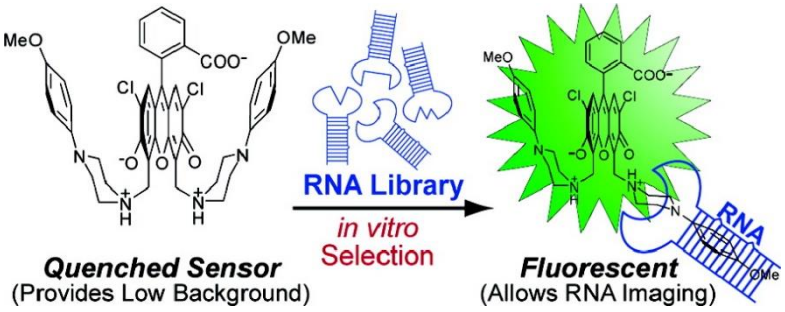

Figure 7. Detection mechanism of the proposed probe in the presence of RNA. This figure is adopted from reference 25.

Using the DCF-piperazine scaffold, PET-based probes for the enzyme carbonic anhydrase IX (CA IX)[30] and cell channel receptor, human Ether a-go-go-Related Gene (hERG),[31] were developed. Specific recognition of the targets was provided by attaching target-specific ligands to the nitrogen atom of the piperazine ring. Variable success of *ca.* 1.4-times and 2.5-fold fluorescence enhancement were achieved for CA IX and hERG, respectively. For the latter, the same group also did a study where they changed

the fluorophore to naphthalimide and witnessed an improvement to 20-fold fluorescence enhancement for hERG.[32]

In the above examples, the specific binding interactions between the receptor and target form the basis for initial target recognition and subsequent fluorescence detection. Heinlein *et al.* made use of the specific interactions between complementary base pairs to design a DNA probe employing fluorophore-attached singly stranded DNA.[29] The singly stranded DNA adopts a hairpin or stem-loop conformation where an oxazine derivative (*i.e.* fluorophore) attached at the 5'-end of the DNA strand (in end-capped conformation) is quenched via PET by the guanosine residues in the complementary stem. Hybridization of the probe with a target DNA sequence (complementary to the loop sequence) forces the stem apart and restores fluorescence in a concentration-dependent manner (Figure 8). By rational design of the probe, a 20-fold fluorescence enhancement was achieved upon specific binding to the target sequence.

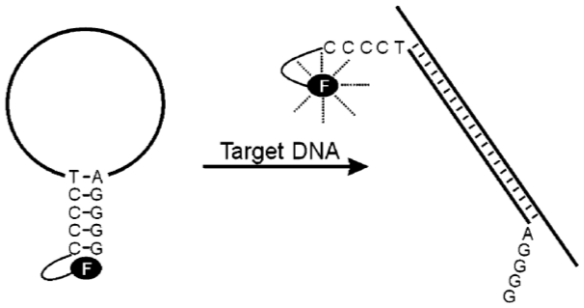

Figure 8. Fluorescence recovery mechanism of the fluorophore-attached singly stranded DNA (in hairpin conformation) in the presence of a complementary target DNA sequence. This figure is adopted from reference 29.

Host-guest interactions were also explored in the design of PET-based probes. Our group prepared a cyanine dye-ferrocene (Cy5-Fc) dyad which formed an inclusion

complex with β-cyclodextrin (β-CD) and led to recovery of quenched fluorescence.[33] In the absence of β-CD, PET occurs from Fc to the excited Cy5 and quenched Cy5's emission. The addition of β-CD led to formation of an inclusion complex where Fc is encapsulated in the cavity of β-CD. This resulted in an increased spatial separation between Fc and Cy5 which restored the latter's fluorescence. (At 2 mM of β-CD, a fluorescence recovery of ~2-times was observed.) These results formed the basis for the design of a "turn-off" probe consisting of Cy5 conjugated to Fc and β-CD (*i.e.* a triad) to sense biologically relevant molecules. The triad naturally exhibits fluorescence due to inhibition of PET in the Fc-β-CD inclusion complex. In the presence of other guest molecules which can displace Fc from β-CD (represented by a cone structure), PET can occur again between Fc and Cy5 and fluorescence of the triad is quenched (Figure 9). Using this triad, sodium lithocholate (a), amantadine hydrochloride (b) and adamantanecarboxylic acid (sodium salt; c) can be detected with sufficient sensitivity in water and synthetic urine.

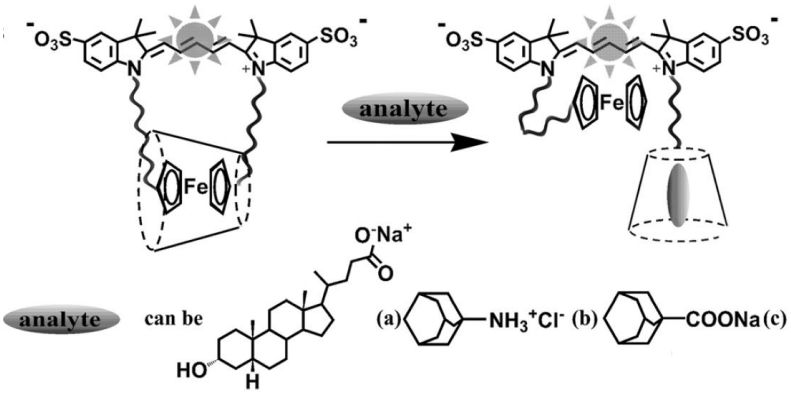

Figure 9. Fluorescence quenching mechanism of the Cy5-Fc- β-CD triad in the presence of an analyte that is capable of displacing Fc from β-CD (represented by a cone structure). The analytes tested include sodium lithocholate (a), amantadine hydrochloride (b) and adamantanecarboxylic acid (sodium salt; c). This figure is adopted from reference 33.

In all cases, rational design of the probes through careful selection of the fluorophore and quencher (with suitable redox potentials and change in free energy (ΔG) of PET efficiency) as well as consideration of the conformations of the probe in the absence and presence of the target (*e.g.* position, orientation, motion of the quencher and/or fluorophore) are necessary to develop a highly efficient PET-based sensing system.[25, 29]

1.4.2 FRET

The FRET mechanism is described by a transfer of energy from an excited donor to an acceptor through non-radiative dipole-dipole coupling.[11] The efficiency of such a process is dependent on several factors including the spectral overlap between the emission spectrum of the donor and absorption spectrum of the acceptor, and their relative orientations and proximity (efficiency is proportional to r^{-6}, where r is the donor-acceptor distance; generally <10 nm).[4, 34] An energy donor-acceptor pair, also known as a FRET pair, can be constructed from combinations of different (usually fluorescent) materials. Traditional FRET pairs were constructed from organic dyes while recent developments have seen increasing applications of materials such as gold nanoparticles, graphene oxide and UCNP in the design of FRET-based detection systems.[35-40] Selected examples using UCNP as the donor are illustrated.

Liu *et al.* designed a FRET-based system to monitor the activity of caspase-3 (an important enzyme involved in cell apoptosis) using a Rhodamine B (RB)-labelled peptide sequence conjugated to Yb/Er-doped $NaGdF_4$ (Gd = gadolinium).[35] The DEVDG fragment in the peptide sequence is specifically recognized and cleaved by caspase-3. In the absence of the enzyme, the conjugated UCNP displayed low UCL intensity upon 980 nm excitation due to quenching by RB through FRET. The addition

of caspase-3 cleaves the RB-DEVDG fragment and led to UCL recovery of UCNP in a concentration-dependent manner (Figure 10). Other systems utilizing a similar FRET quenching effect for quantification of target concentration have also been reported for detection of an antigen[36] and DNA[37] based on the specific interactions of antigen-antibody and complementary oligonucleotide sequences, respectively.

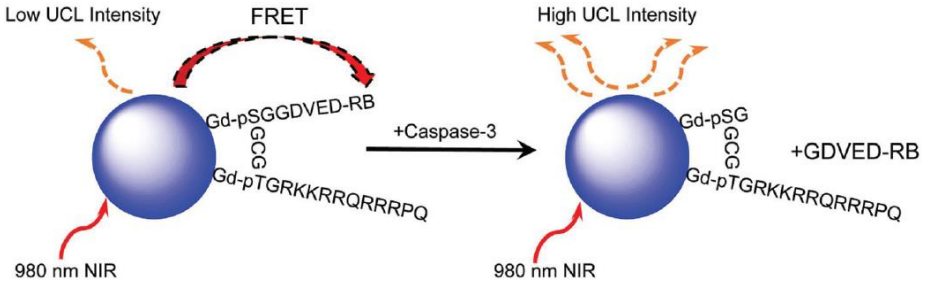

Figure 10. Schematic diagram showing UCL recovery of UCNP in the presence of caspase-3. This figure is adopted from reference 35.

Small molecule detection on UCNP was demonstrated by Nguyen *et al.* and they designed a simple system using dye-conjugated UCNP to sense glutathione based on a ring-opening process.[41] A derivative of RB (RBD) was used, which is non-fluorescent in its ring-closed form. As a result, the conjugated UCNP displayed emission (monitored at 540 nm) in the absence of glutathione. The addition of glutathione triggers ring-opening of RBD, which forms a fluorescent structure that quenched the 540 nm emission of UCNP. At the same time, an increase in the emission intensity at 592 nm due to the ring-opened RBD was observed (Figure 11). Both wavelengths could be linearly correlated to the glutathione concentration, and applications in human serum and urine were carried out with satisfactory recoveries.

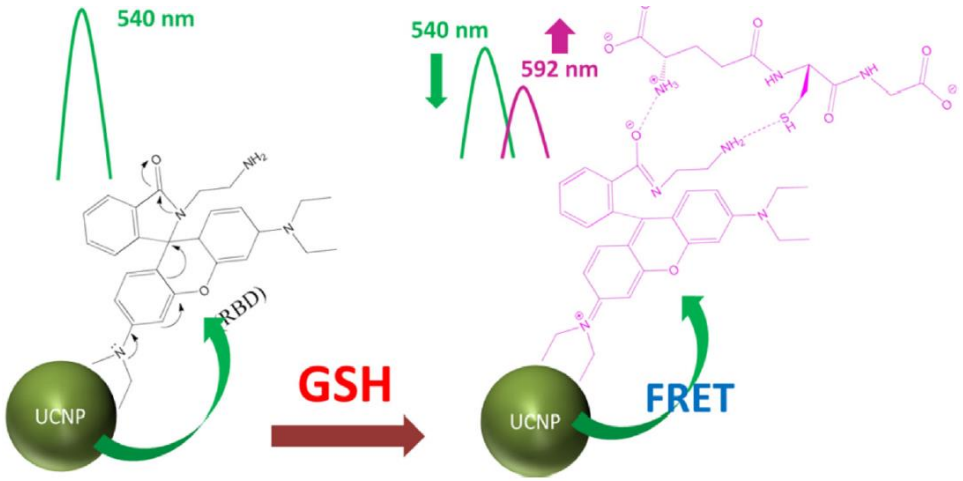

Figure 11. Schematic diagram showing the detection mechanism of RBD-conjugated UCNP in the presence of glutathione (GSH). This figure is adopted from reference 41.

1.5 Vancomycin and its detection methods

In Chapters 2 and 3, two molecular PET-based probes were designed to detect vancomycin (Van), which is a first-line antibiotic for treatment of Gram-positive bacterial infections. In this section, a detailed discussion on the various methods reported to date for Van detection is included.

Van (Figure 12) exerts its antibacterial activity against Gram-positive bacteria mainly by binding to a D-alanyl-D-alanine (D-Ala-D-Ala) sequence and inhibiting the final stage of bacterial cell wall synthesis.[42] Other bactericidal mechanisms of Van such as inhibition of RNA synthesis and alteration of cell membrane permeability have also been identified.[43-45] The antibiotic is prescribed to patients who are allergic to penicillin or infected with penicillin-resistant bacterial strains (*e.g.* the deadly methicillin-resistant *Staphylococcus aureus*).[42, 46] Therefore, it has been termed the drug of "last resort", used in treatment only when other antibiotics have failed.[47-48]

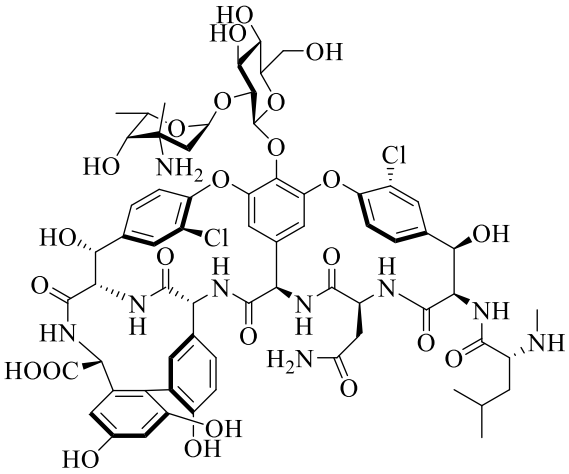

Figure 12. Chemical structure of Van.[49]

Following the emergence of Van-resistant enterococci (VRE) and detection of low-level Van resistance in *Staphylococcus aureus*,[42] the need for effective treatment with optimal drug levels while avoiding resistance development is of paramount importance. Furthermore, Van has a narrow therapeutic window, for which under-dosing often leads to ineffective treatments and even reports of hypersensitive reactions while overdosing is associated with nephrotoxicity and ototoxicity.[48, 50] These has drove clinical laboratories to adopt therapeutic drug monitoring (TDM) practices for Van. The high inter- and intra-patient variability towards Van therapy also make such practices of great value to achieve individualized dosing regimens.[51] Routine monitoring of Van levels on a daily basis is highly recommended for patients with renal dysfunction as there is a higher tendency of drug accumulation due to prolonged excretion time.[52] Frequent monitoring is also recommended for patients undergoing aggressive or prolonged Van therapy.[50]

The excessive use and misuse of Van have led to its detection in aquatic sources and animal-derived foods, which increase the risk of bacterial resistance development and pose a threat to human health.[43, 46, 53] Therefore, monitoring of Van levels in water

samples and animal products are also of great importance. Among the various analytical methods developed for Van quantification in different media, the established ones include high performance liquid chromatography (HPLC), immunoassays and bioassays.[54]

1.5.1 HPLC

HPLC is a type of chromatographic separation technique that is commonly coupled with UV,[55-57] (photo)diode array (DA),[58-59] fluorescence,[60] mass spectrometry (MS)[51, 61-63] or electrochemical[64] detector for the identification and quantification of the analyte(s) of interest. Due to its high sensitivity and specificity, HPLC has been considered the gold standard for Van quantification among the different analytical methods.[58] Especially in complicated biological fluids, HPLC proves to be an accurate and reliable tool to detect Van at concentrations below the therapeutic range which are often unattainable by immunoassays.[55-56] Another advantage of HPLC over immunoassays is the ability to isolate and quantify the degraded products of Van.[55-56] Furthermore, a simultaneous detection of Van and other commonly co-prescribed antibiotics has been performed on HPLC systems which improves the efficiency of analysis.[53, 63] However, traditional HPLC systems have several drawbacks[50, 56, 61-62] that limited its widespread use in routine laboratories and prompt ongoing efforts to improve existing HPLC techniques. These include: (1) a slow turnaround time owing to tedious sample preparation and lengthy analysis time which makes it impractical for the fast-paced, high-throughput requirement in routine laboratories, (2) requirement of large sample volumes which would be burdensome especially on the elderly and paediatric patients, and (3) substantial investment due to the high instrument and maintenance

costs and need to employ skilled operators, which restricted its use to a few laboratories in certain countries.

Some of these drawbacks can be overcome with the use of ultra performance liquid chromatography (UPLC) columns, which has sub-2 μm particle packing compared to the 3-10 μm particle packing found in normal HPLC columns.[62] The advantage of a smaller particle packing is exemplified in the higher separation efficiency and resolution of UPLC systems, achievable with a smaller sample volume (*e.g.* 50 μL) and lower flow rate.[51, 56, 61-62] With a shorter runtime per sample (within 3-5 min), the overall cost-effectiveness of the system is enhanced compared to HPLC systems. When coupled with MS detectors, the sensitivity of detection is increased compared to UV detectors[50] although one group reported comparable performance using a home-built 2D-HPLC-UV system.[56] However, their setup is complicated involving the use of three columns and three column-switching devices, and 200 μL of plasma volume is required. One of the motivations of this group comes from the high instrument and maintenance costs of MS detectors, which is a valid concern especially for applications in less wealthy countries.

In an attempt to reduce costs without compromising on the detection sensitivity, D'Hondt *et al.* utilized a cheaper single quad MS detector instead of the higher-end triple quadrupole MS instrument commonly used in previous studies.[65] These new MS detectors are commercially available and directly compatible with existing H/UPLC equipment and analysis software. Their group developed a UPLC-UV/MS method whereby two forms of detection, namely UV and MS, were used in conjunction and compared the results with those obtained using the traditional HPLC-UV method. With UV detection only, identification of Van B (the major component of the commercial product Van hydrochloride) using the latter method was done based on its high relative

peak area, while its impurity (aglucovancomycin B) was identified based on its relative retention time to Van B. On the other hand, the UPLC-UV/MS method yielded better resolution separation with appearance of more impurity peaks and tentative assignment of these peaks was achievable based on their MS spectra. Furthermore, lower limits of detection (LODs) were attained, *i.e.* 0.479 μg/mL and 0.220 μg/mL on UV and MS detector, respectively, for the UPLC-UV/MS method *vs.* 1.13 μg/mL on UV detector for the HPLC-UV method. Therefore, using the former method, the authors demonstrated the ability to perform impurity profiling of Van and other therapeutic peptides on top of sensitive quality control investigations. However, the analysis time of 30 min for Van remains undesirably long for routine considerations and is not significantly reduced compared to the HPLC-UV method (*i.e.* 35 min). Furthermore, post-column treatment was necessary to remove ion suppression effect and yield accurate data on MS.

Recently, Song *et al.* developed a new HPLC technique that utilizes an evaporative light scattering detector (ELSD) for the simultaneous determination of Van and seven other cyclopolypeptide antibiotics in animal feed.[53] The ELSD is a general detector that gives signals based on the concentration of the analyte and not its optical properties. As such, no additional derivatization step is required for those antibiotics that lack chromophores or fluorophores. Although the LODs for two antibiotics were improved, the corresponding values obtained for the remaining antibiotics including Van were found to be slightly higher than reported methods which the authors attributed it to the different scale of analysis, *i.e.* macro analysis in their study *vs.* micro and ultra-micro analysis in the reported methods. Nonetheless, one distinct disadvantage of their method is that it requires several steps for sample preparation, including extraction, purification and concentration of the antibiotics on solid-phase extraction (SPE) cartridge and a final filtration step. Not only is it time-consuming and laborious, the SPE

cartridges are expensive and intended for single-use only, increasing the cost of analysis.[58]

1.5.2 Immunoassays

Immunoassays are detection methods that employ Van-specific antibodies as recognition elements.[66-67] Free Van and labelled Van (either with a fluorophore, radioactive isotope or enzyme for fluorescence polarization immunoassay (FPIA), radioimmunoassay (RIA) or enzyme immunoassay (EIA), respectively) compete for a fixed number of binding sites on the antibody. The signal derived from the amount of bound labelled-Van is either directly (as in enzyme-multiplied immunoassay (EMIT) of EIA) or inversely proportional (as in FPIA and RIA) to the concentration of (free) Van in a sample.[67-69] Compared to HPLC, immunoassays are cheaper, faster and can be easily performed using commercial kits and automated analyzers (*e.g.* TDx from Abbott Laboratories for FPIA) with good precision, accuracy and sensitivity; therefore it is widely adopted in most routine laboratories.[70-72] However, immunoassays do have several disadvantages which will be elaborated specific to each assay in the following paragraphs.

1.5.2.1 FPIA

FPIA is often reported to overestimate serum Van concentrations due to cross-reactivities with the crystalline degraded products of Van (Van CDP-1) and other drugs.[54, 73] The degradation of Van to the inactive Van CDP-1 is a spontaneous process that is both time- and temperature-dependent.[74-75] For example, when maintained at 20-25 ℃, 50% and 90% of the initial Van weight were converted to Van CDP-1 in 16 h and 40 h, respectively.[74] The overestimation is more pronounced in patients with renal

dysfunction due to prolonged half-life of the antibiotic in the body (*e.g.* half-life up to 11 h in normal patients *vs.* up to 5 days in patients with renal dysfunction and even longer in dialyzed patients).[72, 74] The instability of the FPIA calibrators can also cause overestimation of serum Van concentrations, especially if they are used for more than 30 days after the package is opened.[76] Another disadvantage of FPIA is the need for specialized and costly equipment for automated operation.[50, 54, 73] Despite the demerits, FPIA is still the most commonly used Van detection method in routine laboratories due to its high-throughput capability (*e.g.* can run up to 80 tests per hour)[66] and sufficient sensitivity with a LOD of 2 μg/mL for clinical significance.[57]

1.5.2.2 RIA

Unlike the fluorescent label used in FPIA, RIA uses a γ-emitting iodine isotope (^{125}I) to label Van.[66] This method can detect Van precisely and accurately, but is less efficient and more expensive than FPIA.[54, 77] RIA-derived calibration curves also have limited stability (*i.e.* stable for less than 24 h), for which fresh curves have to be generated daily.[66, 77] This increases the amount of labour and reagents needed which makes the assay inefficient and adds to the cost of analysis.[77] Other disadvantages of RIA include the need for proper handling and disposal of radioactive chemicals,[66, 77] extensive sample preparation steps, short shelf life of the reagents and possible interferences from other γ-emitting isotopes such as ^{67}Ga or ^{99}Tc.[54, 66]

1.5.2.3 EIA

There are two types of EIA, namely EMIT and enzyme-linked immunosorbent assay (ELISA), which are classified as homogeneous and heterogeneous assays, respectively.[69, 78] The latter involves a physical separation step whereby bound

complexes formed after incubation are retained on a solid phase and unbound materials are washed away.[78] This is not necessary in the homogeneous assay which greatly enhances its efficiency.[67, 69] Similar to FPIA, commercial kits for EMIT are available and the operation can be automated (*e.g.* Du Pont's aca® system, Syva's Solaris® system and Cobas Bio™ centrifugal analyser from Roche Analytical Instruments, Inc.).[72, 79-80] EMIT utilizes a monoclonal antibody and was found to exhibit better selectivity than FPIA which uses a polyclonal antibody due to absence of cross-reaction with Van CDP-1.[54, 72, 76] However, the former displays low precision at Van concentrations higher than 30 μg/mL[55, 57, 76] and has lower sensitivity compared to ELISA due to the lack of a separation step to remove interfering materials.[67] Furthermore, it can only detect a single target whereas multiple target detection is achievable using ELISA (*e.g.* indirect ELISA).[81]

For the purpose of Van quantification, both direct[82] and indirect[43, 81] ELISA in competitive format have been developed. The former is simple and rapid, and has been applied in commercial kits such as DEIANJ11 by Creative Diagnostics.[82] In this assay, an antigen (*i.e.* Van conjugated to a carrier, usually protein) is first immobilized on a microwell plate (Figure 13). Van (standard or sample) and an enzyme-labelled (Van-specific) antibody are then added to the well and incubated for a period of time, during which Van and the antigen compete for the antibody. The unbound materials (free Van or antibody, or Van-antibody complex) are subsequently removed, and a substrate for the enzyme is added. The product is usually coloured which allows for UV quantification. The signal obtained would be in negative correlation to the Van concentration. By comparing the signal to a calibration curve, the actual Van concentration in an unknown sample can be readily determined.

In the indirect method, an additional secondary antibody is used and this enables signal amplification which enhances the sensitivity of detection.[83] In this assay, Van and the immobilized antigen compete for an unlabelled primary antibody (Van-specific) (Figure 13). After incubation for a period of time, the unbound materials are removed and an enzyme-labelled secondary antibody (specific for the primary antibody) is added. The rest of the procedure leading to UV detection is similar to the direct method. Since more than one secondary antibody can bind to the primary antibody, signal amplification is achieved and consequently, indirect ELISA offers higher sensitivity than the direct method.

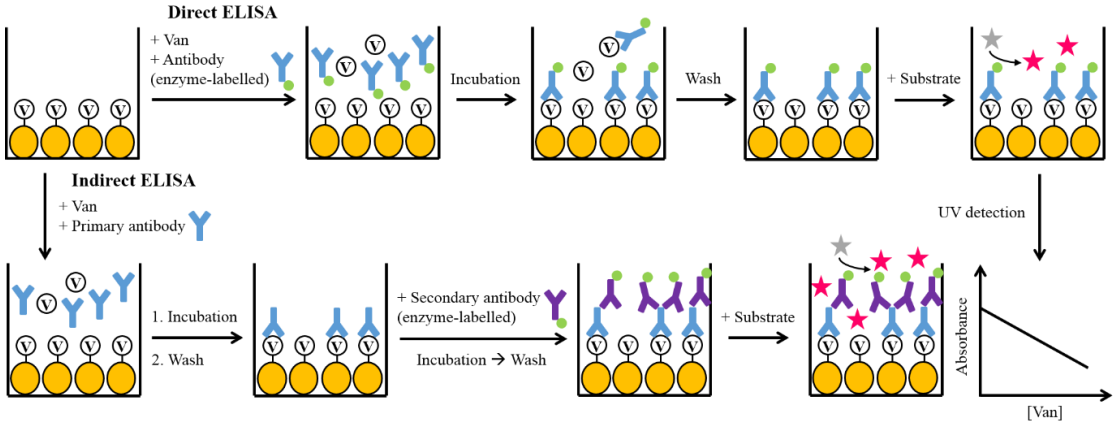

Figure 13. Schematic diagram showing the steps involved in direct and indirect ELISA. The diagram is not drawn to scale.

In 2015, Odekerken *et al.* developed an indirect competitive ELISA (ic-ELISA) for the detection of Van and gentamicin (Gen) in two protein-rich biological fluids, namely serum and wound exudate.[81] In the first part of their study, specific assays were established for each antibiotic using Van-conjugated bovine serum albumin (BSA) as antigen for Van detection and Gen-conjugated BSA for Gen detection. The results showed that Van and Gen quantification can be achieved with high specificity and

sensitivity for the concentration range of 20-5000 ng/mL and 2-500 ng/mL, respectively. The LODs obtained were also improved compared to that of selected fluorescence-based methods and HPLC, where the performance of the latter is often hampered by a high protein content. However, the authors did acknowledge some limitations of ELISA which is exemplified in the lack of ready-to-use protocols due to the need for rigorous optimization of the assay depending on the antibiotic as well as complexity of the sample composition. Furthermore, they could not exclude the possibility of aspecific interactions of other antibiotics (not tested in their study) with the Van- or Gen-specific antibody which could potentially compromise the selectivity of the assay. In the second part of their study, the group investigated the possibility of conjugating both Van and Gen to one BSA (*i.e.* one antigen expressing two antibiotics on its surface) and demonstrated that the modified antigen affords detection of Van or Gen by their respective antibodies with results comparable to the individual assays. In addition, when the new assay was used to determine Gen concentration, no cross-reactivity was detected in the presence of Van and vice versa. These results are promising from an efficiency point of view as it is now possible to produce one antigen for multiple target detection.

Two years later in 2017, an ic-ELISA based on a lab-prepared monoclonal antibody (3H4) was developed by Kong *et al.* which boasts of a higher detection sensitivity for Van than the previous group.[43] A LOD of 0.06 ng/mL was attained under the optimized buffer conditions of pH 7.4, 0.4% sodium chloride (m/v) and 5% acetonitrile (v/v). Satisfactory recovery rates ranging from 89.2-121.5% were also reported in raw milk and animal feed samples, with the latter showing comparable results as the HPLC-MS/MS method (also tested in their study). However, as aforementioned, rigorous optimization of the sampling conditions such as pH, ionic

strength (*i.e.* concentration of sodium chloride) and amount of organic solvent added was necessary to achieve the high sensitivity as reported. In addition, the assay was found to display a relatively high cross-reactivity value of 40% for norvancomycin (norVan), a compound with similar structure and therapeutic performance as Van. To improve the selectivity of the assay, the authors suggested the preparation of another antibody that is specific for norVan. Although this is doable and under preparation by the authors, the preparation of another antibody would incur higher costs, and more importantly, the performance and batch-to-batch reproducibility of the new antibody remains to be validated. Another interesting investigation by this group is the development of a lateral-flow immunochromatographic assay (ICA) strip employing the 3H4 antibody for a visual detection of Van. This method offers the advantages of being simpler and more rapid than ELISA, and does not require any instrument for analysis, making it highly suitable for preliminary on-site evaluations. However, this method is only semi-quantitative and has to be supported by other quantitative methods for exact values of Van concentrations.

To sum up, immunoassays are simple, rapid, cheap and suitable for high-throughput sample analysis. However, the use of protein-based antibodies and enzymes has always raised concerns regarding their stability (*e.g.* to assay conditions, shelf life, storage and transport requirements) and batch-to-batch consistency, which are often cited as inadequacies of immunoassays.[69, 84] To resolve this, molecularly imprinted materials (MIM) have been developed as synthetic alternatives to natural antibodies.

1.5.3 MIM as synthetic alternatives to antibodies in ELISA-like assays

MIM are prepared in the presence of a template, *i.e.* analyte, to generate binding sites that are complementary in size, shape and electrostatic environment to the analyte.[85-86] These synthetic materials thus behave like a monoclonal antibody displaying high selectivity and specificity to its analyte, but without the associated stability issues and inconsistencies arising from batch-to-batch variability.[44] Other advantages of MIM include the low cost, ease and speed of production of the imprints with the availability of automated synthesis.[44]

Materials such as polymers and silica have been employed by Chianella's and Piletska's groups, respectively, to generate Van imprints that are used to replace antibodies as recognition elements in corresponding ELISA-like assays. Chianella *et al.* determined an apparent dissociation constant (K_d) of 0.48 nM between the prepared molecularly imprinted polymer nanoparticles (nanoMIP) and Van, affirming the high affinity interaction, and subsequently demonstrated a LOD of 2.5 pM of the developed ELISA-like assay in buffer and serum for the concentration range of 1 pM-70 nM (Figure 14).[44] They also examined the stability of the prepared nanoMIP-coated microplates and showed that the assay performance is not affected even after one month of storage at room temperature and in a separate experiment to mimic the conditions of unrefrigerated delivery, storage at 40 ℃ for one week.

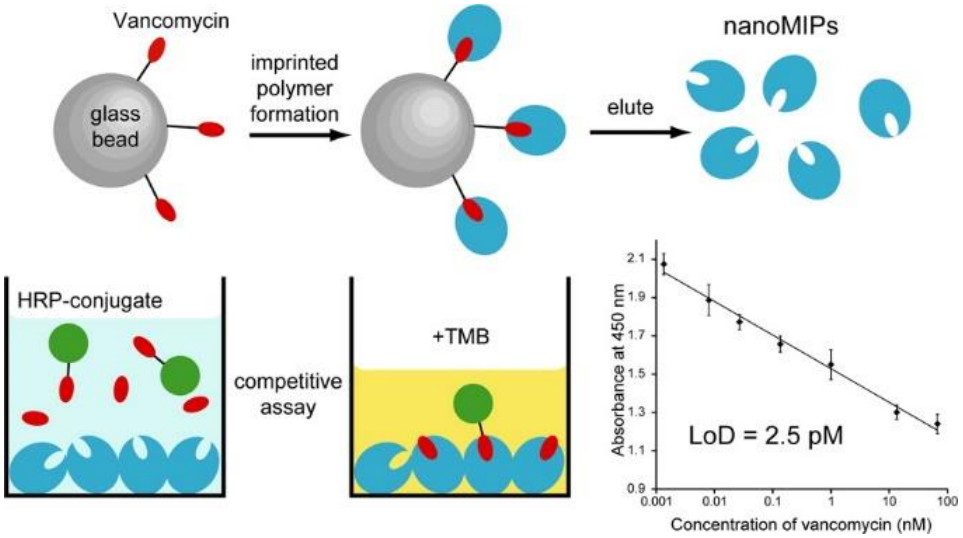

Figure 14. Schematic diagram showing the preparation of nanoMIP and its application in an ELISA-like assay which yielded a LOD of 2.5 pM. The figure is adopted from reference 44.

Contrary to the automated synthesis of nanoMIP using different monomers by Chianella's group, Piletska *et al.* prepared molecularly imprinted silica nanoparticles (nanoMIS) by Ostwald ripening, a process whereby smaller particles dissolve preferentially due to less stable surface energies and are deposited onto larger particles (Figure 15).[86] It was hypothesized that the formation of the nanoMIS starts with the weak, non-specific association between the silica nanoparticles and the Van template. This is followed by condensation of silicic acid, produced from the dissolution of smaller silica particles or particles with rough surfaces, around the regions of contact between the nanoparticles and Van template, thereby strengthening the association and converting the cavity on the silica nanoparticle into a specific binding site for Van. The prepared nanoMIS were able to detect Van without cross-reactivity with teicoplanin, another glycopeptide antibiotic bearing high structural similarity to Van. However, the silica nanoparticles were found to be unstable at high pH and in the presence of phosphate ions which resulted in the loss of recognition sites after 1 h of incubation in

a phosphate buffer of pH 8.5. The application of the nanoMIS for Van quantification in spiked serum was also tested, for which a shorter linear detection range was obtained due to increased sample complexity.

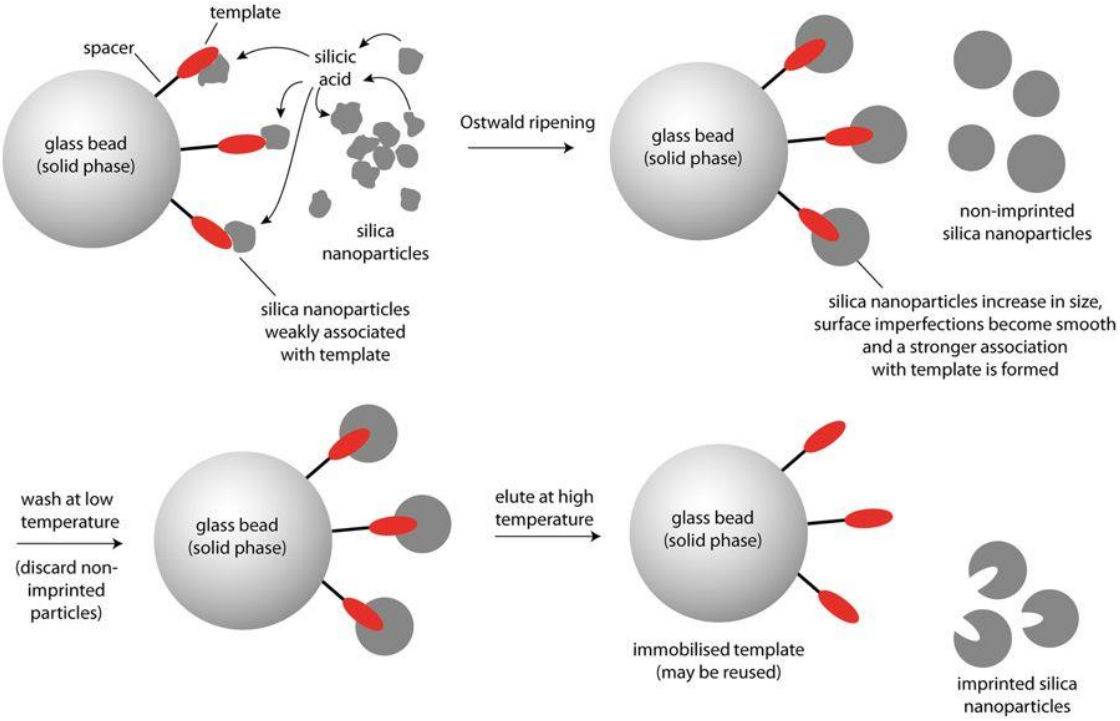

Figure 15. Schematic diagram showing the formation of the nanoMIS. The figure is adopted from reference 86.

In the two methods aforementioned, enzymes are still required to produce a detectable UV signal that is used to derive the Van concentration in a sample. A recent report by Canfarotta *et al.* features the development of a novel thermal detection platform for Van relying on nanoMIP coated on thermocouples without the need for enzymatic reactions.[85] The set-up includes a heat source and two thermocouples in a liquid flow cell, where the temperature (T1) of one of the thermocouples is controlled at 37 ℃ and not coated with the nanoMIP, and the other sensing thermocouple has a floating temperature T2 and is coated with the nanoMIP (Figure 16). Thermal detection

of Van is afforded when the antibiotic binds with high affinity to the nanoMIP and causes a reduction in the directional heat-flow to the sensing thermocouple (Figure 16). This results in a lower T2 measured. Using this method, the authors claimed a fast measurement time of less than 5 min per sample and determined a LOD of (4 ± 1) nM for the linear concentration range of 0-100 nM. These merits, on top of the simple operation and data interpretation, presents the reported method as a viable option for real-time applications. However, on further examination, it was found that prior to the first measurement, an initial stabilization time of 45 min in blank buffer and subsequently, a 30 min interval between each addition (either of different Van concentrations to construct the calibration curve, or different samples) are required, which make the whole procedure undesirably time-consuming and inefficient. In addition, the LOD was attained with a relatively large error of *ca.* 25% and at the maximum Van concentration tested, *i.e.* 1000 nM, only a 0.65% decrease in thermal response was observed; suggesting a low sensitivity of the reported method. To effect a larger change in thermal response and hence improve the detection sensitivity, the authors suggested performing the measurements at lower temperatures, but added that this could affect the stability of the current temperature control unit, for which further adaptations are necessary. Another disadvantage of this method is that it yielded a relatively low selectivity factor (*i.e.* ratio of response of analyte *vs.* competitor) of 1.7 in the presence of teicoplanin, which does not make it exactly distinguishable from Van. Nevertheless, according to the authors, this work is the first reported thermal detection method that applies nano-recognition elements on thermocouples and they have demonstrated its wide applicability to detect compounds with sizes ranging from small molecules to proteins.

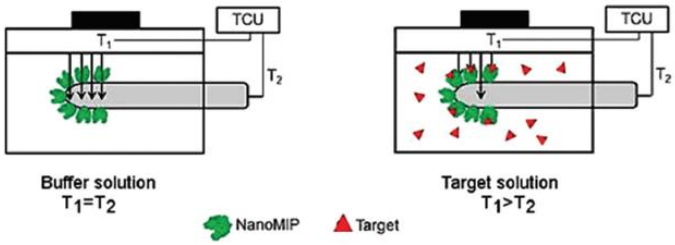

Figure 16. Schematic diagram showing the set-up and working principle of the proposed thermal detection platform. The figure is adopted from reference 85.

1.5.4 Bioassays

Apart from HPLC and immunoassays, bioassays represent another established method for Van quantification and two examples are the agar diffusion technique and turbidimetric assay.[87] In both methods, the inhibition of bacterial growth in the presence of varying antibiotic concentrations is monitored. This can be done by measuring the size of the inhibition zone on an agar plate (as in the agar diffusion technique) or absorbance of a mixture of the bacteria and antibiotic in a liquid medium (as in turbidimetric assay), which is then plotted against the Van concentration to identify a linear relationship to construct the calibration curve. Bioassays are inexpensive, have small sample volume requirements and measures only the active drug (*i.e.* no response would be obtained for the inactive Van CDP-1).[66, 88] However, it is both time- and labour-intensive, yielding a turnaround time of at least 6 h, lacks precision and does not present good sensibility or reproducibility.[64, 66, 71, 88-90] Furthermore, the presence of co-administered antibiotics that are not completely removed or inactivated would result in significant interference in the detection of Van.[66, 89] Taken together, these factors make bioassays unsuitable as routine detection methods for Van.

A literature search of publications in the past 20 years has revealed ongoing efforts by the research community to seek improvements and/or new developments to

overcome one or more of the limitations of the established Van detection methods.[46, 48, 52, 68, 73, 84, 91-98] Clearly, the monitoring of Van levels continues to hold great significance and importance, especially in TDM practices with one of the main aims to tackle drug resistance development.[99] As mentioned in section 1.5.3, MIM represents one of the improvements for immunoassays. The following sections would be dedicated to the discussion of other new techniques that have been developed for Van quantification over the years.

1.5.5 Pyrolysis mass spectrometry (Pyr-MS)

High temperature degradation or pyrolysis of Van was found to produce characteristic fragments that could be identified and quantified on a mass spectrometer. Such method has been employed by Ghassempour *et al.* to determine the concentrations of Van and its degraded products in human serum.[91] A characteristic peak with a mass-to-charge ratio (*m/z*) of 108, corresponding to the $C_6H_4O_2$ fragment of Van, was chosen and quantitative analysis was done by comparing the relative abundance of this peak to an internal standard. Compared to a traditional HPLC method, Pyr-MS offers the advantages of higher sensitivity, shorter analysis time and does not require large sample volumes or large quantities of toxic and expensive solvents. However, this method destroys the sample and is unable to quantify Van and Van CDP-1 separately due to production of the same fragment upon thermal degradation, which resulted in an overlap of signals. Such interference is not present in HPLC which is able to separate and quantify both compounds individually, in which case it proves to be superior to Pyr-MS.

1.5.6 Capillary electrophoresis (CE)-based methods

Analytical tools utilizing CE for separation have been reported by several groups for Van detection in biological and environmental samples.[52, 73, 92-94] This miniaturized technique yields separation with high efficiency and resolution, and only requires minute volumes of sample and reagents.[92] Consequently, waste generation is reduced and overall cost-effectiveness increased for CE-based analytical methods.[93] A hyphenated technique applying competitive immunoassay on CE coupled with laser-induced fluorescence polarization (LIFP) detection was described by Lam *et al.* in 2002.[92] The group used commercial FPIA kits which were shown to be compatible with CE analysis and thus eliminated the need for an extra step to label Van. After separation by CE, the highly sensitive LIFP detection enabled identification of the larger antibody-Van tracer (*i.e.* Van with fluorescent label) complexes from the smaller, unbound materials due to a significantly slower rotation, which polarized the fluorescence signal to a greater extent. Subsequent data analysis is similar to FPIA where the measured fluorescence signal and Van concentration are in negative correlation. However, the proposed method offers several advantages over FPIA as it requires very small sample volumes (*i.e.* 1 μL) and only 1/10 of the reagent consumption recommended for FPIA, and yields a LOD that is 10 times better. Furthermore, the method displayed high selectivity with no detectable cross-reactivities with Gen and digoxin, two antibiotics commonly prescribed prior to Van therapy which could potentially interfere with the analysis. For applications in human plasma, no extraction step was necessary, though the authors suggested a protein precipitation step for samples known to have a high protein content to improve reproducibility of measurements.

Micellar electrokinetic capillary chromatography (MECC) is a modification of CE where separation of the analyte is based on partitioning between a pseudostationary

phase comprising of micelles and an aqueous buffer.[73, 94] Using this method with UV detection, sample introduction via direct serum injection or after a protein removal step were demonstrated by Kitahashi's and Wang's groups, respectively. Clearly, the former is more efficient and while this could damage and reduce the lifetime of HPLC columns, its application on capillary tubes which are cheaper, more durable and require lower solvent volumes makes it more economical than HPLC.[73] The MECC method developed by Kitahashi's group also provides many other merits such as no need of an internal standard, high selectivity with no interference from 32 other antibiotics, nanoliter sample requirement (suitable for testing neonates) and ability to quantify total Van concentration (free and protein-bound). Wang's group thought that the concentration of the ionic surfactant sodium dodecyl sulfate (SDS) used by Kitahashi's group (*i.e.* 100 mM) is relatively high and is likely to cause an increase in the current and Joule heating, which in turn would reduce the separation efficiency and prolong analysis time.[93] As such, their group used 50 mM of SDS instead and added 2% sulfobutyl-β-cyclodextrin (β-CD) to the borate buffer (pH 9.5). The addition of β-CD was found to improve the separation of Van from serum proteins and impurities, plausibly due to an additional partitioning cavity. The lower limit of quantification (LLOQ) and applicable concentration range using this method were determined to be 1 μg/mL and 8.53-35.22 μg/mL, respectively, for which the latter was found to be comparable to that obtained using HPLC, *i.e.* 9.30-33.25 μg/mL. Thus, the authors presented this method as an alternative Van-TDM approach to HPLC for patients with peritoneal dialysis-associated peritonitis (PDAP).

Towards the goal of developing easily accessible point-of-care diagnostic tools, further miniaturization of MECC was realized on portable microchips that is coupled with laser-induced fluorescence (LIF)[94] or conductivity[52] detection. For microchip

electrophoresis (MCE), pre-concentration of Van is necessary due to the small sample injection volume and short optical path length, which diminish the detection sensitivity. This was accomplished with striking results, being achievable within 50 s[52] and in a separate report, yielding sensitivity enhancement factors as high as ~300-times.[94] When a polymeric micelle, poly(styrene sulfonic acid) sodium salt (PSS), was used as the pseudostationary phase in place of SDS, the aforementioned problems associated with the use of high SDS concentrations were avoided as PSS does not require a critical micelle concentration to maintain its polymer structure, hence enabling its use in lower concentrations (*ca.* 0.116 mM) while retaining a high separation efficiency.[94] This method coupled with LIF detection was demonstrated to be able to simultaneously analyze three antibiotics including Van within 3 min. However, MCE has its own limitations which include the need for specialized equipment(s), skilled operators, derivatization of analyte(s) to introduce fluorescent labels (*e.g.* Cy5) for systems using fluorescence detection[94] and several sample preparation steps (*e.g.* filtration, SPE/liquid-liquid extraction (LLE), desalting) for detection in real samples.[52, 94]

1.5.7 Cantilever arrays

Cantilevers as sensing platforms rely on specific binding events to induce nanomechanical responses, from which qualitative and quantitative data can be extracted.[95] When one side of the cantilever was functionalized with the peptide L-Lys-D-Ala-D-Ala (Lys = lysine), the introduction of Van in solution led to specific binding interactions which caused the cantilever to bend due to a change in surface stress (Figure 17).[84, 99] A linear relationship between the change in surface stress and Van concentration was found, which allowed construction of a calibration curve for quantitative analysis of the antibiotic. By fitting the data with an appropriate equation,

a value for K_d was also determined.[99] The signal transduction mechanism of cantilevers is advantageous as it allows for direct detection of Van without the need for any labelling or external probes.

Furthermore, with the fabrication of cantilever arrays expressing different ligands, it is possible to perform multiple analyses in parallel under the same experimental conditions, making such arrays highly efficient analytical tools. For example, Ndieyira *et al.* fabricated arrays of cantilevers coated with three different ligands, namely D-Ala-D-Ala, D-Ala-D-Lac (Lac = lactate) and triethylene glycol (PEG) (Figure 17).[99] While D-Ala-D-Ala is the specific ligand for Van, D-Ala-D-Lac is a mutated sequence that confers bacterial resistance to Van and a reference was included using the inert PEG coating.

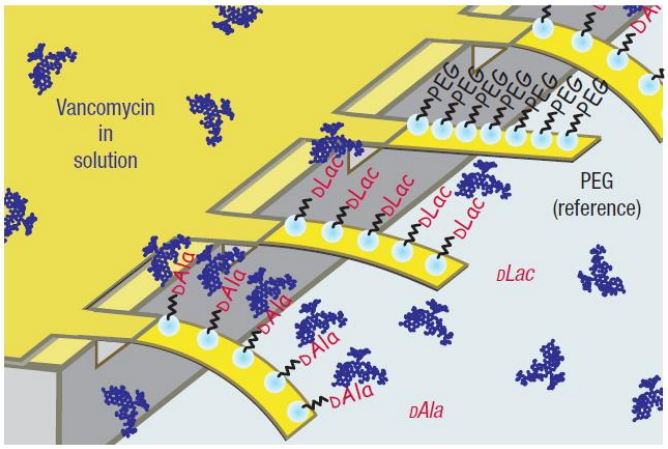

Figure 17. Schematic diagram showing cantilevers that are functionalized with different ligands (D-Ala, D-Lac and PEG) and the extent of bending in the presence of Van. The latter is dependent on the strength of interaction, *i.e.* K_d, between the antibiotic and the ligand. The figure is adopted from reference 99.

Upon injection of Van samples, the deflection of all three cantilevers was monitored in parallel and differential measurements (obtained after subtraction of the

background signal recorded on the reference cantilever) were analyzed. The results indicated a successful discrimination between the two peptide sequences, of which the D-Ala-D-Lac sequence, being short of one hydrogen bond to Van, displayed a much reduced affinity with a derived K_d value that is 800-fold larger than that for D-Ala-D-Ala; in consistent with results obtained by surface plasmon resonance. Using this method, Van detection limits as low as 10 nM was attainable and more importantly, applications in biological samples revealed satisfactory coverage of the clinically relevant concentration range. Though not proven, it is postulated that by expressing different ligands specific for different antibiotics on the cantilever surface, cantilever arrays have the potential to perform simultaneous screening for a plethora of drugs. It is expected that this would require further optimization and method validation in order to obtain detection limits with adequate or high sensitivity for the analytes of interest.

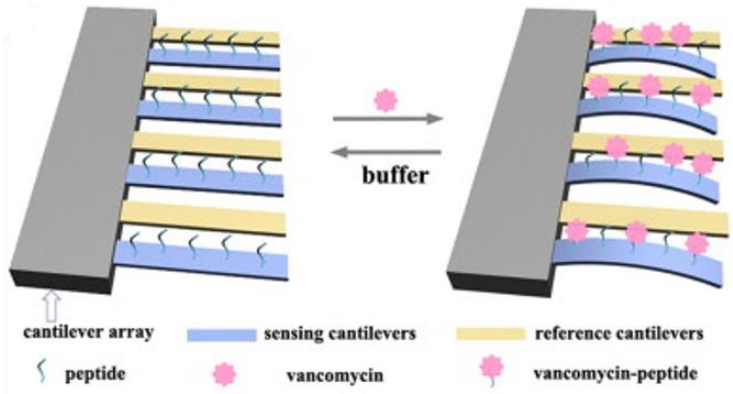

Figure 18. Schematic diagram showing the reversibility of the sensing cantilevers for repeated Van measurements. The figure is adopted from reference 84.

Another distinct advantage of cantilever arrays is its reversibility, where the binding between Van and the immobilized peptides can be reversed by flushing with the running buffer, thereby regenerating the cantilever surface for the next round of

sampling (Figure 18). The same group performed more than 100 measurements and reported reproducible signals (*e.g.* average surface stress signal at 250 μM of Van = -34.6 ± 0.9 mN m^{-1}), affirming the high reliability of cantilever arrays. As an extra washing step, 10 mM of hydrochloric acid (HCl) solution was injected to ensure complete removal of Van. This was considered to be a rather harsh regeneration condition, for which Bai *et al.* demonstrated that it was unnecessary and reported significant reduction on time spent on intermediate washing steps (*i.e.* from the *ca.* 1 h for two washing steps in the previous method to several minutes in their method), which in turn greatly enhances the efficiency between consecutive analyses.[84]

Compared to the antibodies and enzymes used in immunoassays, the use of peptides as recognition elements have considerable advantages such as better stability (over time, *e.g.* the modified cantilevers can be stored at -20 ℃ for more than a month, and to harsh experimental conditions, *e.g.* 10 mM of HCl), lower cost of production and ease of immobilization on cantilever surfaces.[84, 99] Nonetheless, the operation of cantilever arrays requires specialized equipment (*e.g.* home-built gravity flow microfluidics system)[99] and technical expertise, and the detection sensitivity can be compromised by the varying ionic strength of different running buffers used, especially at high Van concentrations,[84] for which further optimization is necessary.

1.5.8 Chemiluminescence (CL)-based methods

In 2014 and 2015, Khataee *et al.* published Van quantification methods employing flow-injection CL detection based on two different systems, luminol-hydrogen peroxide-copper oxide nanosheets (luminol-H_2O_2-CuO NS)[96] and potassium permanganate-morin-cadmium sulfide quantum dots ($KMnO_4$-morin-CdS QD),[46] respectively. In both systems, CL was readily produced upon mixing of two solutions

(a and b) and this emitted light coming from the formation of respective oxidized products was recorded on a luminometer (D) (Figure 19).

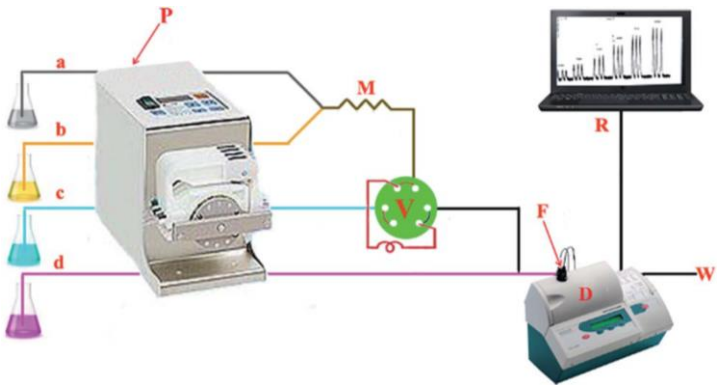

Figure 19. Schematic diagram showing the flow-injection CL system. Using the $KMnO_4$-morin-CdS QD system as an example: (a) acid solution, (b) mixture of Van (standard or sample), morin and CdS QD, (c) water as carrier, (d) $KMnO_4$ solution, (P) pump, (M) mixing tube, (V) injection valve, (F) flow cell, (D) luminometer, (W) waste, (R) recorder (*i.e.* personal computer). The figure is adopted from reference 46.

The rapid response, simple set-up, operation and analysis, and inexpensive equipment and reagents are some important benefits of these CL-based methods. Coupled with flow-injection, the corresponding CL-based method is capable of high-throughput analysis (*e.g.* 120 samples per hour) and has hence driven developments for food, environmental, clinical and pharmaceutical applications.

However, traditional CL-based methods often suffer from poor detection sensitivity owing to the low quantum yield of the oxidized product. Khataee *et al.* reported on improved quantum yields with the introduction of semiconductor nanomaterials such as CuO NS and CdS QD as signal amplifier catalysts, for which the former was shown to increase the CL intensity of the reaction between luminol and H_2O_2 by ~9-times. Upon the addition of Van, however, the enhanced CL intensity decreased

(for the CuO NS system) or further increased (for the CdS QD system) in a manner dependent on the antibiotic concentration, thus affording quantitative analysis of Van and successful applications in spiked environmental water samples and human serum, and commercial pharmaceutical formulations have been demonstrated.

Both of their systems displayed high sensitivity and a wide linear range of about 2-4 orders of magnitude. For example, a LOD of 1.4 μg/L was determined for the Van concentration range of 0.004-19 mg/L using the $KMnO_4$-morin-CdS QD system. However, it was found that the presence of Cu^{2+} ions caused significant interference to which the authors suggested its removal in real samples using a chelating agent (*e.g.* ethylenediaminetetraacetic acid (EDTA)) or by running the sample through a strong cation exchange column prior to analysis. The use of nanomaterials also entails stringent control of its size and/or morphology (for CuO NS) which affect its catalytic properties and hence reproducibility of the results. Furthermore, although selectivity tests were performed in the presence of commonly occurring substances in real samples, the selectivity of the proposed method for Van in the presence of other antibiotics, commonly co-administered or with high structural similarity, was not illustrated, which presents a loophole of their systems.

Before ending the discussion on Van detection methods in this chapter, it is worth mentioning a very interesting report, published in 2016, featuring the development of an integrated system utilizing hollow microneedles for extraction of sub-nanoliter sample volumes and optofluidic detection which allows a rapid and straightforward analysis of Van concentrations in interstitial fluids.[48] This system was designed with the aim to provide a minimally invasive and less painful point-of-care alternative to commercial TDM kits which require frequent (*e.g.* 3-4 times daily)

extraction of large (blood) sample volumes (>1 mL) from patients undergoing Van treatment, in the process inflicting much pain on them.

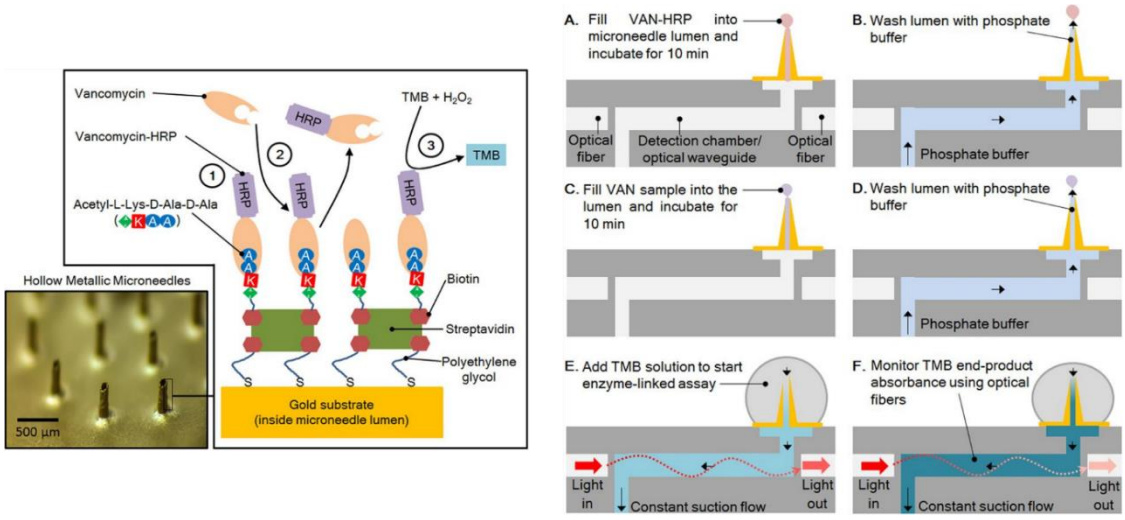

Figure 20. Van detection scheme inside the microneedle lumen (left). A stepwise detection procedure is shown on the right. The figure is adopted from reference 48.

The microneedles under study were fabricated with sub-millimeter dimensions and their inner lumen coated with ligands expressing the Lys-D-Ala-D-Ala peptide sequence to capture Van (Figure 20). When inserted into the skin, the microneedle extracts only 0.6 nL of interstitial fluid by capillary action. Van in the fluid then competes with a pre-loaded enzyme-labelled Van (Van-HRP) for the immobilized peptides and displaces it from the surface (Figure 20). TMB, a substrate for HRP, is added in the next step (step E) and is converted by the remaining bound Van-HRP to a coloured product, which is detected by UV spectroscopy in the integrated optofluidic device (step F). A high UV signal would mean a low concentration of Van in the interstitial fluid and vice versa. Low-loss light propagation in the optofluidic device was achieved by integrating air mirrors along the optimized 5 mm detection chamber to ensure total internal reflection. This greatly enhanced the detection sensitivity of the

whole system, yielding a LOD of 84 nM for the Van concentration range of 0.3-40 μM. The proposed system boasts of a significantly reduced LOD compared to that of commercial immunoassay kits (*e.g.* both QMS® VANCO and EMIT® 2000 kits have a LOD of 1.35 μM), rapid analysis time (*i.e.* <5 min) and an efficient, integrated detection assay that saves the time to transfer the samples from place to place and/or equipment to equipment.

Fluorescence-based methods have also been developed for Van detection, the discussion of which is included in Chapter 2.

1.6 Aims of thesis

Fluorescence-based techniques are at the heart of highly sensitive analytical tools which also display great flexibility to be tailored to detect various targets using different mechanisms and materials. Often, the targets include biologically significant materials such as ions, small molecules, proteins and DNA. The rational design of suitable fluorescence-based detection systems for such targets enables monitoring of important physiological processes, disease states as well as elucidation of the pharmacokinetics and pharmacodynamics of various drugs in therapeutic drug monitoring practices; these are areas receiving increasing attention over the years.

In Chapters 2 and 3, two molecular PET-based probes were designed for Van detection. The first probe consists of a triad made up of a squaraine dye conjugated to two anthraquinone molecules via Lys-D-Ala-D-Ala peptides. In the absence of Van, electron transfer occurs from the excited squaraine dye to anthraquinone and quenches the emission of the dye (Chapter 2). A similar quenching phenomenon can also be effected by the opposite hole-transfer mechanism, where hole transfer instead of electron transfer takes place from an excited cyanine dye to Fc in the second probe

(Chapter 3). In the same chapter, an investigation on the influence of the length of the linker between the dye and the quencher on the hole-transfer quenching efficiency in the triad was also conducted.

In Chapter 4, a novel FRET-based probe utilizing UCNP as the sensing platform was designed to sense epinephrine (EP), which is an important neurotransmitter involved in the regulation of various physiological processes in the sympathetic nervous system. The synthesis of the nanoparticles and its application for EP detection are discussed in this chapter.

1.7 References

1. Li, B.; Yu, Q.; Duan, Y. *Crit. Rev. Biotechnol.* **2015,** *35* (1), 82-93.
2. Wolfbeis, O. S. *Chem. Soc. Rev.* **2015,** *44* (14), 4743-4768.
3. Zhong, W. *Anal. Bioanal. Chem.* **2009,** *394* (1), 47-59.
4. Chinen, A. B.; Guan, C. M.; Ferrer, J. R.; Barnaby, S. N.; Merkel, T. J.; Mirkin, C. A. *Chem. Rev.* **2015,** *115* (19), 10530-10574.
5. Cardoso Dos Santos, M.; Hildebrandt, N. *Trends Analyt. Chem.* **2016,** *84*, 60-71.
6. S, M.; N, P. *J. Mater. Sci. Nanotechnol.* **2016,** *4* (1).
7. Wang, X.; Valiev, R. R.; Ohulchanskyy, T. Y.; Agren, H.; Yang, C.; Chen, G. *Chem. Soc. Rev.* **2017,** *46* (14), 4150-4167.
8. Resch-Genger, U.; Grabolle, M.; Cavaliere-Jaricot, S.; Nitschke, R.; Nann, T. *Nat. Methods* **2008,** *5* (9), 763-75.
9. Klymchenko, A. S. *Acc. Chem. Res.* **2017,** *50* (2), 366-375.
10. Han, J.; Burgess, K. *Chem. Rev.* **2010**, *110*, 2709-2728.
11. Chen, G.; Qiu, H.; Prasad, P. N.; Chen, X. *Chem. Rev.* **2014,** *114* (10), 5161-214.

12. Luo, S.; Zhang, E.; Su, Y.; Cheng, T.; Shi, C. *Biomaterials* **2011,** *32* (29), 7127-38.

13. Chen, J.; Zhao, J. X. *Sensors (Basel)* **2012,** *12* (3), 2414-35.

14. Wu, X.; Chen, G.; Shen, J.; Li, Z.; Zhang, Y.; Han, G. *Bioconjug. Chem.* **2015,** *26* (2), 166-75.

15. Nadort, A.; Sreenivasan, V. K.; Song, Z.; Grebenik, E. A.; Nechaev, A. V.; Semchishen, V. A.; Panchenko, V. Y.; Zvyagin, A. V. *PLoS One* **2013,** *8* (5), e63292.

16. Ang, L. Y.; Lim, M. E.; Ong, L. C.; Zhang, Y. *Nanomedicine* **2011**, *6* (7), 1273-1288.

17. Wang, M.; Abbineni, G.; Clevenger, A.; Mao, C.; Xu, S. *Nanomedicine* **2011,** *7* (6), 710-29.

18. Zhang, H.; Li, Y.; Lin, Y.; Huang, Y.; Duan, X. *Nanoscale* **2011,** *3* (3), 963-6.

19. Qiu, H.; Yang, C.; Shao, W.; Damasco, J.; Wang, X.; Agren, H.; Prasad, P. N.; Chen, G. *Nanomaterials (Basel)* **2014,** *4* (1), 55-68.

20. Lin, M.; Zhao, Y.; Wang, S.; Liu, M.; Duan, Z.; Chen, Y.; Li, F.; Xu, F.; Lu, T. *Biotechnol. Adv.* **2012,** *30* (6), 1551-61.

21. Shen, J.; Chen, G.; Ohulchanskyy, T. Y.; Kesseli, S. J.; Buchholz, S.; Li, Z.; Prasad, P. N.; Han, G. *Small* **2013,** *9* (19), 3213-7.

22. Li, Z.; Zhang, Y. *Nanotechnology* **2008,** *19* (34), 345606.

23. Doose, S.; Neuweiler, H.; Sauer, M. *ChemPhysChem* **2009,** *10* (9-10), 1389-98.

24. Wong, J. K.; Todd, M. H.; Rutledge, P. J. *Molecules* **2017,** *22* (2).

25. Sparano, B. A.; Koide, K. *J. Am. Chem. Soc.* **2007**, *129*, 4785-4794.

26. Kobayashi, H.; Ogawa, M.; Alford, R.; Choyke, P. L.; Urano, Y. *Chem. Rev.* **2010**, *110*, 2620-2640.

27. Dias, G. G.; King, A.; de Moliner, F.; Vendrell, M.; da Silva Junior, E. N. *Chem. Soc. Rev.* **2018,** *47* (1), 12-27.

28. Zhang, W.; Ma, Z.; Du, L.; Li, M. *Analyst* **2014,** *139* (11), 2641-9.

29. Heinlein, T.; Knemeyer, J.-P.; Piestert, O.; Sauer, M. *J. Phys. Chem. B* **2003**, *107*, 7957-7964.

30. Zhang, S.; Yang, C.; Lu, W.; Huang, J.; Zhu, W.; Li, H.; Xu, Y.; Qian, X. *Chem. Commun. (Camb)* **2011,** *47* (29), 8301-3.

31. Liu, Z.; Wang, B.; Ma, Z.; Zhou, Y.; Du, L.; Li, M. *Anal. Chem.* **2015,** *87* (5), 2550-4.

32. Liu, Z.; Zhou, Y.; Du, L.; Li, M. *Analyst* **2015,** *140* (24), 8101-8.

33. Wu, X.; Liu, F.; Wells, K. L.; Tan, S. L.; Webster, R. D.; Tan, H. S.; Zhang, D.; Xing, B.; Yeow, E. K. *Chemistry* **2015,** *21* (8), 3387-98.

34. Jin, B.; Wang, S.; Lin, M.; Jin, Y.; Zhang, S.; Cui, X.; Gong, Y.; Li, A.; Xu, F.; Lu, T. J. *Biosens. Bioelectron.* **2017,** *90*, 525-533.

35. Liu, L.; Zhang, H.; Song, D.; Wang, Z. *Analyst* **2018,** *143* (3), 761-767.

36. Xu, S.; Dong, B.; Zhou, D.; Yin, Z.; Cui, S.; Xu, W.; Chen, B.; Song, H. *Sci. Rep.* **2016,** *6*, 23406.

37. Chen, Z.; Chen, H.; Hu, H.; Yu, M.; Li, F.; Zhang, Q.; Zhou, Z.; Yi, T.; Huang, C. *J. Am. Chem. Soc.* **2008**, *130*, 3023-3029.

38. Saleh, S. M.; Ali, R.; Hirsch, T.; Wolfbeis, O. S. *J. Nanopart. Res.* **2011,** *13* (10), 4603-4611.

39. Alonso-Cristobal, P.; Vilela, P.; El-Sagheer, A.; Lopez-Cabarcos, E.; Brown, T.; Muskens, O. L.; Rubio-Retama, J.; Kanaras, A. G. *ACS Appl. Mater. Interfaces* **2015,** *7* (23), 12422-9.

40. Liu, C.; Wang, Z.; Jia, H.; Li, Z. *Chem. Commun. (Camb)* **2011,** *47* (16), 4661-3.

41. Nguyen, T.-T. T.; Huy, B. T.; Tawfik, S. M.; Zayakhuu, G.; Cho, H. H.; Lee, Y.-I. *Arab J. Chem.* **2018**.

42. Tariq, M. H.; Naureen, H.; Abbas, N.; Akhlaq, M. *J. Anal. Bioanal. Tech.* **2015**, *6*, 1-5.

43. Kong, D.; Xie, Z.; Liu, L.; Song, S.; Kuang, H.; Xu, C. *Food Agric. Immunol.* **2017,** *28* (3), 414-426.

44. Chianella, I.; Guerreiro, A.; Moczko, E.; Caygill, J. S.; Piletska, E. V.; De Vargas Sansalvador, I. M.; Whitcombe, M. J.; Piletsky, S. A. *Anal. Chem.* **2013,** *85* (17), 8462-8.

45. de Souza Botelho, T.; Rebello Lourenco, F.; de Jesus. Andreoli Pinto, T. *Curr. Pharm. Anal.* **2013,** *9* (2), 172-176.

46. Khataee, A.; Lotfi, R.; Hasanzadeh, A. *RSC Advances* **2015,** *5* (101), 82645-82653.

47. Sharaf El-Din, M. K.; Ibrahim, F.; Kamal El-Deen, A.; Shimizu, K. *J. Food. Drug. Anal.* **2018,** *26* (2), 834-841.

48. Ranamukhaarachchi, S. A.; Padeste, C.; Dubner, M.; Hafeli, U. O.; Stoeber, B.; Cadarso, V. J. *Sci. Rep.* **2016,** *6*, 29075.

49. Ashford, P. A.; Bew, S. P. *Chem. Soc. Rev.* **2012,** *41* (3), 957-78.

50. Javorska, L.; Krcmova, L. K.; Solichova, D.; Solich, P.; Kaska, M. *J. Sep. Sci.* **2016,** *39* (1), 6-20.

51. Brozmanova, H.; Kacirova, I.; Urinovska, R.; Sistik, P.; Grundmann, M. *Clin. Chim. Acta* **2017,** *469*, 136-143.

52. Chong, K. C.; Thang, L. Y.; Quirino, J. P.; See, H. H. *J. Chromatogr. A* **2017,** *1485*, 142-146.

53. Song, X.; Xie, J.; Zhang, M.; Zhang, Y.; Li, J.; Huang, Q.; He, L. *J. Chromatogr. B Analyt. Technol. Biomed. Life Sci.* **2018,** *1076*, 103-109.

54. Somerville, A. L.; Wright, D. H.; Rotschafer, J.C. *Pharmacotherapy*, **1999**, *19*, 702-707.

55. Usman, M.; Hempel, G. *Springerplus* **2016,** *5*, 124.

56. Sheng, Y.; Zhou, B. *J. Chromatogr. A* **2017,** *1499*, 48-56.

57. Jesus Valle, M. J.; Lopez, F. G.; Navarro, A. S. *J. Pharm. Biomed. Anal.* **2008,** *48* (3), 835-9.

58. Lima, T. M.; Seba, K. S.; Goncalves, J. C. S.; Cardoso, F. L. L.; Estrela, R. C. E. *J. Chromatogr. Sci.* **2018,** *56* (2), 115-121.

59. Wicha, S. G.; Kloft, C. *J. Chromatogr. B Analyt. Technol. Biomed. Life Sci.* **2016,** *1028*, 242-248.

60. Abu-Shandi, K. H. *Anal. Bioanal. Chem.* **2009,** *395* (2), 527-32.

61. Javorska, L.; Krcmova, L. K.; Solich, P.; Kaska, M. *J. Pharm. Biomed. Anal.* **2017,** *142*, 59-65.

62. Barco, S.; Castagnola, E.; Gennai, I.; Barbagallo, L.; Loy, A.; Tripodi, G.; Cangemi, G. *J. Chemother.* **2016,** *28* (5), 395-402.

63. Bijleveld, Y.; de Haan, T.; Toersche, J.; Jorjani, S.; van der Lee, J.; Groenendaal, F.; Dijk, P.; van Heijst, A.; Gavilanes, A. W.; de Jonge, R.; Dijkman, K. P.; van Straaten, H.; Rijken, M.; Zonnenberg, I.; Cools, F.; Nuytemans, D.; Mathot, R. *J. Chromatogr. B Analyt. Technol. Biomed. Life Sci.* **2014,** *951-952*, 110-8.

64. Favetta, P. Guitton, J.; Bleyzac, N.; Dufresne, C.; Bureau, J. *J. Chromatogr. B* **2001**, *751*, 377-382.

65. D'Hondt, M.; Gevaert, B.; Wynendaele, E.; De Spiegeleer, B. *J. Pharm. Anal.* **2016,** *6* (1), 24-31.

66. Pfaller, M. A.; Krogstad, D. J.; Granich, G. G.; Murray, P. R. *J. Clin. Microbiol.* **1984**, *20*, 311-316.

67. Slagle, K. M.; Ghosn, S. J. *Lab. Med.* **1996**, *27*, 177-183.

68. Yu, L.; Zhong, M.; Wei, Y. *Anal. Chem.* **2010**, *82*, 7044-7048.

69. O'Kennedy, R.; Byrne, M.; O'Fagain, C.; Berns, G. *Biochem. Educ.* **1990**, *18*, 136-140.

70. Hagihara, M.; Sutherland, C.; Nicolau, D. P. *J. Chromatogr. Sci.* **2013,** *51* (3), 201-7.

71. Vila, M.; Oliveira, R.; Goncalves, M.; Tubino, M. *Quim. Nova* **2007**, *30*, 395-399.

72. Saunders, N. J.; Want, S. V.; Adams, D. J. *J. Antimicrob. Chemother.* **1995**, *36*, 411-415.

73. Kitahashi, T.; Furuta, I. *Clin. Chim. Acta* **2001**, *312*, 221-225.

74. Melichercik, P.; Klapkova, E.; Landor, I.; Judl, T.; Sibek, M.; Jahoda, D. *Bratisl. Med. J.* **2014,** *115* (12), 796-799.

75. Murphy, J. E. *Clinical Pharmacokinetics*, 5th ed.; American Society of Health-System Pharmacists: Maryland, 2012, pp364.

76. Morishige, H.; Shuto, H.; Ieiri, I.; Otsubo, K.; Oishi, R. *Ther. Drug Monit.* **1996**, *18*, 80-5.

77. Ackerman, B. H.; Berg, H. G.; Strate, R. G.; Rotschafer, J. C. *J. Clin. Microbiol.* **1983**, *18*, 994-995.

78. Engvall, E. *Methods Enzymol.* **1980**, *70*, 419-439.

79. Yeo, K.-T.; Traverse, W.; Horowitz, G. L. *Clin. Chem.* **1989**, *35*, 1504-1507.

80. Wilson, J. F. *Drug Eicosanoids: Second Messengers*; Springer Science+Business Media LLC: New York, 1995, pp1640.

81. Odekerken, J. C.; Logister, D. M.; Assabre, L.; Arts, J. J.; Walenkamp, G. H.; Welting, T. J. *Springerplus* **2015,** *4*, 614.

82. Creative Diagnostics. https://www.creative-diagnostics.com/pdf/DEIANJ11.pdf (accessed Aug 25, 2018).

83. BosterBio. https://www.bosterbio.com/media/pdf/ELISA_Handbook.pdf (accessed Aug 25, 2018).

84. Bai, X.; Lu, B.; Chen, X.; Zhang, B.; Tang, J. *Biosens. Bioelectron.* **2014,** *62*, 145-50.

85. Canfarotta, F.; Czulak, J.; Betlem, K.; Sachdeva, A.; Eersels, K.; van Grinsven, B.; Cleij, T. J.; Peeters, M. *Nanoscale* **2018,** *10* (4), 2081-2089.

86. Piletska, E.; Yawer, H.; Canfarotta, F.; Moczko, E.; Smolinska-Kempisty, K.; Piletsky, S. S.; Guerreiro, A.; Whitcombe, M. J.; Piletsky, S. A. *Sci. Rep.* **2017,** *7* (1), 11537.

87. Francisco, F. L.; Saviano, A. M.; Almeida Tde, S.; Lourenco, F. R. *J. Microbiol. Methods* **2016,** *124*, 28-34.

88. Pohlod, D. J.; Saravolatz, L. D.; Somerville, M. M. *J. Clin. Microbiol.* **1984**, *20*, 159-161.

89. Filburn, B. H.; Shull, V. H.; Tempera, Y. M.; Dick, J. D. *Antimicrob Agents Chemother.* **1983**, *24*, 216-220.

90. Walker, C. A.; Kopp, B. *Antimicrob Agents Chemother.* **1983**, *24*, 216-220.

91. Ghassempour, A. Darbandi, M. K.; Asghari, F. S. *Talanta* **2001**, *55*, 573-580.

92. Lam, M. T.; Le, X. C. *Analyst* **2002,** *127* (12), 1633-1637.

93. Wang, J.; Cao, Y.; Wu, S.; Wang, S.; Zhao, X.; Zhou, T.; Lou, Y.; Fan, G. *Molecules* **2017,** *22* (4).

94. Wu, M.; Gao, F.; Zhang, Y.; Wang, G.; Wang, Q.; Li, H. *J. Pharm. Biomed. Anal.* **2015,** *103*, 91-8.

95. Mckendry, R.; Zhang, J.; Arntz, Y.; Strunz, T.; Hegner, M.; Lang, H. P.; Baller, M. K.; Certa, U.; Meyer, E.; Guntherodt, H.-J.; Gerber, C. *PNAS* **2002**, *99*, 9783-9788.

96. Khataee, A. R.; Hasanzadeh, A.; Iranifam, M.; Fathinia, M.; Hanifehpour, Y.; Joo, S. W. *Spectrochim. Acta A Mol. Biomol. Spectrosc.* **2014,** *122*, 737-43.

97. Liang, W.; Liu, S.; Liu, Z.; Li, D.; Wang, L.; Hao, C.; He, Y. *New J. Chem.* **2015,** *39* (6), 4774-4782.

98. Lee, S.; Park, I. S.; Jung, Y.-S.; Kim, J.-M. *J. Nanosci. Nanotechnol.* **2014,** *14* (10), 7693-7699.

99. Ndieyira, J. W.; Watari, M.; Barrera, A. D.; Zhou, D.; Vogtli, M.; Batchelor, M.; Cooper, M. A.; Strunz, T.; Horton, M. A.; Abell, C.; Rayment, T.; Aeppli, G.; McKendry, R. A. *Nat. Nanotechnol.* **2008,** *3* (11), 691-6.

Chapter 2 Vancomycin determination by disrupting electron-transfer in a fluorescence turn-on squaraine-anthraquinone triad**

Abstract: This chapter describes the development of a highly sensitive and selective probe for vancomycin (Van) in aqueous and serum samples. The design of the probe is based on a triad consisting of a near-infrared squaraine dye (Seta-640) conjugated to two anthraquinone molecules via Lys-D-Ala-D-Ala peptides. In the absence of Van, the close proximity and efficient electron-transfer from the excited Seta-640 dye to anthraquinone result in significant fluorescence quenching of the dye ("off"-state). When Van is added, the antibiotic molecules bind with high affinity to the -D-Ala-D-Ala ligands in a 2:1 stoichiometry (Van:triad); resulting in fluorescence recovery that is as high as 30-times ("on"-state). Even though bound Van enhances the fluorescence by reducing the rate of (intrinsic) polarity-induced non-radiative decay process, this effect plays only a minor role. Instead, the main reason behind the observed fluorescence recovery after drug binding is the effective inhibition of electron-transfer; plausibly arising from a steric-induced lengthening of the spatial separation between electron donor and acceptor. The probe has detection limits of 7.0 nM and 96.9 nM in buffer and human serum, respectively, operates in the clinically relevant range, is insensitive to Van crystalline degradation product (CDP-1) and easy to operate by using a commonly available fluorescence spectrometer.

Except for the part of the introduction in section 2.1, this chapter has been published in Ng, S. M.; Wu, X.; Khyasudeen, F.; Nowakowski, P. J.; Tan, H.-S.; Xing, B.; Yeow, E. K. L. *ACS Sens.* **2018, *3*, 1156-1163.

2.1 Introduction

Vancomycin (Van) is a glycopeptide antibiotic that is used to treat patients afflicted with infections caused by penicillin-resistant Gram-positive bacteria, and is the drug of "last resort" for tackling the deadly methicillin-resistant *Staphylococcus aureus* (MRSA). In order to administer optimal dosages and to avoid ototoxicity/nephrotoxicity during systematic treatment of patients, therapeutic drug monitoring of Van is routinely performed in hospitals.[1-2] Van determination in aquatic environment is also commonly conducted to ensure that elevated drug concentration is not present which will otherwise lead to adverse repercussions to the ecosystem.[3] Therefore, the development of efficient and cost-effective methods to determine Van in both human serum and aqueous samples is necessary.

Up to now, various methods have been developed for quantification of Van in different media. These include high performance liquid chromatography (HPLC),[4-6] immunoassays,[7-9] bioassays,[10] capillary electrophoresis,[11-13] cantilever arrays[14-15] and chemiluminescence-based methods.[16-17] However, these methods are often limited by time-consuming procedures and a low throughput, cross-reactions with other structurally similar compounds including Van crystalline degradation product (CDP-1) (*e.g.* fluorescence polarization immunoassay), use of radioactive and/or unstable reagents (*e.g.* enzyme-based methods), lack of standard assay protocols (*e.g.* enzyme-linked immunosorbent assay), and need for designated instruments from manufacturers (*e.g.* for commercially available immunoassays).

Fluorescence-based methods have also been developed for Van quantification and are advantageous because of their high sensitivity, rapidity and simplicity. Yu *et al.* prepared a molecular probe consisting of an organic dye (*i.e.* Alexa Fluor 680) conjugated to a peptide sequence Lys-D-Ala-D-Ala and used it to detect three

glycopeptide antibiotics (Van, teicoplanin and telavancin) in a direct fluorescence polarization assay.[18] When the antibiotic binds specifically to the -D-Ala-D-Ala sequence of the probe, the resulting (bulkier) complex would cause the fluorescence polarization signal to increase. By monitoring the increase in polarization signal as the concentration of the antibiotic is increased, a linear relationship was found for all three antibiotics within certain concentration ranges, thus affording quantification of the three antibiotics using the proposed assay. The assay demonstrated high selectivity toward the class of glycopeptide antibiotics, for which no significant change in polarization signal was noted for other antibiotics tested. Furthermore, the activity of the synthesized probe was unaffected even after storage in the dark at room temperature for 9 months, exhibiting excellent stability over the proteinaceous reagents that are used in immunoassays. However, it was found that the working concentration range of the probe barely covers the clinically relevant concentration range for Van and teicoplanin. Consequently, additional steps are required to dilute the blood samples prior to analysis (shown for teicoplanin only).

Lee *et al.* also prepared a molecular probe consisting of a biphenyl derivative conjugated to two D-Ala-D-Ala moieties (BPDC-2DADA **1**) which displayed aggregation-induced enhanced emission (AIEE) in the absence of Van (Figure 1).[19] The aggregation behaviour, facilitated by aromatic and hydrogen-bonding NH and COOH groups, led to the formation of fibrous structures that were observed using scanning electron microscope (SEM) and optical microscope. The addition of Van, which binds to D-Ala-D-Ala, induced a morphological change from fibers to nanoparticles over time (Figure 1) and a decrease in fluorescence intensity was observed. The change could be reversed by adding free peptide which binds to Van and displaces it from BPDC-2DADA **1**. Consequently, aggregation occurs again and the fibrous structure was

regenerated with recovery of fluorescence intensity. A low LOD of 57 μM was attained using this method. However, the Van concentrations tested (*i.e.* 0.17-17 mM) were orders of magnitude higher than its therapeutic range and the use of an excitation wavelength of 265 nm, which can also excite biological compounds, can cause significant background noise in the analysis of real samples.

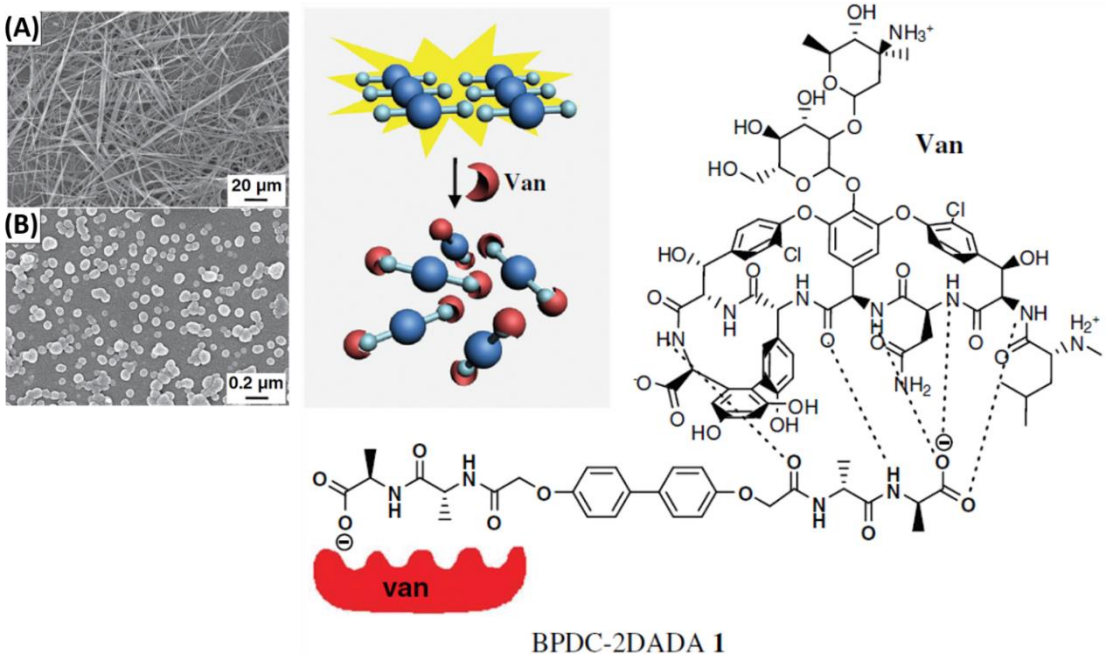

Figure 1. Schematic diagram showing the morphological change of BPDC-2DADA **1** in the absence and presence of Van. Representative SEM images are also included. The figure and images are adopted from reference 19.

Instead of using molecular probes, Liang *et al.* utilized cadmium telluride quantum dots (CdTe QD) as the sensing element and demonstrated that the fluorescence of the quantum dots was quenched in the presence of Van.[20] The quenching phenomenon was due to a disruption of the electron-hole recombination in CdTe QD in the presence of Van upon excitation at 350 nm (Figure 2). The fluorescence intensity was monitored at 542 nm which is away from the autofluorescence of biomolecules, hence avoiding the

potential interference issues of the previous method. They reported an extremely high sensitivity of their method toward Van with a LOD of 0.4605 ng/mL for the linear concentration range of 1.534 ng/mL-20 μg/mL. They even prepared a sample containing exactly 1.534 ng/mL of Van (*i.e.* the limit of quantification) to verify the accuracy of their method. The measured change in fluorescence intensity (*i.e.* 4.68 a.u.) was compared to the value derived from the calibration curve (*i.e.* ~5.05 a.u.) and an accuracy of ~93 % was determined. However, this result is dubious as the small change of 4.68 a.u. (which is *ca.* <0.1 % decrease from 5192 a.u. measured in the absence of Van) easily falls under experimental and/or instrumental error.[21] A visual examination of the fluorescence spectra recorded in the absence and presence of 1.534 ng/mL of Van also revealed 'superimposed' spectra at first glance, for which an enlarged view was included in order to illustrate the small magnitude decrease in fluorescence intensity. Another disadvantage of this method is a long equilibration time of 10 min for the fluorescence signal to stabilize. It is worth mentioning that no specific interaction between Van and CdTe QD was involved in the quenching mechanism (Figure 2), which therefore leads to questionable selectivity of their method toward other structurally similar compounds such as Van CDP-1.

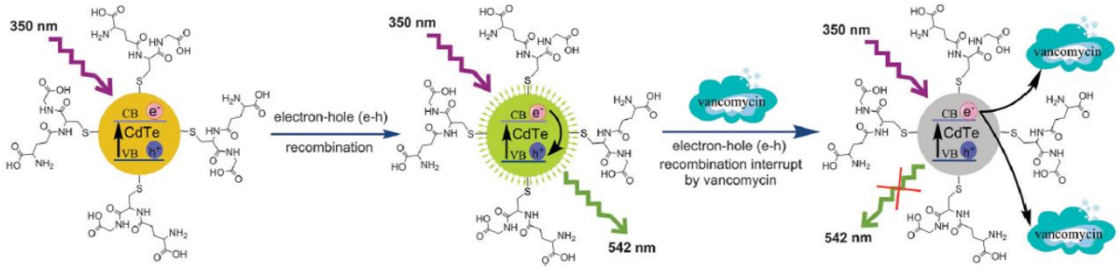

Figure 2. Schematic diagram showing the mechanism of fluorescence quenching of CdTe QD in the presence of Van. The figure is adopted from reference 20.

The last two detection methods are examples of fluorescence "turn-off" systems. There are advantages and disadvantages of such quenching systems. One disadvantage is the multiple pathways by which fluorescence decay can take place, which can complicate mechanistic studies. The opposite fluorescence "turn-on" systems, on the other hand, produce signals from specific binding events.[22] Thus, it would appear that the mechanistic investigations for such systems are more straightforward. Furthermore, fluorescence "turn-on" systems are thought to display higher sensitivity due to a larger signal-to-noise ratio attainable against a dark background.[22-23]

Herein, we proposed a novel fluorescence "turn-on" probe for Van based on a molecular triad consisting of a near-infrared squaraine dye (Seta-640)[24] conjugated to two anthraquinone molecules (AQ) via Lys-D-Ala-D-Ala peptides (Van-specific) (Figure 3). Squaraine dyes have previously been utilized to detect biomolecules (*e.g.* proteins, nucleic acids), where the association between the two moieties changes the polarity of the environment around the dye and induces a fluorescence enhancement behaviour. In the case of our triad, significant fluorescence quenching occurs in both buffer solution and deproteinized human serum due to a charge-transfer reaction between the squaraine dye and conjugated anthraquinone, with the latter being a good electron-acceptor. In the presence of Van, the drug binds to the two -D-Ala-D-Ala ligands which effectively reduces the emission quenching and restores fluorescence by as much as 30 times. The working mechanism of the triad probe is investigated using time-resolved spectroscopy which reveals that, apart from altering the microenvironment polarity, the bound Van impedes electron-transfer efficiency, possibly by imposing a steric effect.

2.2 Experimental

2.2.1 Materials

All chemicals were used as received unless otherwise stated. Vancomycin hydrochloride (Van·HCl), anthraquinone-2-carboxylic acid, (+)-*tert*-Butyl D-lactate, triisopropylsilane (TIPS), ammonium acetate, *N*-(3-dimethylaminopropyl)-*N'*-ethylcarbodiimide hydrochloride (EDC·HCl) and human serum from human male AB plasma (USA origin, sterile-filtered) were purchased from Sigma-Aldrich. Fmoc-D-Ala-Wang resin, 2-chlorotrityl chloride resin, Fmoc-D-Ala-OH, Fmoc-Lys(Ac)-OH, Boc-Lys(Fmoc)-OH and *O*-(benzotriazol-1-yl)-*N,N,N',N'*-tetramethyluronium hexafluoro-phosphate **(**HBTU) were purchased from GL Biochem (Shanghai) Co., Ltd. Piperidine, trifluoroacetic acid (TFA), *N*,*N*-diisopropylethylamine (DIPEA) and 4-dimethylaminopyridine (DMAP) were purchased from Alfa Aesar. Seta-640 di-NHS (product number K8-1662) was purchased from SETA BioMedicals. Van CDP-1 was purchased from Toronto Research Chemicals Inc. and purified by RP-HPLC before use. Phosphate buffered saline (PBS, 1X, pH 7.4) was purchased from Thermo Fisher Scientific. Reagent or HPLC grade solvents were used without further purification.

2.2.2 Synthesis

Semi-preparative and analytical HPLC were performed on a Shimadzu HPLC system with a Kromasil C-18 (250 × 10 mm) and C-18 (250 × 4.6 mm) reverse phase column using a mobile phase (50 mM ammonium acetate in water and acetonitrile, unless otherwise stated) with a flow rate of 3 mL min^{-1} and 1 mL min^{-1}, respectively. ESI mass spectra were obtained on Thermo LCQ Deca XP Max and Water Q-Tof Premier instruments. ^{1}H NMR spectra were recorded on a Bruker AV 400 spectrometer (400 MHz). The chemical shifts (δ) were reported in ppm relative to the residual solvent

peak and coupling constants (*J*) in Hz. The peptides and their derivatives were prepared using solid-phase synthesis based on fluorenylmethyloxycarbonyl (Fmoc) chemistry.

H_2N-Lys(AQ)-D-Ala-D-Ala-OH. 2-chlorotrityl chloride resin (500 mg, 0.5 mmol) was activated in dichloromethane (DCM) in a peptide synthesizer with N_2 flow for 10 min. Fmoc-D-Ala-OH (1.5 equiv.) dissolved in a mixture of DIPEA (4 equiv.) and DCM (4 mL) was loaded onto the swelled resin and agitated for 1.5 h. The resin was then washed with DCM and the capping of unreacted resin was performed with a solution of DIPEA (4 equiv.), methanol and DCM (1:1 v/v) for 15 min. Subsequently, the resin was washed with DCM followed by *N*,*N*-dimethylformamide (DMF) and a solution of 20% piperidine in DMF (v/v) was added to remove Fmoc for 20 min. The resin was then washed several times with DMF and subjected to the following series of coupling-deprotection-washing cycles: (i) coupling with the second Fmoc-D-Ala-OH (2 equiv.) followed by Boc-Lys(Fmoc)-OH (2 equiv.) and anthraquinone-2-carboxylic acid (2 equiv.) in the presence of HBTU (2 equiv.), DIPEA (4 equiv.) and DMF (4 mL) for 2 - 3 h, (ii) Fmoc deprotection with 20% piperidine in DMF (v/v) for 20 min, and (iii) repeated washing with DMF. The resin was then washed with DCM, and a mixture of TFA, TIPS and DCM (30:2:68 v/v/v) was added to cleave the peptide from the resin and to deprotect Boc. The cleaved products were collected after 1.5 h of reaction and the solvents were removed under vacuum. Cold diethyl ether (DE) was added to precipitate the peptide, which was then purified using RP-HPLC (30 to 60% acetonitrile over 20 min). The collected fractions were lyophilized to give the peptide as a light yellow solid. ESI $[M + H]^+$ m/z calcd. for $[C_{27}H_{31}N_4O_7]$ 523.22, found 523.29. ^{1}H NMR (400 MHz, D_2O) δ = 7.72 (s, 1H, Ar-H), 7.68-7.54 (m, 6H, 6 × Ar-H), 4.28-4.23 (q, *J* = 7.1 Hz, 1H, CH), 4.06-4.01 (q, *J* = 7.1 Hz, 1H, CH), 3.37-3.34 (t, *J* = 6.8 Hz, 1H, CH), 3.25-3.22

(m, 2H, CH_2), 1.64-1.51 (m, 4H, 2 × CH_2), 1.41-1.31 (m, 2H, CH_2), 1.30-1.28 (d, *J* = 7.2 Hz, 3H, CH_3), 1.25-1.23 (d, *J* = 7.2 Hz, 3H, CH_3).

H_2N-Lys(Ac)-D-Ala-D-Ala-OH. This compound was prepared on Fmoc-D-Ala-Wang resin in a similar way as described above. After Fmoc removal, Fmoc-D-Ala-OH (1.5 equiv.) and Fmoc-Lys(Ac)-OH (1.5 equiv.) were loaded onto the resin in sequence. The peptide was cleaved from the resin using a solution of 95% TFA in DCM (v/v) and purified using RP-HPLC (5 to 45% acetonitrile over 20 min). The collected fractions were lyophilized to give the peptide as a white solid. ESI $[M + H]^+$ m/z calcd. for $[C_{14}H_{27}N_4O_5]$ 331.20, found 331.17. ^{1}H NMR (400 MHz, D_2O) δ = 4.40-4.35 (q, *J* = 7.3 Hz, 1H, CH), 4.18-4.12 (q, *J* = 7.2 Hz, 1H, CH), 4.02-3.99 (t, *J* = 6.6 Hz, 1H, CH), 3.21-3.17 (t, *J* = 6.8 Hz, 2H, CH_2), 1.99 (s, 3H, CH_3), 1.93-1.87 (m, 2H, CH_2), 1.60-1.53 (quint, *J* = 7.2 Hz, 2H, CH_2), 1.44-1.35 (m, 8H, 2 × CH_3, CH_2).

H_2N-Lys(AQ)-D-Ala-D-Lac-OH. This compound was prepared using both liquid- and solid-phase synthesis:

Fmoc-D-Ala-D-Lac-OtBu. (+)-*tert*-Butyl D-lactate (100 mg, 0.687 mmol) and Fmoc-D-Ala-OH (257 mg, 0.825 mmol) were dissolved with stirring in dry DCM (5 mL) at 0 °C. DMAP (9.00 mg, 0.0737 mmol) and EDC·HCl (159 mg, 0.829 mmol) were added in sequence, and the mixture was stirred for 20 min at 0 °C and another 18 h at room temperature. The reaction mixture was extracted with ethyl acetate and brine, and dried over anhydrous sodium sulphate. The organic layer was concentrated under vacuum and purified using silica gel chromatography (0 to 20% ethyl acetate in hexane). The product was obtained as a colorless oil. ESI $[M + H]^+$ m/z calcd. for $[C_{25}H_{30}NO_6]$ 440.21, found 462.11 $[M + Na]^+$. ^{1}H NMR (400 MHz, DMSO) δ = 7.90-7.88 (d, *J* = 7.2 Hz, 2H, 2 × Ar-H), 7.84-7.82 (d, *J* = 7.6 Hz, 1H, NH), 7.73-7.70 (t, *J* = 6 Hz, 2H, 2 × Ar-H), 7.44-7.40 (t, *J* = 7.4 Hz, 2H, 2 x Ar-H), 7.35-7.31 (t, *J* = 7.6 Hz, 2H, 2 × Ar-H),

4.88-4.83 (q, *J* = 7.1 Hz, 1H, CH), 4.30-4.28 (m, 2H, CH_2), 4.24-4.20 (t, *J* = 6.8 Hz, 1H, CH), 4.18-4.11 (quint, *J* = 7.4 Hz, 1H, CH), 1.39-1.37 (m, 12H, 4 × CH_3), 1.35-1.33 (d, *J* = 7.2 Hz, 3H, CH_3).

Solid-phase synthesis. The procedure is similar to the one described for H_2N-Lys(AQ)-D-Ala-D-Ala-OH. Before loading onto the resin, Fmoc-D-Ala-D-Lac-OtBu was deprotected to give Fmoc-D-Ala-D-Lac-OH using a mixture of TFA, TIPS and DCM (9:1:0.1 v/v/v) for 1 h at room temperature. Fmoc-D-Ala-D-Lac-OH was loaded onto the resin followed by Boc-Lys(Fmoc)-OH. The final product was obtained as a light yellow solid. ESI $[M + H]^+$ m/z calcd. for $[C_{27}H_{30}N_3O_8]$ 524.20, found 524.29. The ^1H NMR spectra were obtained in DMSO and D_2O to reveal all peaks. ^1H NMR (400 MHz, DMSO) δ = 8.99-8.97 (t, *J* = 5.4 Hz, 1H, NH), 8.69-8.67 (d, *J* = 7.2 Hz, 1H, NH), 8.65-8.64 (d, *J* = 1.6 Hz, 1H, Ar-H), 8.35-8.22 (m, 4H, 4 x Ar-H), 7.97-7.95 (m, 2H, 2 x Ar-H), 4.78-4.73 (q, *J* = 6.9 Hz, 1H, CH), 4.28-4.21 (quint, *J* = 7.2 Hz, 1H, CH), *3.56-3.52 (t, J = 6.6 Hz), 3.32-3.30 (m),* 1.72-1.53 (m, 4H, 2 × CH_2), 1.41-1.29 (m, 8H, 2 × CH_3, CH_2). ^1H NMR (400 MHz, D_2O) δ = 7.66-7.57 (m, 7H, 7 × Ar-H), 4.51-4.46 (q, *J* = 7.1 Hz, 1H, CH), 4.10-4.07 (t, *J* = 6.8 Hz, 1H, CH), 3.32 (m, 2H, CH_2), 2.01-1.96 (m, 2H, CH_2), 1.68-1.63 (m, 2H, CH_2), 1.47-1.43 (m, 8H, 2 × CH_3, CH_2).

In the NMR spectrum derived using DMSO, a broad water peak overlapped with the two signals in italics, resulting in inaccurate integration. Therefore, another NMR spectrum was obtained in D_2O to reveal the number of protons corresponding to the two peaks. Note that in this case, the most downfield CH signal (δ = 4.78-4.73 in DMSO) was masked by the water residual peak.

*Triad **1** and dyad **4**.* H_2N-Lys(AQ)-D-Ala-D-Ala-OH (10 equiv.) was first dissolved with sonication in a mixture of 100 mM sodium bicarbonate and DMSO (10:1 v/v). Seta-640 di-NHS dissolved in 40 μL of anhydrous DMSO was transferred

dropwise into the solution under vigorous stirring. After 3 h, the reaction was stopped and **1** and **4** were isolated from the crude reaction mixture using RP-HPLC (5 to 50% acetonitrile over 35 min). The collected fractions were lyophilized to give **1** and **4** as blue solids. **1**: HRMS (ESI) $[M]^+$ m/z calcd. for $[C_{98}H_{112}N_{10}O_{30}S_4]$ 2036.6429, found 2036.6395. **4**: HRMS (ESI) $[M]^+$ m/z calcd. for $[C_{71}H_{84}N_6O_{24}S_4]$ 1532.4420, found 1532.4391.

*Triad **2***. H_2N-Lys(AQ)-D-Ala-D-Lac-OH and DMAP were first dissolved in anhydrous DMSO. Seta-640 di-NHS dissolved in anhydrous DMSO was transferred dropwise into the solution under vigorous stirring. After 4 h, the reaction was stopped and **2** was isolated from the crude reaction mixture using RP-HPLC (5 to 50% acetonitrile over 35 min). The collected fractions were lyophilized to give **2** as a blue solid. HRMS (ESI) $[M + H]^+$ m/z calcd. for $[C_{98}H_{111}N_8O_{32}S_4]$ 2039.6187, found 2039.6190.

*Reference compounds **5** and **6***. **5** and **6** were synthesized from H_2N-Lys(Ac)-D-Ala-D-Ala-OH using the same procedure as described for triad **1**. The products were purified using RP-HPLC with an elution profile of 5 to 35% acetonitrile over 35 min. Both compounds were obtained as blue solids. **5**: HRMS (ESI) $[M + H]^+$ m/z calcd. for $[C_{72}H_{105}N_{10}O_{26}S_4]$ 1653.6084, found 1653.6173. **6**: HRMS (ESI) $[M]^+$ m/z calcd. for $[C_{58}H_{80}N_6O_{22}S_4]$ 1340.4209, found 1340.4204.

*Triad **3***. H_2N-Lys(AQ)-D-Ala-D-Ala-OH (6 equiv.) was dissolved with sonication in a mixture of 100 mM sodium bicarbonate and DMSO (10:1 v/v), and added to Cy5-bis-NHS ester in a vial under vigorous stirring. After 1 h, the reaction was stopped and **3** was isolated from the crude reaction mixture using RP-HPLC (20 to 50% acetonitrile with 0.1% TFA in water with 0.1% TFA over 45 min). The collected fractions were lyophilized to give **3** as a blue solid. HRMS (ESI) $[M]^+$ m/z calcd. for

[$C_{91}H_{103}N_{10}O_{22}S_2$] 1751.6690, found 1751.6666. ^{1}H NMR (400 MHz, D_2O) δ = 8.04-8.03 (d, *J* = 1.6 Hz, 1H, Ar-H), 7.87-7.75 (m, 5H, 5 × Ar-H), 7.70-7.67 (m, 2H, 2 × Ar-H), 7.59-7.52 (t, *J* = 13.2 Hz, 2H, 2 × Ar-H), 7.22-7.19 (d, *J* = 8.4 Hz, 1H, CH), 5.87-5.81 (t, *J* = 12.2 Hz, 2H, 2 × CH), 5.73-5.70 (d, *J* = 13.2 Hz, 2H, 2 × CH), 4.44-4.38 (q, *J* = 7.2 Hz, 1H, CH), 4.35-4.32 (dd, *J* = 10, 4 Hz, 1H, CH), 4.18-4.12 (q, *J* = 7.2 Hz, 1H, CH), 3.77-3.75 (m, 2H, CH_2), 3.41-3.38 (t, *J* = 6.2 Hz, 2H, CH_2), 2.40-2.39 (m, 2H, CH_2), 1.92-1.27 (m, 24H, 6 x CH_2, 4 x CH_3). The ^{1}H NMR spectrum is given in Annex at the end of the chapter (Figure A1).

The purity of compounds **1**-**6** was confirmed by HPLC which shows a single sharp peak for each compound (Figure 4A).

Seta-640 di-carboxylic acid. Seta-640 di-carboxylic acid was prepared by hydrolyzing the commercially purchased Seta-640 di-NHS in PBS for at least 1 h at room temperature.

Van CDP-1. The commercial product was found to contain a mixture of Van CDP-1 (minor and major product, abbreviated as Van CDP-1m and Van CDP-1M, respectively) and Van. Therefore, the chemical was purified before use. Van CDP-1 was dissolved by sonication in DMSO and purified using RP-HPLC (5 to 40% acetonitrile over 30 min). Van CDP-1m and Van CDP-1M were collected together and lyophilized to give pure Van CDP-1 as a light yellow solid. ESI $[M + H]^+$ m/z calcd. for [$C_{66}H_{75}Cl_2N_8O_{25}$] 1449.42, found 1449.10, 725.31 $[M + 2H]^{2+}$ (Van CDP-1m) and 1449.12, 725.30 $[M + 2H]^{2+}$ (Van CDP-1M).

2.2.3 Calibration curve in PBS

To obtain the calibration curve of triad **1** in PBS, appropriate amounts of the Van stock solutions were added to the triad to achieve the desired final Van concentrations.

The sample was left to stand for three min before its absorbance and fluorescence were measured. The quantum yield (Φ) of triad **1** at each Van concentration was calculated using the following equation:

$$\Phi_{Van} = \Phi_{std} \left(\frac{1-10^{-A_{std}}}{1-10^{-A_{Van}}} \right) \left(\frac{\alpha_{Van}}{\alpha_{std}} \right)$$

where Φ_{Van} and Φ_{std} are the quantum yields of Van sample and standard sample, respectively, A_{Van} and A_{std} are the absorbance of Van sample and standard sample at the excitation wavelength (*i.e.*, 590 nm), respectively, and α_{van} and α_{std} refer to the area under the fluorescence spectra for Van sample and standard sample, respectively. Seta-640 di-carboxylic acid was used as the standard (Φ = 0.13, value provided by the manufacturer). A similar procedure was used to obtain the calibration curve for reference compound **5**.

2.2.4 Calibration curve in human serum

Pre-treatment of human serum (HS). For tests in HS, the serum was first deproteinized using a modified procedure.[25-26] Methanol followed by acetonitrile were added to the thawed serum (1.25:1.25:1 v/v/v) and the mixture was vortexed for 10 min. The suspension was centrifuged (A23-6x100 rotor, SORVALL LYNX 6000 centrifuge, Thermo Scientific) at 12000 rpm for 10 min at 4 ^{o}C, and the supernatant was decanted and lyophilized. The dried powder was reconstituted in water, with a volume equal to the original volume of serum used. Any undissolved material was removed by ultracentrifugation (F23-48x1.5 rotor, SORVALL LYNX 6000 centrifuge, Thermo Scientific) at 23000 rpm for 10 min at 4 ^{o}C. The clear supernatant was left to stand in the dark for 2 h at room temperature before it is used in the serum tests.

*Calibration curve of triad **1** in HS.* The procedure to obtain the calibration curve in HS is the same as described for PBS, except that the equilibration time was five min. The limit of detection (LOD) of triad **1** in both PBS and HS was determined from the equation LOD = $3\sigma/b$, where σ is the standard deviation obtained from the fluorescence measurements of the triad in the absence of Van in PBS or HS and b is the slope derived after linearly fitting the calibration curves within certain ranges.

Preparation of Van-spiked HS samples for recovery tests. The HS samples containing 3 μM or 9 μM of Van were separately prepared by spiking 5 mL of the untreated serum with an appropriate amount of the Van stock solution. The spiked samples were vortexed for one min and deproteinized in a similar way as described above, except that there is an additional washing step before the supernatant is lyophilized. This washing step was added to improve the recovery of Van by re-suspending the protein precipitates in a mixture of methanol, acetonitrile and water (1.25:1.25:1 v/v/v), and centrifuging the suspension at 12000 rpm for 10 min at 4 ^{o}C. The supernatant was decanted and added to the first batch of liquid. This was repeated for three times and the collected fractions of liquid were lyophilized. The % recovery is given by: $B/A \times 100\%$, where A is the added [Van] (*i.e.* 3 μM or 9 μM) and B is the concentration of Van determined from the calibration curve.

2.2.5 Electrochemistry

Cyclic voltammograms were recorded at a scan rate of 100 mV s^{-1} using a computer-controlled Eco Chemie Autolab PGSTAT 100 with an ADC fast scan generator. A three-electrode system in a single-compartment voltammetric cell was used. The working electrode, reference electrode and counter electrode are glassy carbon, Ag/AgCl (in 3 M KCl) and platinum, respectively. The solvent and supporting

electrolyte is PBS. Prior to each measurement, the solution was purged with N_2 for five min at room temperature.

2.2.6 Steady-state absorption and fluorescence spectroscopy

Steady-state absorption and fluorescence spectra were recorded on a UV/Vis spectrometer (Cary 100, Varian) and fluorescence spectrometer (Cary Eclipse, Varian), respectively. The dye concentrations used were ~ 1.4 μM. For fluorescence measurements, the samples were excited at 590 nm.

2.2.7 Time-resolved measurements

Time-resolved fluorescence spectroscopy measurements were carried out on a TCSPC spectrofluorimeter (FluoroCube, Horiba Jobin Yvon) with an excitation wavelength of 638 nm generated using a pulsed diode laser (NanoLED-635L, Horiba Jobin Yvon). The fluorescence lifetime decay profiles were collected at 650 nm and fitted using the Horiba Jobin Yvon Datastation software. The goodness of fit was evaluated from the reduced chi-square (χ^2) value and the randomness of the weighted residuals.

For the fs-TA spectroscopy measurements, samples were dissolved in PBS to provide solutions with an OD of ~ 0.2 at ~ 640 nm in a 1 mm cell. A commercial Ti:sapphire regenerative amplifier laser (Coherent Legend) operating at 1 kHz produced pulses of ~ 120 fs duration which were centered at 800 nm. This beam was split into two portions. The major portion was directed into a non-collinear optical parametric amplifier (TOPAS White, Light Conversion) to generate a pump pulse centered at 640 nm. The pump beam was attenuated to 10 nJ $pulse^{-1}$ and compressed using an acousto-optic programmable dispersive filter pulse shaper (DAZZLER, Fastlite) to achieve ~ 45

fs pulses (< 1.3 times transform limited pulse). The minor portion of the 800 nm light was focused onto a 2 mm sapphire window to generate a white light continuum which was used as a probe beam. This beam was then chopped using a mechanical chopper to remove scattered light from the pump and subsequently passed through a motorized translation stage with the femtosecond time step precision to introduce a delay between the pump and probe pulses. The polarization of the probe beam was set, using a half-wave plate and a polarizer, to 54.7° (magic angle) relative to the pump beam. Both pump and probe pulses were then focused using a spherical mirror onto the sample. The probe beam was then collimated and measured using a spectrometer (HORIBA Jobin Yvon, TRIAX 190) with a CCD detector (Princeton Instruments, Pixis 100). The transient absorption spectra was measured by measuring the probe spectra with and without the pump pulse by means of a mechanical chopper.

All measurements were performed at room temperature and repeated two to three times to ensure reproducible results.

2.3 Results and discussion

2.3.1 Squaraine-anthraquinone triad *vs.* Cy5-anthraquinone triad

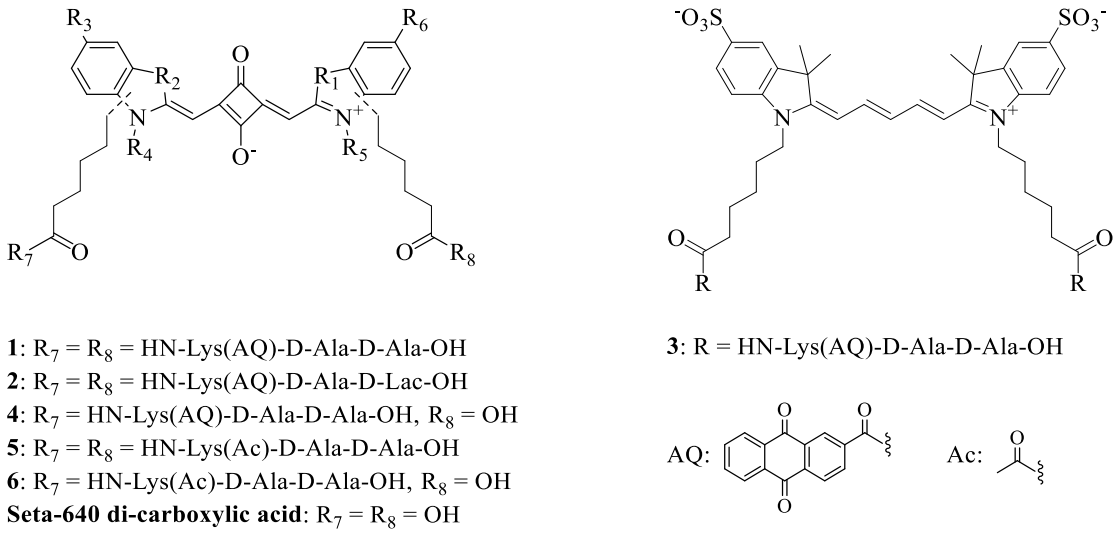

Figure 3. Chemical structures of all compounds used in this work. As the exact structure of the Seta-640 dye is not known, a general structure of the SETA series dyes reported by Patsenker *et al.*[24] from SETA BioMedicals is shown.

The compounds used in this work were prepared according to procedures described under experimental section and their purity were confirmed by reversed phase-high performance liquid chromatography (RP-HPLC; Figure 4A). The triad **1**, presented in this work, consists of a squaraine dye (Seta-640)[24] covalently attached to two Lys(AQ)-D-Ala-D-Ala peptides (the bracket refers to conjugation of the functional group, *i.e.* anthraquinone (AQ), at the side chain of Lys) (Figure 3). As will be discussed in the sections below, the quenched emission of triad **1** displays significant fluorescence recovery upon binding with Van in aqueous solutions (~ 30-times) and serum samples (~ 21-times). Furthermore, the fluorescence quantum yield (Φ) of triad **1** in the presence

of Van (32 μM) remains relatively constant over a period of 12 h, making it a highly stable probe (Figure 4B).

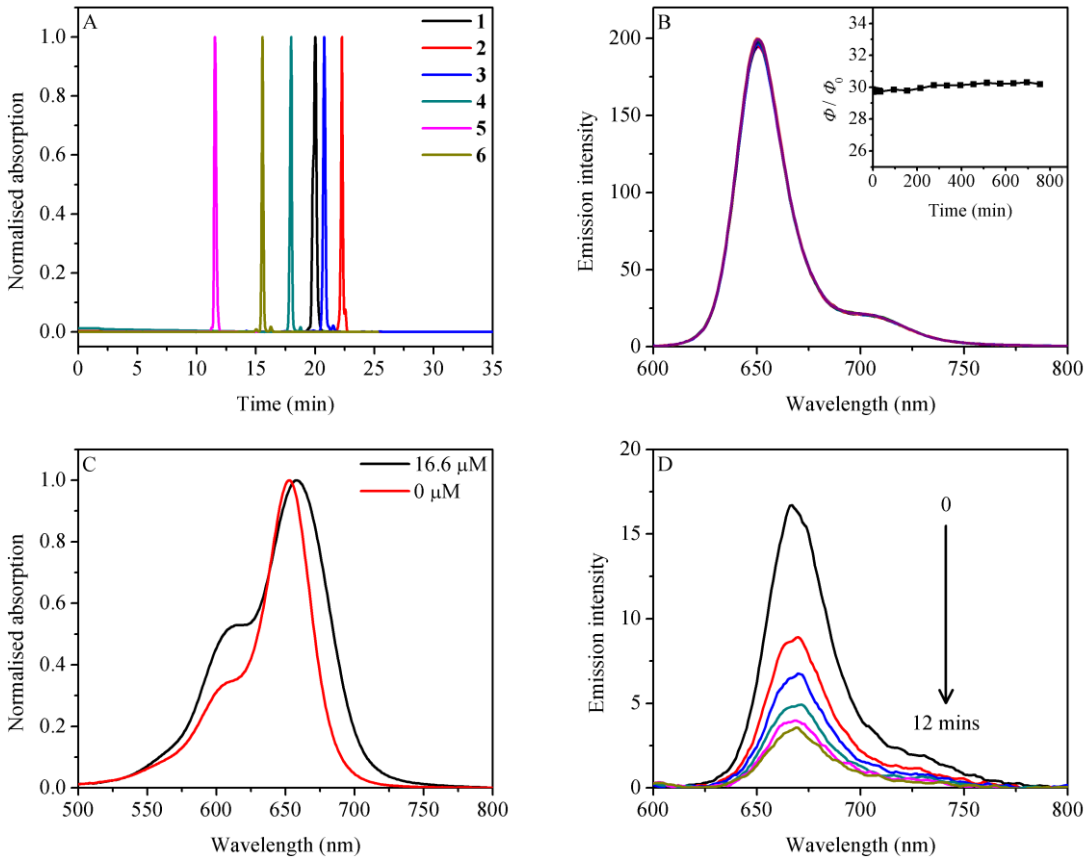

Figure 4. (A) Normalized HPLC chromatograms of compounds **1**-**6** obtained by UV detection at a wavelength of 650 nm. (B) Fluorescence spectra of triad **1** (~ 1.4 μM) in the presence of 32 μM of Van in PBS over a period of ~ 12 h. Spectra were recorded at time intervals of 1 min/scan for the first 10 mins, 5 mins/scan for the next 25 mins, and 1 h/scan for another 12 h. Inset shows the corresponding plot of Φ/Φ_0 *vs.* time, where Φ_0 is the quantum yield of triad **1** in the absence of Van at time 0. (C) Normalized absorption spectra of triad **3** in the absence and presence of 16.6 μM of Van in PBS. (D) Fluorescence spectra of triad **3** decreases in intensity with time in the presence of 16.6 μM of Van in PBS.

However, when the Seta-640 dye in triad **1** is replaced with a cyanine Cy5 dye (triad **3** in Figure 3), a weak fluorescence recovery takes place in the presence of Van in phosphate buffered saline (PBS) (*e.g.*, 3.6-times when the concentration of Van, [Van] = 16.6 μM). When bound to Van, the absorption spectrum of triad **3** is broadened and its fluorescence intensity decreases with standing time (Figures 4C and 4D, respectively). Furthermore, this is accompanied by the precipitation of blue solid, which indicates the formation of insoluble aggregates of the triad **3**-Van complex. The exact reason for this observation is not clear at the moment, however, it can be concluded that triad **3** is unstable and does not perform satisfactorily as a Van probe. Therefore, unlike triad **1**, triad **3** is not a suitable probe for Van, and the choice of the dye is important to ensure stability of the probe as well as efficient fluorescence quenching and recovery in the absence and presence of the analyte, respectively.

2.3.2 Electron transfer in triad 1

The absorption and fluorescence spectra of triad **1** and reference compound **5** (*i.e.*, Seta-640 dye conjugated to two Lys(Ac)-D-Ala-D-Ala peptides, where the anthraquinone group is replaced by an acetate (Ac) group; Figure 3) in PBS are shown in Figure 5A. Triad **1** absorbs and emits with peak maxima at λ_{abs} = 641 nm and λ_{em} = 646 nm, respectively; both values are close to the reference compound **5** (λ_{abs} = 638 nm and λ_{em} = 648 nm). The lack of a significant band shift or distortion of band shape indicates the absence of strong electronic couplings between the ground-states of the Seta-640 molecule and anthraquinone in triad **1**.

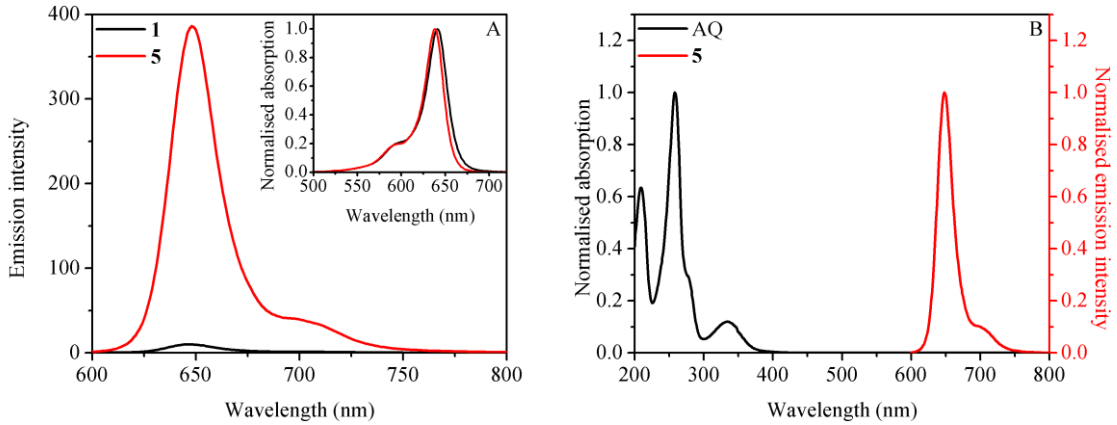

Figure 5. (A) Fluorescence spectra of triad **1** and reference compound **5** in PBS. Excitation wavelength λ_{ex} = 590 nm and concentrations of **1** and **5** are ~ 1.4 μM. Inset shows the normalized absorption spectra of **1** and **5**. (B) Normalized absorption and fluorescence spectra of anthraquinone-2-carboxylic acid (AQ) and reference compound **5**, respectively, in PBS.

Figure 5A shows that the fluorescence of triad **1** in PBS is significantly quenched when compared to reference compound **5**. In particular, the fluorescence quantum yields of triad **1** and reference compound **5** are 0.006 and 0.19, respectively. Clearly, the presence of the anthraquinone molecules in triad **1** causes the fluorescence quantum yield of the squaraine dye to be reduced by *ca*. 32-times. This is plausibly due to either an energy or charge-transfer process. Since there is no spectral overlap between the absorption spectrum of anthraquinone-2-carboxylic acid and emission spectrum of reference compound **5** (Figure 5B), resonance energy transfer is not likely to be responsible for the observed fluorescence quenching in triad **1**.

To assess the feasibility of charge-transfer, the Gibbs free energy for electron-transfer from Seta-640 di-carboxylic acid to anthraquinone-2-carboxylic acid, ΔG_{et}, is calculated using the Rehm-Weller equation: $\Delta G_{et} = E_{ox}(D) - E_{red}(A) - E_{oo}$, where $E_{ox}(D)$ is the oxidation potential of the electron donor *D*, $E_{red}(A)$ is the reduction potential of

the electron acceptor *A* and E_{oo} is the excited-state energy of *D*. From cyclic voltammetry experiments, the first oxidation potential of Seta-640 di-carboxylic acid and reduction potential of anthraquinone-2-carboxylic acid in PBS were determined to be $E_{ox}(D)$ = 0.537 eV and $E_{red}(A)$ = -0.452 eV, respectively (Figure 6). A value of ΔG_{et} = -0.941 eV is obtained for E_{oo} = 1.93 eV. Therefore, electron-transfer from an excited Seta-640 dye to anthraquinone is an energetically favourable process.

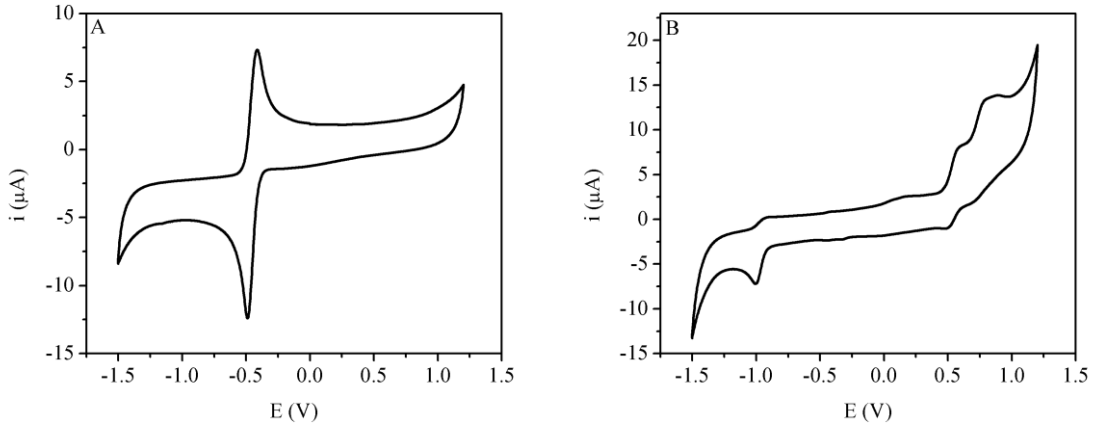

Figure 6. Cyclic voltammograms of (A) anthraquinone-2-carboxylic acid and (B) Seta-640 di-carboxylic acid in PBS. The first oxidation potential of Seta-640 di-carboxylic acid and the reduction potential of anthraquinone-2-carboxylic acid are 0.537 eV and -0.452 eV, respectively.

The fluorescence lifetime decay profiles of triad **1** and reference compound **5** in PBS, recorded using a time-correlated single photon counting (TCSPC) instrument, are given in Figure 7A. The bi-exponential lifetime decay of reference compound **5** yields lifetime components τ_1 = 1290 ± 4 ps (contribution to the decay α_1 = 67 %) and τ_2 = 548 ± 9 ps (α_2 = 33 %). On the other hand, the emission lifetime profile of triad **1** decays significantly faster and is described using a tri-exponential decay function with τ_1 = 1081 ± 6 ps (α_1 = 34 %), τ_2 = 425 ± 8 ps (α_2 = 50 %) and a short component τ_3 = 100

± 10 ps (α_3 = 16 %). The latter is shorter than the resolution of the TCSPC instrument; suggesting that ultrafast quenching processes are present that are not detected by the TCSPC measurements. Nonetheless, the time-resolved emission lifetime experiments clearly show that the fluorescence lifetime of the Seta-640 dye in the triad is quenched by the conjugated anthraquinones.

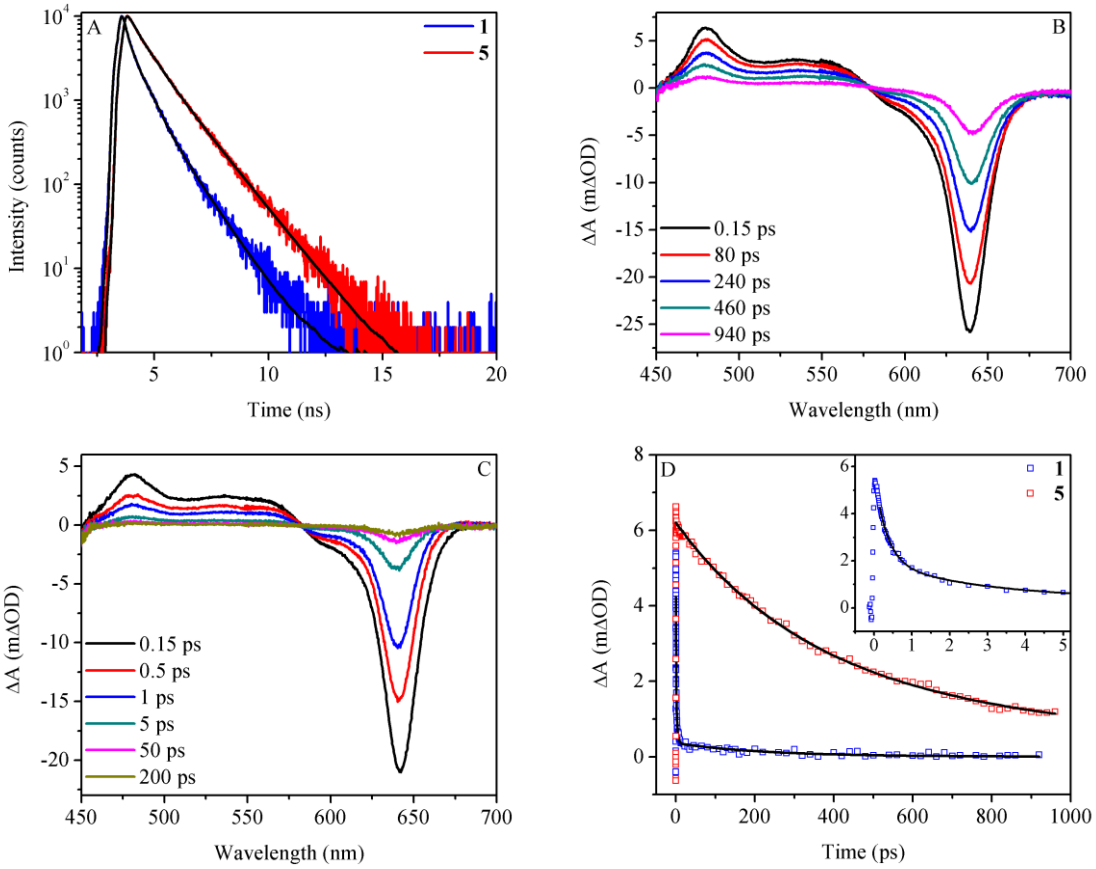

Figure 7. (A) Fluorescence lifetime decay profiles of triad **1** and reference compound **5** in PBS (λ_{ex} = 638 nm and monitoring emission at λ_{em} = 650 nm). Transient absorption spectra at different probe delay times of (B) reference compound **5** and (C) triad **1** in PBS (pump wavelength λ_{ex} = 640 nm), and (D) kinetic profiles extracted at 481 nm for **1** and **5**. Inset shows the kinetic profile of **1** for the first 5.2 ps.

Femtosecond-transient absorption (fs-TA) measurements were conducted to examine the ultrafast quenching processes. Both reference compound **5** and triad **1** in PBS were pumped with a 640 nm laser pulse excitation and their fs-TA spectra recorded at various delay times are shown in Figures 7B and 7C, respectively. The -Δ*A* band between 580 - 700 nm is attributed to ground-state bleaching and stimulated emission. Since the absorption range of the monocations of typical squaraine dyes has previously been reported to overlap with that of the neutral species,[27-29] the -Δ*A* band of triad **1** in Figure 7C may also contain contribution from the absorption of the monocation of the Seta-640 dye after electron-transfer to anthraquinone.

The S_1 excited-state absorption (ESA) of reference compound **5** and triad **1** occurs at wavelengths < 580 nm (*i.e.*, +Δ*A* bands). The kinetic trace of reference compound **5**, probed at 481 nm, is described using a bi-exponential decay function with the long lifetime component fixed at τ_1 = 1290 ps (α_1 = 31 %) (from TCSPC) and a short lifetime component τ_2 = 330 ± 10 ps (α_2 = 69 %) (Figure 7D). Given that the maximum time-window of the fs-TA experiments is ~ 1 ns, the extracted τ_2 component is comparable to that of the TCSPC result (*i.e.*, 548 ps). τ_1 and τ_2 are therefore the lifetimes of the excited S_1 state.[30]

Compared to reference compound **5**, the kinetic trace of triad **1** at 481 nm decays at a significantly faster rate due to electron transfer from the excited S_1 state of the Seta-640 dye to an anthraquinone (Figure 7D). The tri-exponential decay fit to the kinetic trace yields lifetime components τ_1 = 230 ± 30 ps (α_1 = 6 %), τ_2 = 2.9 ± 0.3 ps (α_2 = 29 %) and τ_3 = 0.32 ± 0.01 ps (α_3 = 65 %). Since the extinction coefficient of the absorption peak maximum of anthraquinone radical anion (AQ^-) at 556 nm is low (*i.e.*, 11.2×10^{-3} M^{-1} cm^{-1}),[31] its contribution to the kinetic decay in Figure 7C is assumed to be small.

Results from both the TCSPC and fs-TA measurements indicate the existence of a wide range of electron-transfer rates in triad **1**. This is because the electron donor and acceptor, in a fluid aqueous environment, are able to adopt several spatial conformations with respect to each other due to the flexible linker. The Marcus rate transfer for non-adiabatic charge-transfer is expressed as:[32]

$$k_{ET} = \eta^{-1}|V|^2 \left(\frac{\pi}{\lambda k_B T}\right)^{0.5} \exp[-(\Delta G^o + \lambda)^2/4\lambda k_B T]$$

where V is the electronic coupling between donor and acceptor separated by a distance r, ΔG^o is the free energy change for charge-transfer and λ is the total reorganization energy. When the Seta-640 dye is within close proximity to anthraquinone (*i.e.*, short r), the electron-transfer reaction is highly efficient which results in the ultrafast quenching processes. Since V decreases exponentially with increasing r, at longer donor-acceptor spatial separations (*i.e.*, long r), the electron-transfer rate becomes significantly slower. It is interesting to note that for triad **1**, the ~ 1 ns lifetime component observed in the TCSPC measurement due to structures with long donor-acceptor distances are not present in the fs-TA kinetic trace. This is possibly due to a small population of triad **1** with such conformations; in agreement with the low fluorescence quantum yield observed.

2.3.3 Vancomycin inhibits electron transfer in triad 1

Upon the addition of Van to reference compound **5** in PBS, the absorption spectrum is slightly red-shifted as illustrated in Figure 8A (*e.g.*, when [Van] = 32 μM, λ_{abs} is red-shifted by 3 nm). The fluorescence of reference compound **5** is enhanced in the presence of increasing concentrations of Van (Figure 8B). In particular, the emission quantum yield is increased from Φ_0 = 0.19 in the absence of Van to Φ = 0.35 when [Van] = 32 μM (*i.e.*, 1.8-times increase) (see the plot of Φ/Φ_0 *vs.* [Van] in the inset of

Figure 8B, where Φ are the quantum yields in the presence of different Van concentrations).

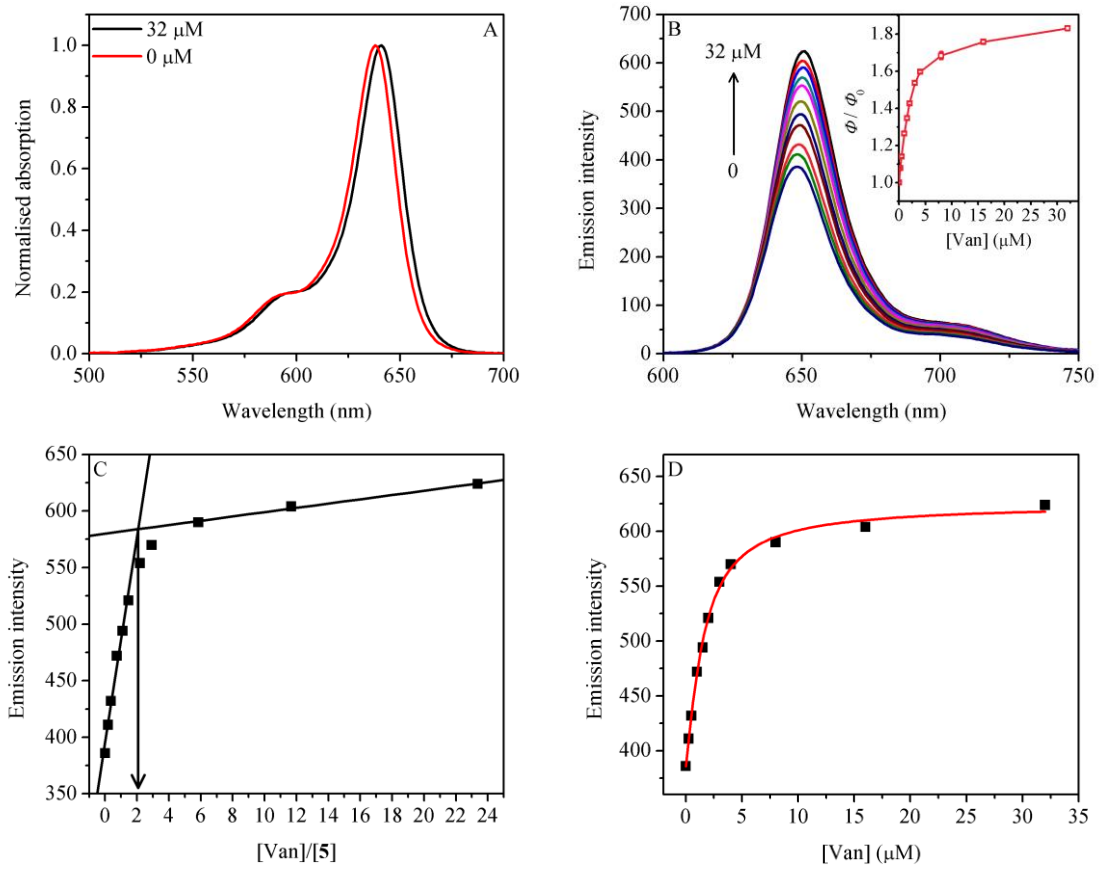

Figure 8. (A) Normalized absorption spectra of reference compound **5** in the absence and presence of 32 μM of Van in PBS. (B) Fluorescence spectra of reference compound **5** (~1.4 μM) in the presence of different concentrations of Van in PBS ([Van] = 0, 0.25, 0.5, 1, 1.5, 2, 3, 4, 8, 16, 32 μM). Inset shows the plot of Φ/Φ_0 *vs.* [Van]. (C) Plot of emission intensity *vs.* [Van]/[**5**] ratio. (D) Plot of emission intensity *vs.* [Van] for reference compound **5** in PBS. The red curve shows the fit of experimental data according to equation (1).

The binding stoichiometry between reference compound **5** and Van was determined using the mole ratio method to be 1:2 (Figure 8C). Assuming that the

formation of the 1:2 complex follows a stepwise equilibrium reaction between **5** and Van:

$$\mathbf{5} + \text{Van} \rightleftharpoons \mathbf{5}\text{:Van} \quad (\text{Step 1}, K_{11})$$

$$\mathbf{5}\text{:Van} + \text{Van} \rightleftharpoons \mathbf{5}\text{:(Van)}_2 \quad (\text{Step 2}, K_{12})$$

where K_{11} is the association constant for the formation of the 1:1 complex (Step 1) and K_{12} is the stepwise association constant of **5**:(Van)$_2$ (Step 2). In this case, the titration curve is described using the following nonlinear expression (Figure 8D):[33-35]

$$F = \frac{F_0 + F_{11}K_{11}[H] + F_{12}K_{11}K_{12}[H]^2}{1 + K_{11}[H] + K_{11}K_{12}[H]^2} \qquad (1)$$

where F, F_0, F_{11} and F_{12} refer to the fluorescence intensity of **5** at various concentrations of Van, when [Van] = 0, when **5** exists as 1:1 complex with Van and when **5** exists as 1:2 complex with Van, respectively, and [H] is the initial concentration of Van. From the fit, K_{11} and K_{12} were determined to be 0.75 μM^{-1} and 0.51 μM^{-1}, respectively. The value of K_{11} is in good agreement with the association constant reported previously for the binding between Van and -D-Ala-D-Ala ligand in phosphate buffer (*i.e.*, 0.77 μM^{-1}).[36] It is noted that the binding of the first Van does not significantly impede the binding of the second Van. The α (= $4K_{12}/K_{11}$) parameter which describes the extent of cooperative binding was calculated to be 2.7 (> 1); suggesting the presence of positive cooperativity in the system, and the favourable formation of the 1:2 complex (**5**:(Van)$_2$) over the formation of the 1:1 complex (**5**:Van).[37] This corresponds well with the result from the mole ratio method (Figure 8C).

If the initial concentrations of **5** and Van are $[5]_0$ and $[\text{Van}]_0$, respectively, then the following expressions can be written:

$$K_{11} = \frac{[\mathbf{5}\text{:Van}]}{[\mathbf{5}][\text{Van}]}$$

$$K_{12} = \frac{[\mathbf{5}\text{:(Van)}_2]}{[\mathbf{5}\text{:Van}][\text{Van}]}$$

where [**5**:$(Van)_2$] = *y*, [**5**:Van] = *x* – *y*, [**5**] = $[\mathbf{5}]_0$ – *x*, and [Van] = $[Van]_0$ – (*x* + *y*). When the initial concentration of **5** is $[\mathbf{5}]_0$ = 1.4 μM, then at 2 equivalents of Van (*i.e.*, $[Van]_0 = 2[\mathbf{5}]_0$), the proportions of **5** in the form of **5**:$(Van)_2$, **5**:(Van) and unbound **5** in solution are 28.4 %, 37.6 % and 34.0 %, respectively. On the other hand, at 21.4 equivalents of Van (*i.e.*, $[Van]_0$ = 30 μM), the proportions of **5** in the form of **5**:$(Van)_0$, **5**:(Van) and unbound **5** in solution are 93.0 %, 6.7 % and 0.3 %, respectively; indicating predominantly 1:2 complex in solution. From Figure 8C, it is noted that the maximum-fold change is not observed when 2 equivalents of Van is present. This is because the solution contains the 1:2 complex, 1:1 complex and unbound **5** in equilibrium. Adding more Van (> 2 equivalents) will shift both Step 1 and 2 to the right of the chemical reactions (*i.e.*, more products are formed). For example, at 21.4 equivalents of Van, the above calculations show > 90 % of **5** exists as the 1:2 complex, and the titration curve approaches the maximum-fold change as observed.

It is worth mentioning that the titration curve for triad **1** (refer to Figure 10B) cannot be described using equation (1) since the fluorescence recovery after binding with Van is dependent on the impediment of electron transfer efficiency which is not homogeneous amongst the molecules due to the distribution of electron donor-acceptor spatial distance. However, by assuming that the association between triad **1** and Van follows a stepwise-reaction and that the conjugated anthraquinones do not significantly affect the binding properties between -D-Ala-D-Ala ligands and Van, a similar explanation is used to rationalize the observation that at 2 equivalents of Van, a mixture of **1**:Van_2, **1**:Van and unbound **1** in equilibrium exist in the solution. At higher Van concentrations, more 1:2 complex is formed causing the titration curve to approach maximum-fold change.

The TCSPC fluorescence lifetime profile of reference compound **5** in the presence of 32 μM of Van in PBS is fitted to a bi-exponential decay function with lifetime components τ_1 = 2290 ± 5 ps (α_1 = 74 %) and τ_2 = 980 ± 20 ps (α_2 = 26 %) (Figure 9). The corresponding averaged lifetime $<\tau>$ = 2121 ps, calculated from $<\tau> = \sum_i \alpha_i \tau_i^2 / \sum_i \alpha_i \tau_i$, is longer than $<\tau>$ = 1162 ps when [Van] = 0 by 1.8-times (Figure 7A); in agreement with the increase in fluorescence quantum yield.

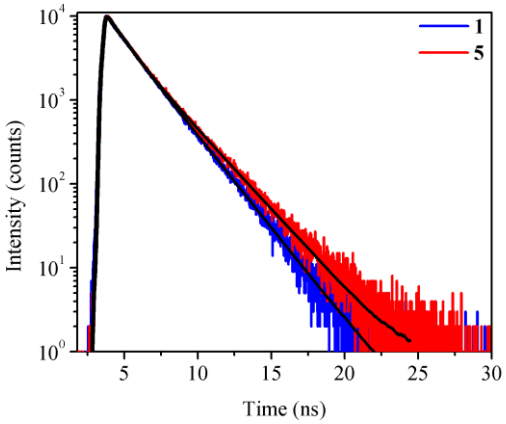

Figure 9. Fluorescence lifetime decay profiles of triad **1** and reference compound **5** in the presence of 32 μM of Van in PBS (λ_{ex} = 637 nm and monitoring emission at 650 nm).

The averaged fluorescence ($<k_f>$) and non-radiative ($<k_{nr}>$) decay constants are computed from:

$$<k_f> = \Phi/<\tau>$$

$$<k_{nr}> = <k_f>(\Phi^{-1} - 1)$$

In the absence of Van, $<k_f>$ = 0.16 ns^{-1} and $<k_{nr}>$ = 0.70 ns^{-1}, whereas for [Van] = 32 μM, $<k_f>$ = 0.17 ns^{-1} and $<k_{nr}>$ = 0.31 ns^{-1}. Upon binding to Van *via* the two -D-Ala-D-Ala ligands, the Seta-640 dye in reference compound **5** comes into close proximity to

the drug molecules, leading to a reduction in the polarity of the surrounding environment. The change in polarity alters $<k_{nr}>$ more significantly than $<k_f>$.[38] In this case, the polarity-induced non-radiative process is less efficient in a more non-polar environment which leads to an enhancement in the fluorescence quantum yield of the dye when bound to Van (inset of Figure 8B).[38]

A control experiment was conducted whereby 50 μM of Van is added to Seta-640 di-carboxylic acid (*i.e.*, dye not conjugated to Lys(Ac)-D-Ala-D-Ala) in PBS. In this case, the emission quantum yield is only enhanced by 1.1-times (Figure 10A). This is because the dye molecule does not bind to Van and its fluorescence intensity is thus unaffected by the presence of free drug molecules in solution.

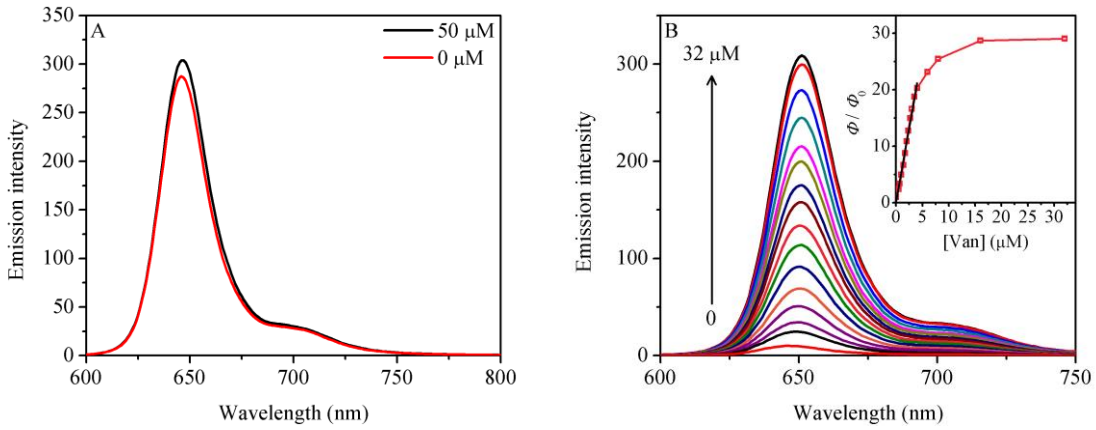

Figure 10. (A) Fluorescence spectra of Seta-640 di-carboxylic acid (~ 1.4 μM) in the absence and presence of 50 μM of Van in PBS. (B) Fluorescence spectra of triad **1** in the presence of different concentrations of Van in PBS ([Van] = 0, 0.5, 0.7, 1, 1.4, 1.7, 2, 2.3, 2.7, 3, 3.5, 4, 6, 8, 16, 32 μM). Inset shows the plot of Φ/Φ_0 *vs.* [Van] and the black line in shows the linear fit for the range of [Van] from 0 to 4 μM.

For triad **1** in PBS, the addition of Van causes the fluorescence intensity and quantum yield to increase significantly (Figure 10B). For example, Φ_0 = 0.006 in the

absence of Van is increased to Φ = 0.18 when [Van] = 32 μM (*i.e.*, *ca*. 30-times enhancement) (see the plot of Φ/Φ_0 *vs*. [Van] in the inset of Figure 10B). The influence of bound Van on the intrinsic polarity-induced non-radiative decay (*i.e.*, 1.8-times increase in Φ) is unable to completely explain the increase in fluorescence quantum yield observed in Figure 10B. We propose that the reduction in polarity due to the bound Van may reduce the electron-transfer efficiency in triad **1**. In addition, when Van molecules bind to the -D-Ala-D-Ala ligands in triad **1**, the anthraquinones are likely to be pulled away from the Seta-640 dye due to steric effect (Scheme 1). The increase in spatial separation between the electron donor and acceptor in the presence of Van reduces the charge-transfer quenching efficiency and results in the observed enhancement in fluorescence intensity.

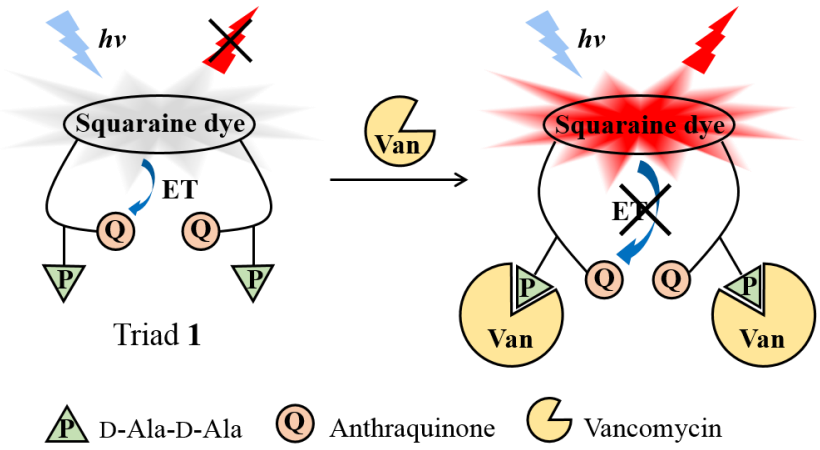

Scheme 1. Proposed mechanism of fluorescence recovery of triad **1** in the presence of Van. In the absence of Van, the anthraquinone molecules are in close proximity to the squaraine dye and electron-transfer (ET) from the photo-excited dye to anthraquinone occurs. When the triad binds to Van *via* -D-Ala-D-Ala ligands, the anthraquinone molecules are positioned further away from the dye; possibly due to steric hindrance. This results in the decrease of ET efficiency and fluorescence recovery occurs.

The fluorescence recovery of triad **1** reaches a plateau at *ca*. [Van] = 30 μM (Figure 10B) with an emission quantum yield (Φ = 0.18) that is lower than that of reference compound **5** in the presence of the same amount of drug (Φ = 0.35). In order to gain further insight into this observation, time-resolved experiments were conducted. In the case of triad **1** in the presence of 32 μM of Van in PBS, the fluorescence lifetime profile from TCSPC shows a bi-exponential decay with components τ_1 = 1975 ± 3 ps (α_1 = 90 %) and τ_2 = 740 ± 30 ps (α_2 = 10 %) (Figure 9). The averaged lifetime $<\tau>$ = 1926 ps is close in value to that of reference compound **5** in the presence of the same amount of antibiotic (*i.e*., 2121 ps), and arises from triad conformers that do not undergo electron-transfer quenching due to the long electron donor-acceptor separation after binding with Van. However, we note that $<\tau>$ is unable to account for the discrepancy observed in the emission quantum yields of triad **1** and reference compound **5** when bound to Van. Despite the absence of short lifetimes in the TCSPC measurements (*e.g*., those within the time resolution of the TCSPC instrument), ultrafast quenching processes are still present in triad **1** as revealed by fs-TA measurements. From the fs-TA spectra of triad **1** in the presence of 32 μM Van at various delay times (Figure 11A), the fs-TA kinetic trace probed at 481 nm is described using a tri-exponential decay function with τ_1 = 740 ps (α_1 = 35 %) (from TCSPC and fixed), τ_2 = 4.2 ± 0.7 ps (α_2 = 20 %) and τ_3 = 0.54 ± 0.05 ps (α_3 = 45 %) (Figure 11B). Clearly, the short τ_2 and τ_3 lifetimes indicate ultrafast processes; possibly from a portion of Van-**1**-Van triads whose electron donor-acceptor distances are still sufficiently short to induce rapid electron-transfer reactions.

The fluorescence recovery experiment by Van was also conducted on triad **2** (Figure 3), consisting of the Seta-640 dye covalently attached to two Lys(AQ)-D-Ala-D-Lac peptides. In this case, the quenched fluorescence quantum yield of triad **2** in PBS

is Φ_0 = 0.005; similar to the quantum yield of triad **1**. Upon the addition of 50 μM of Van, the fluorescence quantum yield increased only slightly to Φ = 0.006 (Figure 11C). The loss of a hydrogen bond and a gain of an oxygen-oxygen lone pair repulsion between -D-Ala-D-Lac and Van have been reported to give rise to a 1000-fold reduction in affinity between the antibiotic and peptide ligand as compared to -D-Ala-D-Ala.[36] Therefore, the lack of fluorescence recovery for triad **2** is due to the significantly weaker binding between Van and -D-Ala-D-Lac ligand, and supports the existence of specific binding between Van and -D-Ala-D-Ala ligand in triad **1**.

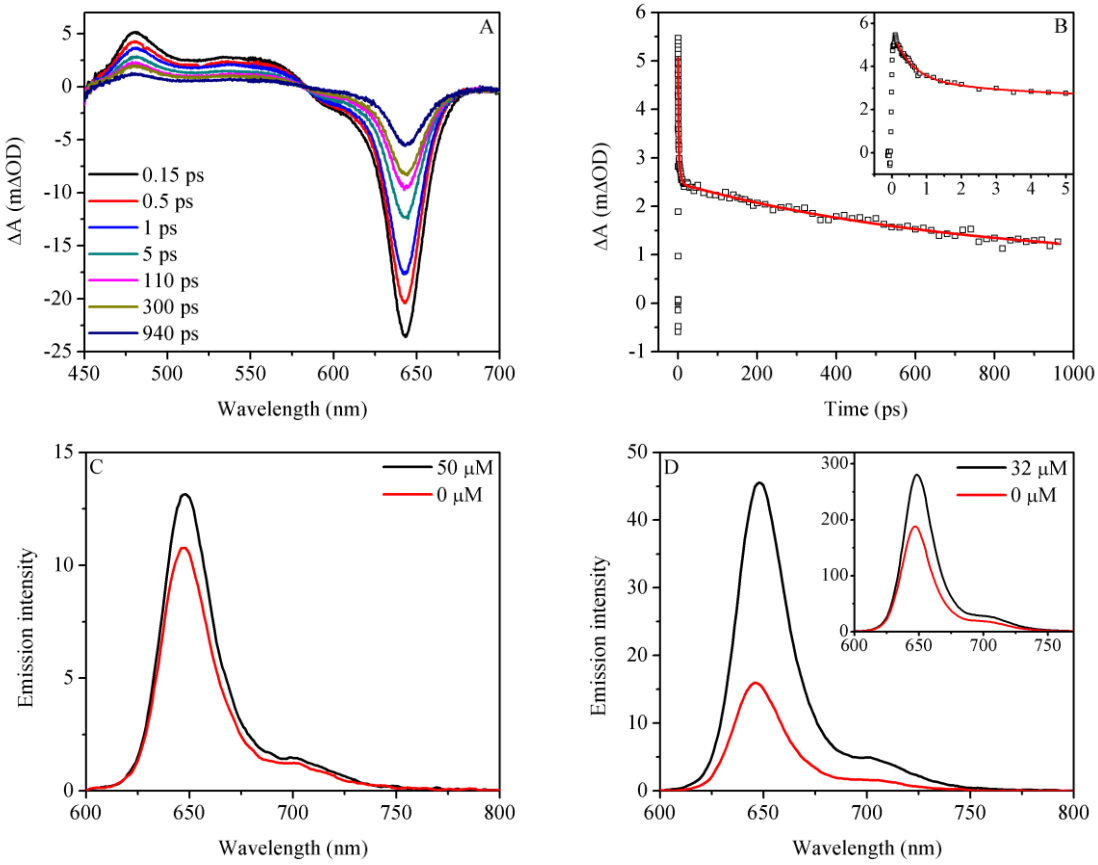

Figure 11. (A) Transient absorption spectra at different probe delay times and (B) kinetic profile extracted at 481 nm for triad **1** in the presence of 32 μM of Van in PBS (pump wavelength = 640 nm). Inset of (B) shows the kinetic decay of **1** for the first 5.2 ps. (C) Fluorescence spectra of triad **2** (~ 1.4 μM) in the absence and presence of 50 μM

of Van in PBS. (D) Fluorescence spectra of dyad **4** and reference compound **6** (inset) (~ 1.4 μM) in the absence and presence of 32 μM of Van in PBS.

The specific binding interaction between Van and triad **1**, and subsequent inhibition of electron-transfer quenching and fluorescence recovery are the driving mechanisms behind the application of triad **1** in the detection and quantification of Van in aqueous solution. The limit of detection (LOD) of triad **1** in PBS was determined to be 7.0 nM (inset of Figure 10B) which is lower than the LOD of chemiluminescence-based methods discussed elsewhere,[16] and is comparable to assays using ultra performance liquid chromatography-tandem mass spectrometry.[39]

A dyad **4** (Figure 3) containing the Seta-640 dye conjugated to one Lys(AQ)-D-Ala-D-Ala peptide displays a quenched fluorescence quantum yield (Φ = 0.007 in PBS) that is increased by only 2.9-times when 32 μM of Van was added into the solution (Figure 11D). The reference compound **6** (Figure 3) containing the dye conjugated to one Lys(Ac)-D-Ala-D-Ala peptide displays a 1.6-times increase in the emission quantum yield at the same Van concentration (inset of Figure 11D). The poor fluorescence recovery in dyad **4** compared to triad **1** implies a smaller degree of electron-transfer inhibition in the dyad upon binding to Van. This could be due to a weaker steric hindrance effect in dyad **4** arising from one bound Van as compared to two bound Vans in triad **1** which allows the flexibly linked anthraquinone to remain close to the dye in the dyad.

2.3.4 Selectivity and interference tests

To investigate whether triad **1** responds to other commonly used antibiotics, 100 μM of tobramycin, gentamicin, amikacin and penicillin G were separately added to a

PBS solution of the probe. From Figure 12A, it is clearly seen that while the fluorescence quantum yield of triad **1** is enhanced in the presence of Van (*i.e.*, $\Phi/\Phi_0 >> 1$), it remains relatively invariant (*i.e.*, $\Phi/\Phi_0 \sim 1$) when an excess of the other antibiotics was utilized. This demonstrates that triad **1** does not respond to tobramycin, gentamicin, amikacin and penicillin G, and is selective towards Van.

The interference of some common coexisting substances on the detection of Van was also examined by adding glycine, L-alanine, urea, D-glucose, ascorbic acid, Mg^{2+}, SO_4^{2-} and CO_3^{2-} separately to a PBS solution of triad **1** in the presence of Van (2 μM). The coexisting substance is considered to have an insignificant interference if the fluorescence intensity of the sample is within ± 5% of the intensity of the control sample (*i.e.*, triad **1** with 2 μM of Van only). It is observed in Figure 12B that the addition of the coexisting substances does not perturb the fluorescence quantum yield of triad **1** in the presence of Van.

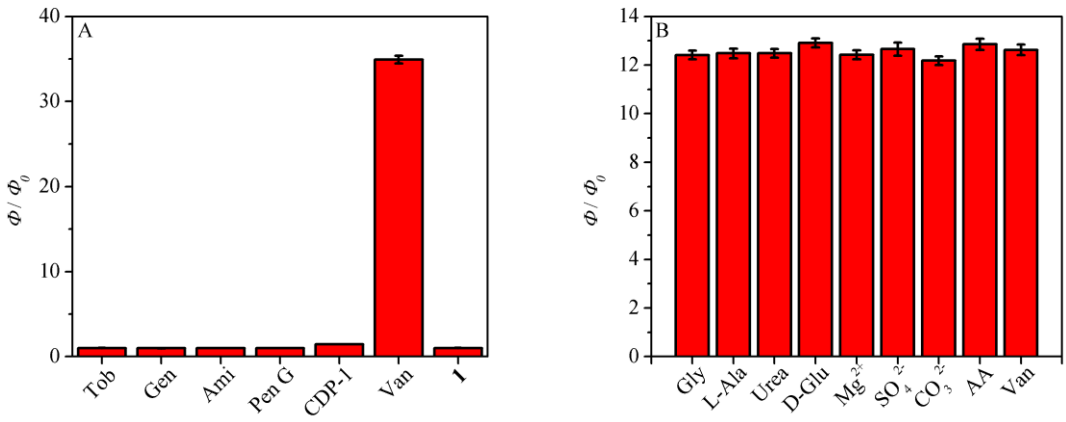

Figure 12. (A) Selectivity of triad **1**. Different antibiotics (32 μM or 100 μM) were added to a PBS solution of triad **1** (~ 1.4 μM) in the absence of Van (Tob: Tobramycin, Gen: Gentamicin, Ami: Amikacin, Pen G: Penicillin G, CDP-1: Van CDP-1 (32 μM), Van (32 μM), Triad **1**). The sample with triad **1** only was used as the control. (B) Interference test. 0.1 or 2 mM of common co-existing substances were added to a PBS

solution of triad **1** (~ 1.4 μM) in the presence of 2 μM of Van (Gly: Glycine, L-Ala: L-Alanine, D-Glu: D-Glucose, Mg^{2+}: $MgCl_2 \cdot 6H_2O$, SO_4^{2-}: Na_2SO_4, CO_3^{2-}: Na_2CO_3 (0.1 mM), AA: Ascorbic acid (0.1 mM)). The sample with triad **1** and 2 μM of Van was used as the control.

A common problem encountered in immunoassays of Van determination is the cross-reactivity of Van crystalline degradation product (CDP-1) which gives false positive results.[40-41] Harris *et al*. have proposed that an additional methylene group in the peptide backbone of Van CDP-1 causes it to assume a conformation that does not facilitate efficient binding with small aliphatic peptides such as Ac-D-Ala-D-Ala; rendering Van CDP-1 inactive against Gram-positive bacteria.[42] When Van CDP-1 (32 μM) was added to a PBS solution of triad **1**, no significant change in the fluorescence quantum yield is observed (Figure 12A). An obvious advantage of triad **1** over immunoassays is therefore its ability to distinguish between Van and its crystalline degradation product with high selectivity towards the former.

2.3.5 Quantification of Van in human serum

Before determination of Van in human serum (HS), the serum is first pre-treated with organic solvents to remove proteins[25-26] (*e.g*., albumin and immunoglobulin A) which can bind with either Van or the squaraine dye.[43-45] Figure 13 shows the fluorescence recovery of triad **1** upon addition of increasing amounts of Van. It is observed that the emission quantum yield of the triad in the absence of Van ($\Phi = 0.003$) is increased by 21-times when 32 μM of Van was added. The maximum recovered fluorescence intensity in the presence of 32 μM of Van is lower in HS as compared to PBS (*i.e*., 30-times in PBS). A plausible explanation for the discrepancy is the presence

of trace amounts of proteins remaining in the serum after the protein precipitation process or endogenous non-protein compounds which bind to Van or the squaraine dye. This decreases the concentrations of free Van or unbound triad, and may also lead to a disruption in the triad-Van association. Nevertheless, the working range of triad **1** covers the clinically therapeutic window of Van (*i.e.*, 7 - 13.5 μM),[46] and the probe is able to achieve Van recovery in spiked serum samples with relatively high accuracy as discussed next.

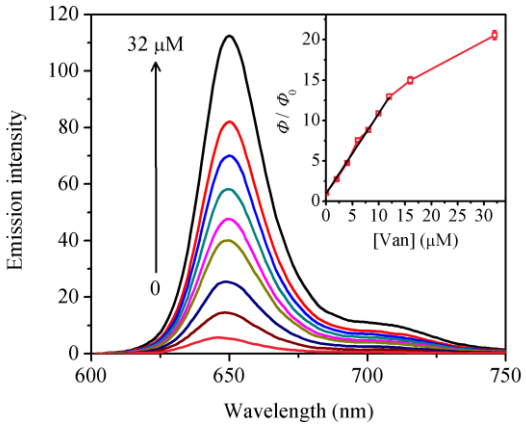

Figure 13. Fluorescence spectra of triad **1** (~ 1.4 μM) in the presence of different concentrations of Van in HS ([Van] = 0, 2, 4, 6, 8, 10, 12, 16, 32 μM). Inset shows the plot of Φ/Φ_0 *vs.* [Van] and the black line shows the linear fit for the range of [Van] from 0 to 12 μM.

HS samples spiked with two concentrations of Van (3 μM and 9 μM) were deproteinized, and the fluorescence spectra of the final solutions containing triad **1** recorded. The [Van] values obtained from the calibration curve indicate a Van recovery within ± 20 % of the actual value (recovered [Van] = 2.38 μM and 9.07 μM) which is comparable to other Van determination assays.[4] In addition, triad **1** detects Van with high sensitivity in HS. A LOD of 96.9 nM is obtained from fitting the linear range of

the calibration curve (inset of Figure 13) which is lower than the LODs of assays using high performance liquid chromatography coupled with various detection methods.[47-49]

2.4 Conclusion

A highly sensitive and selective probe for Van is developed in this study that quantifies the drug in both aqueous and serum samples. In the absence of Van, photo-induced electron-transfer from the excited Seta-640 dye to anthraquinone in triad **1** results in significant fluorescence quenching of the dye. When Van is added, the drug molecules bind with high affinity to the -D-Ala-D-Ala ligands, resulting in fluorescence recovery that can be as high as 30-times. Even though bound Van enhances the fluorescence by reducing the rate of the (intrinsic) polarity-induced non-radiative decay process, this effect plays only a minor role. Instead, the main reason behind the observed fluorescence recovery after drug binding is the effective inhibition of electron-transfer; plausibly arising from a reduction in environmental polarity and steric-induced lengthening of the spatial separation between the squaraine dye and anthraquinone. The proposed Van probe is insensitive to other antibiotics and Van CDP-1, operates in the clinically relevant range, and is easy to operate by using a commonly available fluorescence spectrometer.

2.5 References

1. Hammett-Stabler, C. A.; Johns, T. *Clin. Chem.* **1998**, *44*, 1129-1140.
2. Finch, R. G.; Eliopoulos, G. M. *J. Antimicrob. Chemother.* **2005,** *55 Suppl 2*, ii5-13.
3. Kummerer, K. *Chemosphere* **2009,** *75* (4), 417-34.

4. Javorska, L.; Krcmova, L. K.; Solichova, D.; Solich, P.; Kaska, M. *J. Sep. Sci.* **2016,** *39* (1), 6-20.

5. D'Hondt, M.; Gevaert, B.; Wynendaele, E.; De Spiegeleer, B. *J. Pharm. Anal.* **2016,** *6* (1), 24-31.

6. Song, X.; Xie, J.; Zhang, M.; Zhang, Y.; Li, J.; Huang, Q.; He, L. *J. Chromatogr. B Analyt. Technol. Biomed. Life Sci.* **2018,** *1076*, 103-109.

7. Pfaller, M. A.; Krogstad, D. J.; Granich, G. G.; Murray, P. R. *J. Clin. Microbiol.* **1984**, *20*, 311-316.

8. Odekerken, J. C.; Logister, D. M.; Assabre, L.; Arts, J. J.; Walenkamp, G. H.; Welting, T. J. *Springerplus* **2015,** *4*, 614.

9. Kong, D.; Xie, Z.; Liu, L.; Song, S.; Kuang, H.; Xu, C. *Food and Agricultural Immunology* **2017,** *28* (3), 414-426.

10. Francisco, F. L.; Saviano, A. M.; Almeida Tde, S.; Lourenco, F. R. *J. Microbiol. Methods* **2016,** *124*, 28-34.

11. Lam, M. T.; Le, X. C. *Analyst* **2002,** *127* (12), 1633-1637.

12. Wu, M.; Gao, F.; Zhang, Y.; Wang, G.; Wang, Q.; Li, H. *J. Pharm. Biomed. Anal.* **2015,** *103*, 91-8.

13. Wang, J.; Cao, Y.; Wu, S.; Wang, S.; Zhao, X.; Zhou, T.; Lou, Y.; Fan, G. *Molecules* **2017,** *22* (4).

14. Ndieyira, J. W.; Watari, M.; Barrera, A. D.; Zhou, D.; Vogtli, M.; Batchelor, M.; Cooper, M. A.; Strunz, T.; Horton, M. A.; Abell, C.; Rayment, T.; Aeppli, G.; McKendry, R. A. *Nat. Nanotechnol.* **2008,** *3* (11), 691-6.

15. Bai, X.; Lu, B.; Chen, X.; Zhang, B.; Tang, J. *Biosens. Bioelectron.* **2014,** *62*, 145-50.

16. Khataee, A. R.; Hasanzadeh, A.; Iranifam, M.; Fathinia, M.; Hanifehpour, Y.; Joo, S. W. *Spectrochim. Acta A Mol. Biomol. Spectrosc.* **2014,** *122*, 737-43.

17. Khataee, A.; Lotfi, R.; Hasanzadeh, A. *RSC Advances* **2015,** *5* (101), 82645-82653.

18. Yu, L.; Zhong, M.; Wei, Y. *Anal. Chem.* **2010**, *82*, 7044-7048.

19. Lee, S.; Park, I. S.; Jung, Y.-S.; Kim, J.-M. *J. Nanosci. Nanotechnol.* **2014,** *14* (10), 7693-7699.

20. Liang, W.; Liu, S.; Liu, Z.; Li, D.; Wang, L.; Hao, C.; He, Y. *New J. Chem.* **2015,** *39* (6), 4774-4782.

21. Resch-Genger, U.; Hoffmann, K.; Nietfeld, W.; Engel, A.; Neukammer, J.; Nitschke, R.; Ebert, B.; Macdonald, R. *J. Fluoresc.* **2005,** *15* (3), 337-62.

22. Esser, B.; Swager, T. M. *Angew. Chem. Int. Ed. Engl.* **2010,** *49* (47), 8872-5.

23. Yang, H.; Wang, F.; Zheng, J.; Lin, H.; Liu, B.; Tang, Y. D.; Zhang, C. J. *Chem. Asian J.* **2018,** *13* (11), 1432-1437.

24. Patsenker, L.; Tatarets, A.; Kolosova, O.; Obukhova, O.; Povrozin, Y.; Fedyunyayeva, I.; Yermolenko, I.; Terpetschnig, E. *Ann. N. Y. Acad. Sci.* **2008,** *1130*, 179-87.

25. Muppidi, K. *J. Chromatogr. Sep. Tech.* **2012,** *04* (01).

26. Tariq, M. H.; Naureen, H.; Abbas, N.; Akhlaq, M. *J. Anal. Bioanal. Tech.* **2015**, *6*, 1-5.

27. Volker, S. F.; Renz, M.; Kaupp, M.; Lambert, C. *Chemistry* **2011,** *17* (50), 14147-63.

28. Chen, J.; Winter, R. F. *Chemistry* **2012,** *18* (34), 10733-41.

29. Rao, G. H.; Venkateswararao, A.; Giribabu, L.; Han, L.; Bedja, I.; Gupta, R. K.; Islam, A.; Singh, S. P. *Phys. Chem. Chem. Phys.* **2016,** *18* (21), 14279-85.

30. de Miguel, G.; Marchena, M.; Zitnan, M.; Pandey, S. S.; Hayase, S.; Douhal, A. *Phys. Chem. Chem. Phys.* **2012,** *14* (5), 1796-805.

31. Wightman, R. M.; Cockrell, J. R.; Murray, R. W.; Burnett, J. N.; Jones, S. B. *J. Am. Chem. Soc.* **1976**, *98*, 2562-2570.

32. Wu, X.; Liu, F.; Wells, K. L.; Tan, S. L.; Webster, R. D.; Tan, H. S.; Zhang, D.; Xing, B.; Yeow, E. K. *Chemistry* **2015,** *21* (8), 3387-98.

33. Tablet, C.; Matei, I.; Hillebrand, M. The Determination of the Stoichiometry of Cyclodextrin Inclusion Complexes by Spectral Methods: Possibilities and Limitations. In *Stoichiometry and research - the importance of quantity in biomedicine*; Innocenti, A., Ed.; Intech, 2012, DOI:10.5772/34287.

34. Kusumoto, Y. *Chem. Phys. Letts.* **1987**, *136*, 535-538.

35. Nigam, S.; Durocher, G. *J. Phys. Chem.* **1996**, *100*, 7135-7142.

36. Xing, B.; Jiang, T.; Wu, X.; Liew, R.; Zhou, J.; Zhang, D.; Yeow, E. K. *Chemistry* **2011,** *17* (50), 14170-7.

37. Thordarson, P. *Chem. Soc. Rev.* **2011**, *40*, 1305-1323.

38. Cornelissen-Gude, C.; Rettig, W.; Lapouyade, R. *J. Phys. Chem. A* **1997**, *101*, 9673-9677.

39. Li, B.; Zhang, T.; Xu, Z.; Fang, H. H. *Anal. Chim. Acta* **2009,** *645* (1-2), 64-72.

40. Tanaka, M.; Orii, T.; Gomi, T.; Kobayashi, H.; Kanke, M.; Hirono, S. *Yakugaku Zasshi* **2002**, *122*, 269-275.

41. Somerville, A. L.; Wright, D. H.; Rotschafer, J.C. *Pharmacotherapy*, **1999**, *19*, 702-707.

42. Harris, C. M.; Kopecka, H.; Harris, T. M. *J. Am. Soc. Chem.* **1983**, *105*, 6915-6922.

43. Terpetschnig, E.; Szmacinski, H.; Ozinskas, A.; Lakowicz, J. R. *Anal. Biochem.* **1994**, *217*, 197-204.

44. Sun, H.; Maderazo, E. G.; Krusell, A. R. *Antimicrob. Agents Chemother.* **1993**, *37*, 1132-1136.

45. Butterfield, J. M.; Patel, N.; Pai, M. P.; Rosano, T. G.; Drusano, G. L.; Lodise, T. P. *Antimicrob. Agents. Chemother.* **2011,** *55* (9), 4277-82.

46. Rybak, M. J.; Lomaestro, B. M.; Rotschafer, J. C.; Moellering, R. C.; Craig, W. A.; Billeter, M.; Dalovisio, J. R.; Levine, D. P. *Clin. Infect. Dis.* **2009,** *49* (3), 325-7.

47. Lopez, K. J.; Bertoluci, D. F.; Vicente, K. M.; Dell'Aquilla, A. M.; Santos, S. R. *J. Chromatogr. B Analyt. Technol. Biomed. Life Sci.* **2007,** *860* (2), 241-5.

48. Hagihara, M.; Sutherland, C.; Nicolau, D. P. *J. Chromatogr. Sci.* **2013,** *51* (3), 201-7.

49. Favetta, P. Guitton, J.; Bleyzac, N.; Dufresne, C.; Bureau, J. *J. Chromatogr. B* **2001**, *751*, 377-382.

2.6 Annex

^{1}H NMR spectrum of triad 3

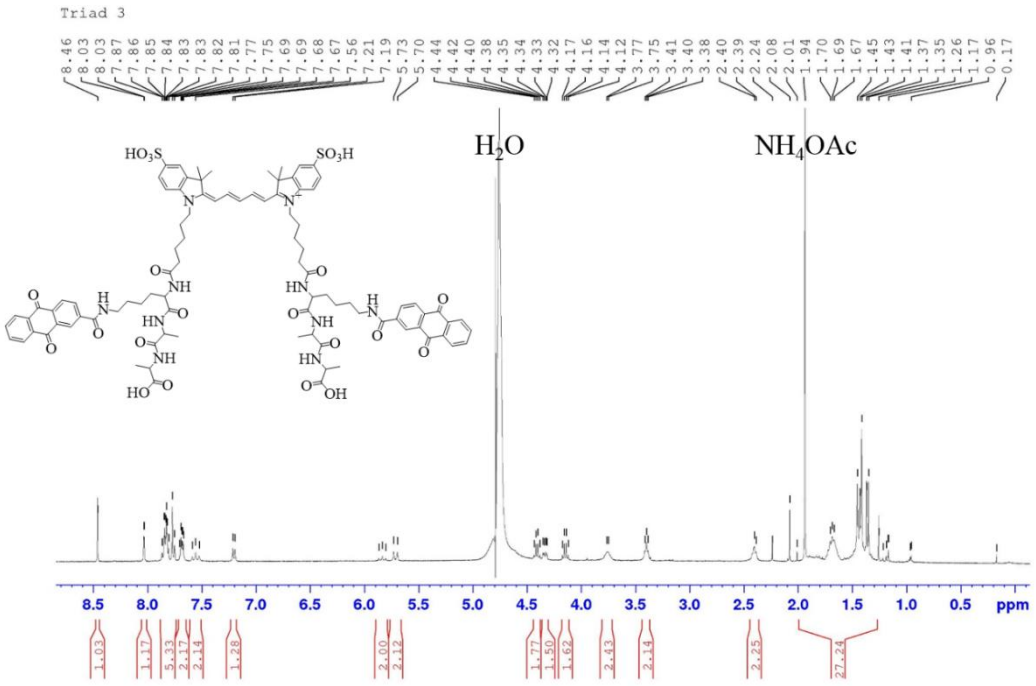

Figure A1. ^{1}H NMR spectrum for triad **3** in D_2O. The water peak appears distorted due to suppression of the water signal when obtaining the spectrum. This could have caused the integration of the neighbouring signals (4-4.5 ppm) to give proton counts larger than 1.

Chapter 3 Fluorescence turn-on probe for vancomycin based on hole-transfer: Influence of linker length on the hole-transfer quenching efficiency

Abstract: In this chapter, a different electron donor-acceptor system consisting of the triad made up of the cyanine dye Cy5 conjugated to two ferrocene (Fc) moieties via Lys-D-Ala-D-Ala peptides was proposed for the detection of vancomycin (Van). In the absence of Van, hole transfer occurs from the excited Cy5 to Fc which quenches the fluorescence of the triad. When Van is added, the binding between the antibiotic and the triad led to fluorescence recovery via a disruption of the hole-transfer efficiency. By synthesizing two triads with a shorter or longer linker between Cy5 and Fc, the distance-dependency of the hole-transfer process was studied using fluorescence spectroscopy.

3.1 Introduction

In this chapter, we continue to explore different electron donor-acceptor systems by varying the dye and/or the quencher in the triad. We have shown in Chapter 2 that when the dye was changed to a near-infrared cyanine dye Cy5, the corresponding triad precipitated in the presence of vancomycin (Van), presumably due to aggregation of triad-Van complexes over time; thus it was not suitable to be used as a Van probe. Herein, we proposed another triad consisting of Cy5 conjugated to two ferrocene (Fc) moieties via Lys-D-Ala-D-Ala peptides. In this case, the quenching of the dye's emission in the absence of Van would occur via a hole-transfer process from the excited Cy5 to Fc. (From here on, the assignment of a hole- or an electron-transfer process is taken from the perspective of the excited species, *i.e.* the dye.) To provide a simple explanation of a hole-transfer process, a 'hole' is generated in the highest occupied molecular orbital (HOMO) upon excitation of the dye which promotes an electron from the HOMO to the lowest unoccupied molecular orbital (LUMO). In the absence of a quencher (or hole acceptor), the excited electron recombines with the hole, producing fluorescence via a radiative decay. The fluorescence can be quenched in the presence of a hole acceptor which accepts the hole by transferring (or donating) an electron to the dye's HOMO. Consequently, the excited electron decays via other pathways and fluorescence is quenched.

Fc is an efficient electron donor due to its low oxidation potential and is commonly used as hole acceptors in hole-transfer mechanistic studies of quantum dots for applications in photovoltaics and photocatalysis.[1-2] When it is conjugated to Cy5, an energetically favourable hole transfer takes place from the excited Cy5 to Fc and the fluorescence of Cy5 in the Cy5-Fc dyad was quenched. We have previously reported the change in free energy (ΔG_{ht}) for this process to be -0.83 eV.[3] By attaching Lys-D-

Ala-D-Ala peptides to the Cy5-Fc dyad to form a triad similar to that discussed in Chapter 2, we attempted to investigate if the corresponding triad can perform as a Van probe satisfactorily. In this case, we anticipated a disruption of the hole-transfer (HT) efficiency between Cy5 and Fc upon binding to Van via the -D-Ala-D-Ala ligands, which would lead to fluorescence recovery (Scheme 1). This is opposite to the fluorescence quenching and recovery mechanism for the squaraine dye-anthraquinone triad which was mediated by an electron-transfer process (*i.e.* electron transfer from the excited dye to anthraquinone which is an efficient electron acceptor).[4-5] In both cases, the charge-transfer efficiency is dependent on the donor-acceptor distance, which is described by the term $e^{-\beta d}$ (where d = donor-acceptor separation).[6] Therefore, in this study, we also investigated the influence of the length of the linker between Cy5 and Fc on the hole-transfer quenching efficiency in the triad.

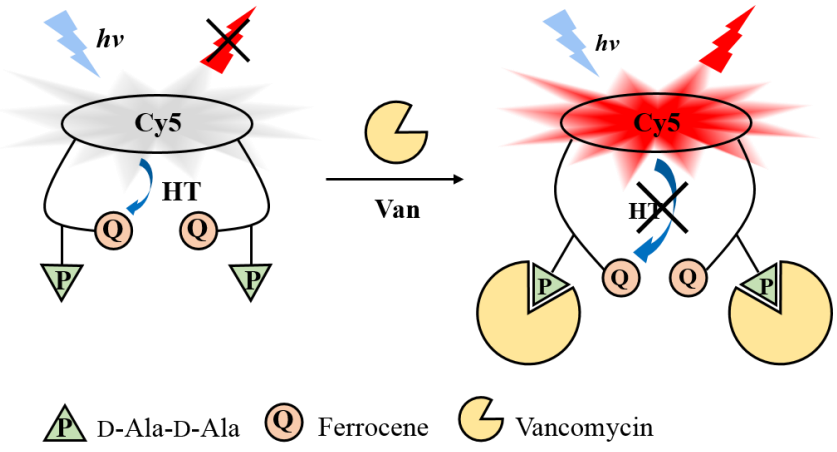

Scheme 1. Proposed mechanism of fluorescence recovery of the triads under study in the presence of Van. In the absence of Van, the Fc moieties are in close proximity to Cy5 and HT from the photo-excited dye to Fc occurs. When the triad binds to Van via the -D-Ala-D-Ala ligands, the Fc moieties are positioned further away from the dye; possibly due to steric hindrance. This results in a decrease of HT efficiency, leading to fluorescence recovery.

3.2 Experimental

3.2.1 Materials

All chemicals were acquired from Sigma-Aldrich (unless otherwise stated) and used as received. 1,2-dichlorobenzene, 3-bromopropionic acid, , trifluoroacetic acid (TFA), *N*,*N*-diisopropylethylamine (DIPEA) and piperidine were purchased from Alfa Aesar. 2,3,3-trimethyl-3H-indole-5-sulfonate (potassium salt) was purchased from Toronto Research Chemicals Inc., ferrocene NHS ester from FIVEphoton Biochemicals and Cy5 bis NHS ester from GE Healthcare. 2-chlorotrityl chloride resin, Boc-Lys-(NH_2)-D-Ala-D-Ala-OH, Fmoc-D-Ala-OH, Fmoc-Lys(Dde)-OH, Boc-Gly-OH and *O*-(benzotriazol-1-yl)-*N,N,N',N'*-tetramethyluronium hexafluoro-phosphate **(**HBTU) were purchased from GL Biochem (Shanghai) Ltd. Phosphate buffered saline (PBS, 1X, pH 7.4) was purchased from Thermo Fisher Scientific. Reagent or HPLC grade solvents were used without further purification. Dry dichloromethane (DCM) was prepared over activated molecular sieves (4 Å) for at least 12 h prior to use while anhydrous solvents were prepared by vacuum distillation.

3.2.2 Synthesis

Semi-preparative and analytical HPLC were performed on a Shimadzu HPLC system with a Kromasil C-18 (250 × 10 mm) and C-18 (250 × 4.6 mm) reverse phase column using a mobile phase (50 mM ammonium acetate in water and 100% ACN, unless otherwise stated) with a flow rate of 3 mL min^{-1} and 1 mL min^{-1}, respectively. ESI mass spectra were obtained on a Thermo LCQ Deca XP Max instrument. ^{1}H NMR spectra were recorded on Bruker AV 500 (500 MHz) and AV 400 (400 MHz) spectrometers. The chemical shifts (δ) were reported in ppm relative to the residual

solvent peak and coupling constants (*J*) in Hz. The peptides and their derivatives were prepared by standard Fmoc chemistry using solid-phase synthesis.

*Compound **1***. 2,3,3-trimethyl-3H-indole-5-sulfonate (101 mg, 0.364 mmol) and 3-bromopropionic acid (556 mg, 3.64 mmol) were heated in 1,2-dichlorobenzene (7.00 mL) at 120℃ under nitrogen. The reaction mixture turned purple immediately and the product precipitated upon formation. The heating was continued for 15 h, after which the reaction mixture was cooled to room temperature and the solvent decanted. The solid obtained was triturated with acetone/diethyl ether (DE) to give the crude product as red powder. The crude product was used without further purification.

*Compound **2***. **1** (4 equiv.) and malonaldehyde bis(phenylimine) monohydrochloride (1 equiv., 0.0410 mmol) were dissolved in 420 μL of 2.5:1 acetic acid:triethylamine (AcOH:TEA; v/v) and heated in a sealed vial at 120℃ for 1 h. After which, DE was added to precipitate the cyanine dye as a dark blue solid which was further washed with DE and ACN. Compound **2** was purified from the crude product by RP-HPLC (20 to 45% ACN in water with 0.1% TFA over 25 min) and lyophilized to give a blue solid (<1 mg). ESI $[M]^+$ m/z calcd. for $[C_{31}H_{35}N_2O_{10}S_2]^+$ 659.17, found 659.33. ^{1}H NMR (500 MHz, DMSO) δ = 8.39-8.34 (t, *J* = 13 Hz, 2H, 2 x CH), 7.80 (d, *J* = 1.4 Hz, 2H, Ar-H), 7.63-7.61 (dd, *J* = 8.3 Hz, 1.5 Hz, 2H, Ar-H), 7.33-7.31 (d, *J* = 8.4 Hz, 2H, Ar-H), 6.61-6.56 (t, *J* = 12.3 Hz, 1H, CH), 6.37-6.34 (d, *J* = 13.7 Hz, 2H, 2 x CH), 4.32-4.30 (t, *J* = 6.9 Hz, 4H, 2 x CH_2), 2.71-2.68 (t, *J* = 7.1 Hz, 4H, 2 x CH_2), 1.68 (s, 12H, 4 x CH_3).

*Compound **3***. To **2** (0.400 mg, 0.606 μmol) in a vial, 40.3 μL and 166 μL of anhydrous *N*,*N*-dimethylformamide (DMF) solutions of *N*-hydroxysuccinimide (NHS; 2.09 mg, 0.0182 mmol) and *N*-(3-dimethylaminopropyl)-*N'*-ethylcarbodiimide hydrochloride (EDC.HCl; 3.49 mg, 0.00182 mmol), respectively, were added

sequentially and the mixture was stirred at room temperature for 4 h. Compound **3** was isolated from the reaction mixture by RP-HPLC (0 to 40% ACN in water with 0.004% TFA over 20 min) and lyophilized to give a blue solid (<1 mg). ESI $[M]^+$ m/z calcd. for $[C_{39}H_{41}N_4O_{14}S_2]^+$ 853.21, found 853.33.

*Boc-Lys(Fc)-D-Ala-D-Ala-OH (**4**).* To a solution of Boc-Lys(NH_2)-D-Ala-D-Ala-OH (8.40 mg, 21.6 μmol) and ferrocene NHS ester (7.70 mg, 23.8 μmol) in anhydrous dimethyl sulfoxide (DMSO; 500 μL), TEA (3.11 μL, 21.6 μmol) was added and the mixture was stirred at 40℃ for 6 h. Compound **4** was isolated from the reaction mixture by RP-HPLC (20 to 100% ACN over 25 min) and lyophilized to give a yellow solid (9.20 mg, 71%). ESI $[M + H]^+$ m/z calcd. for $[C_{28}H_{41}FeN_4O_7]^+$ 601.23, found 600.91. ^{1}H NMR (400 MHz, DMSO) δ = 7.94-7.92 (d, *J* = 7.8 Hz, 1H, NH), 7.90-7.88 (d, *J* = 6.8 Hz, 1H, NH), 7.84-7.81 (t, *J* = 5.8 Hz, 1H, NH), 6.91-6.89 (d, *J* = 7.7 Hz, 1H, NH), 4.78 (s, 2H, 2 x CH), 4.32-4.31 (t, *J* = 1.8 Hz, 2H, 2 x CH), 4.29-4.27 (m, 1H, CH), 4.14 (s, 5H, 5 x CH), 4.04-4.00 (m, 1H, CH), 3.91-3.86 (m, 1H, CH), 3.16-3.11 (q, *J* = 6.3 Hz, 2H, CH_2), 1.59-1.44 (m, 4H, 2 x CH_2), 1.40-1.28 (m, 11H, 3 x CH_3, CH_2), 1.24-1.23 (d, *J* = 7.1 Hz, 3H, CH_3), 1.19-1.17 (d, *J* = 7.0 Hz, 3H, CH_3).

*H-Lys(Fc)-D-Ala-D-Ala-OH (**5**).* To a solution of **4** (9.20 mg, 15.3 μmol) in DCM (5.00 mL), 20% triisopropylsilane (TIPS) and phenol (v/v; 1.00 mL and 1.07 g, respectively), and 30% TFA (v/v; 1.50 mL) were added sequentially. The mixture was stirred at room temperature for 3.5 h. Compound **5** was isolated from the reaction mixture by RP-HPLC (20 to 100% ACN) and lyophilized to give a yellow solid (6.50 mg, 85%). ESI $[M + H]^+$ m/z calcd. for $[C_{23}H_{33}FeN_4O_5]^+$ 501.18, found 501.15.

*H-Gly-Lys(Fc)-D-Ala-D-Ala-OH (**6**).* 2-chlorotrityl chloride resin (1.22 g, 1.22 mmol) was activated in DCM in a peptide synthesizer with N_2 flow for 10 min. Fmoc-D-Ala-OH (1.5 equiv.) dissolved in a mixture of DIPEA (4 equiv.) and DCM (10 mL)

was loaded onto the swelled resin and agitated for 1.5 h. The resin was then washed with DCM and the capping of unreacted resin was performed with a solution of DIPEA (4 equiv.), methanol and DCM (1:1 v/v) for 15 min. Subsequently, the resin was washed with DCM followed by DMF and a solution of 20% piperidine in DMF (v/v) was added to remove Fmoc for 20 min. The resin was then washed several times with DMF and subjected to the following series of coupling-deprotection-washing cycles: (i) coupling with the second Fmoc-D-Ala-OH (2 equiv.) followed by Fmoc-Lys(Dde)-OH (2 equiv.) and Boc-Gly-OH (2 equiv.) in the presence of HBTU (2 equiv.), DIPEA (4 equiv.) and DMF (6-8 mL) for at least 2 h, (ii) Fmoc deprotection with 20% piperidine in DMF (v/v) for 20 min, and (iii) repeated washing with DMF. This yielded the peptide with the sequence Boc-Gly-Lys(Dde)-D-Ala-D-Ala-OH on solid support. The Dde protecting group on the side chain of Lys was then removed using 2% hydrazine in DMF (v/v) for 20 min to expose the amine group for subsequent coupling with ferrocenecarboxylic acid (3 equiv.) in the presence of 1-hydroxybenzotriazole (HOBt; 3 equiv.) and HBTU (3 equiv.) in 4:1 DMF:DCM mixture (v/v) for 3-4 h. The Fc-conjugated peptide was cleaved from the resin under the conditions of 30% TFA, 10% TIPS and phenol (v/v) in DCM for at least 30 min, which also removed the Boc protecting group in the process. The product was collected, followed by concentration under vacuum and cold DE precipitation to yield the crude product, which was purified by RP-HPLC (5 to 60% ACN over 20 min) and lyophilized to give a yellow solid. ESI $[M + H]^+$ m/z calcd. for $[C_{25}H_{36}FeN_5O_6]^+$ 558.20, found 558.19.

*Triad **C3***. To a solution of **3** and **5** in anhydrous DMF (500 μL), anhydrous TEA (10 μL) was added and the mixture was stirred at room temperature for 1.5 h. Triad **C3** was isolated from the reaction mixture by RP-HPLC (0 to 40% ACN over 20 min) and

lyophilized to give a blue solid (<1 mg). ESI $[M]^+$ m/z calcd. for $[C_{77}H_{95}Fe_2N_{10}O_{18}S_2]^+$ 1623.50, found 812.70 $[M + H]^{2+}$.

*Triad **C9***. To a solution of **6** and Cy5 bis-NHS in anhydrous DMF (400 μL), anhydrous TEA (7 μL) was added and the mixture was stirred at room temperature for 30 min. Triad **C9** was isolated from the reaction mixture by RP-HPLC (5 to 50% ACN over 30 min) and lyophilized to give a blue solid (<1 mg). ESI $[M]^+$ m/z calcd. for $[C_{87}H_{113}Fe_2N_{12}O_{20}S_2]^+$ 1821.63, found 911.65 $[M + H]^{2+}$.

3.2.3 Instrumentation

Steady-state absorption and fluorescence spectroscopy. Absorption and fluorescence spectra were recorded on a UV/Vis spectrometer (Cary 100, Varian) and fluorescence spectrometer (Cary Eclipse, Varian), respectively. The samples were excited at 590 nm.

3.3 Results and discussion

3.3.1 Synthesis of triads C3 and C9

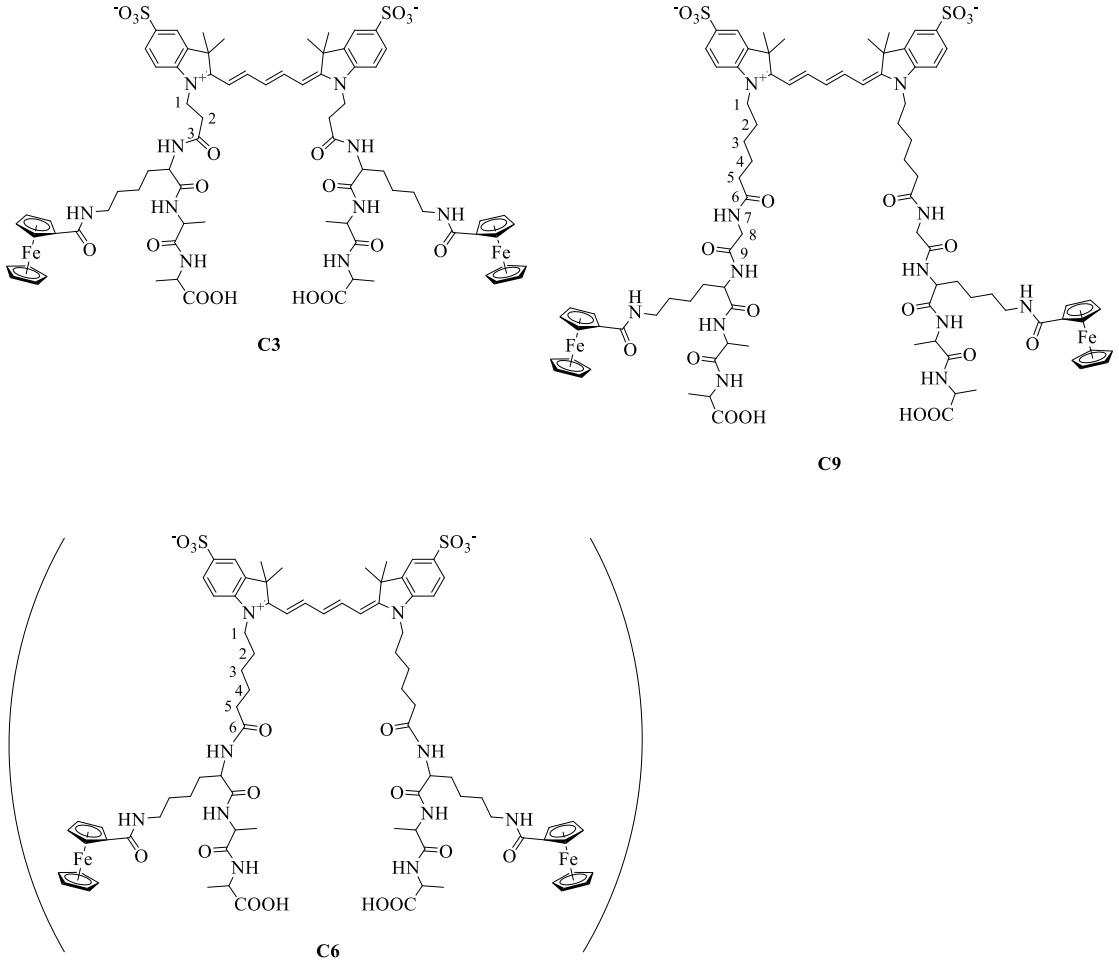

Figure 1. Chemical structures of triads **C3**, **C6** and **C9**.

Figure 1 shows the chemical structures of the three triads that would be discussed in this study. The synthesis of triads **C3** and **C9** would be discussed here, whereas the triad **C6** was prepared previously and its photophysical properties in the absence and presence of Van were investigated by another colleague (unpublished results). These results are included in the discussion and would be used to explain the results obtained for **C3** and **C9**, therefore the structure of **C6** is also included in Figure 1 (in bracket).

The synthesis of **C3** and **C9** involves two parts: the preparation of the cyanine dye and the Fc-conjugated peptide (Scheme 2). For **C3**, a cyanine dye with a 3-atom

linker functionalized with reactive groups (*i.e.* compound **3**) is needed, for which no commercial product was available and had to be synthesized in three steps (a-c). In the first step, a suspension of 2,3,3-trimethyl-3H-indole-5-sulfonate (potassium salt) and 3-bromopropionic acid in dichlorobenzene was heated at 120 ℃ to yield the indoleninium salt **1** via a nucleophilic substitution reaction.[7] The crude product was used in the next step, where it undergoes a condensation reaction[8] with malonaldehyde bis(phenylimine) monohydrochloride to give the cyanine dye **2**. In the last step, the cyanine dye was functionalized with reactive *N*-hydroxysuccinimide (NHS) groups (**3**) via *N*-(3-dimethylaminopropyl)-*N'*-ethylcarbodiimide (EDC) activation. Fc-conjugated Lys-D-Ala-D-Ala peptide (**4**) was prepared by reacting ferrocene NHS ester with Boc-Lys-(NH_2)-D-Ala-D-Ala under basic conditions. This was followed by acidic cleavage of the Boc protecting group to expose the amine group on Lys of compound **5** to react with the cyanine dye NHS ester **3** to yield the final product **C3**.

To obtain a 9-atom linker for **C9** for which a commercial product is also not available, the commercial dye Cy5 bis NHS ester with a 6-atom linker was used and the extension of another three atoms was provided by adding a glycine (Gly) residue to peptide **5** to give Gly-Lys(Fc)-D-Ala-D-Ala (**6**) (the bracket in the peptide sequence indicates conjugation of Fc to the side chain of Lys). The peptide **6** was prepared by standard fluorenylmethyloxycarbonyl (Fmoc) chemistry using solid-phase peptide synthesis (SPPS) and the final coupling reaction with Cy5 bis NHS ester to yield **C9** proceeded as described for **C3**.

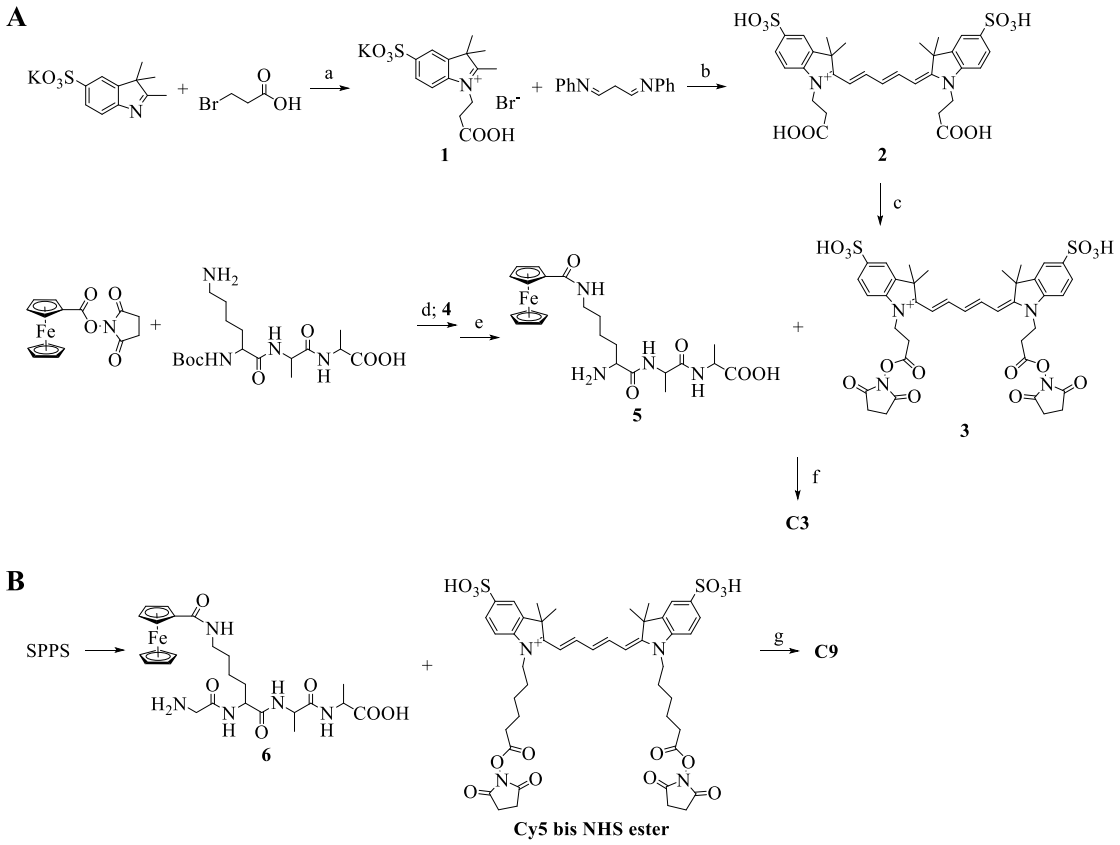

Scheme 2. Synthetic route of (A) **C3** and (B) **C9**.

Reagents and conditions: (a) 1,2-dichlorobenzene, 120℃, 15 h; (b) 2.5:1 AcOH:TEA (v/v), 120℃, 1 h; (c) EDC.HCl, NHS, anhydrous DMF, rt, 4 h; (d) TEA, anhydrous DMSO, 40℃, 6 h; (e) 30% TFA and 20% TIPS and phenol in DCM (v/v), rt, 3.5 h; Anhydrous TEA and DMF, rt, (f) 1.5 h, (g) 30 min.

3.3.2 Spectroscopic studies

In this section, the photophysical properties of a previously prepared triad **C6** are discussed first. These (unpublished) results would form the basis to explain the results obtained for the triads **C3** and **C9**. Figure 2 shows the normalized absorption and fluorescence spectra of **C6** and the reference compound **R6** (*i.e.* Cy5 conjugated to two Lys(Ac)-D-Ala-D-Ala peptides and does not contain Fc; structure not shown) in phosphate buffered saline (PBS) in the absence of Van. **C6** exhibits absorption (λ_{abs})

and emission (λ_{em}) maxima at 651 nm and 663 nm, respectively, which are slightly shifted from the corresponding values for **R6**, *i.e.* λ_{abs} = 649 nm and λ_{em} = 667 nm. The lack of a significant spectral shift or distortion of spectral shape indicates the absence of strong ground-state electronic couplings between Cy5 and Fc in **C6**.

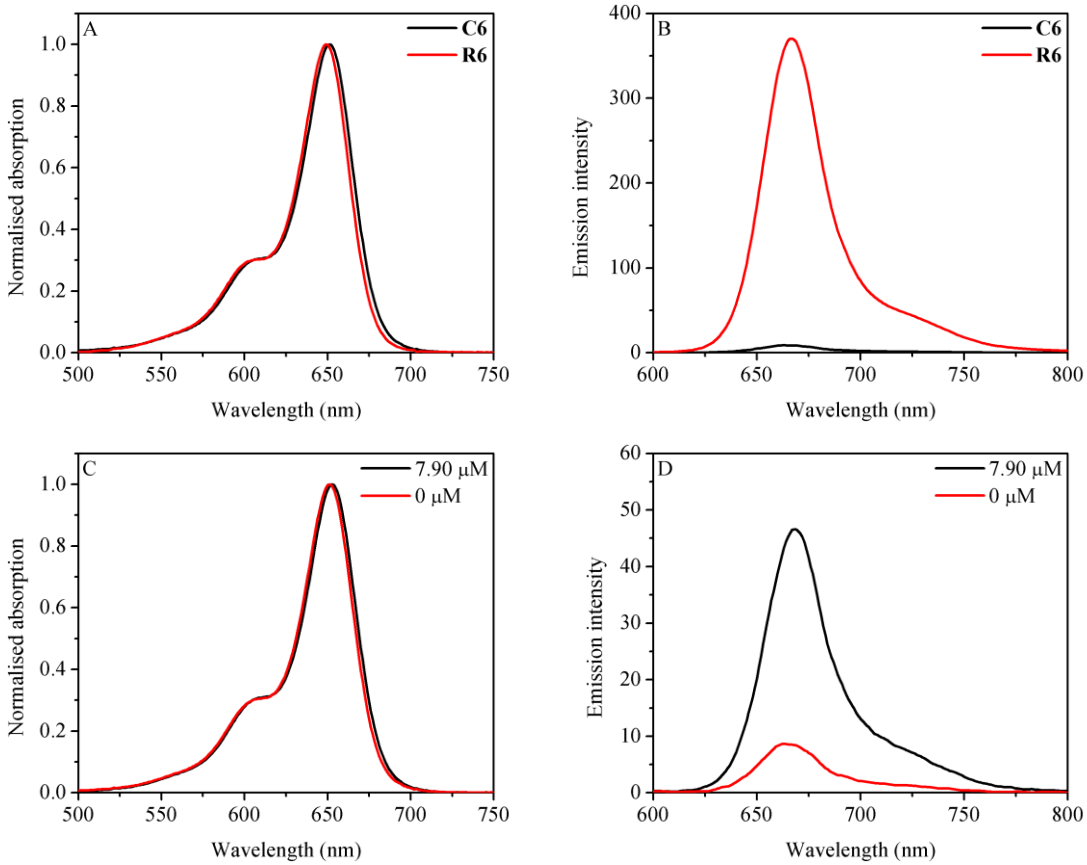

Figure 2. (A) Normalized absorption and (B) fluorescence spectra of **C6** and **R6** in PBS in the absence of Van. (C) Normalized absorption and (D) fluorescence spectra of **C6** in PBS in the presence of 7.90 µM of Van. Excitation wavelength λ_{ex} = 590 nm.

Upon excitation at 590 nm, however, the fluorescence of **C6** was significantly quenched compared to **R6** (Figure 2B). Clearly, the presence of the Fc moieties in **C6** caused the quenched fluorescence and this was ascribed to an energetically favourable

hole transfer from the excited Cy5 to Fc, which we have reported a Gibb's free energy (ΔG_{ht}) of -0.83 eV for a Cy5-Fc dyad without the Lys-D-Ala-D-Ala peptide.[3]

In the presence of 7.90 μM of Van, the absorption spectrum of **C6** was slightly red-shifted (λ_{abs} = 653 nm) while its emission intensity increased by 5.4-times (Figures 2C and 2D, respectively). A similar shift of absorption spectrum was observed for **R6**, but the fluorescence recovery of 1.3-times is smaller compared to **C6** (data not shown). In the absence of Fc, the small increment in emission intensity of **R6** upon binding to Van via the -D-Ala-D-Ala ligands suggests an increase in the hydrophobicity of the microenvironment surrounding Cy5 in the bound complex (similar to reference compound **5** discussed in Chapter 2). Another reason could be due to a restricted rotation of the polymethine chain of Cy5 resulting from a bulkier triad-Van complex, which produces a more rigid molecule and reducing the fluorescence loss due to non-radiative decay. Cyanine dyes with flexible polymethine chains are known to suffer from low quantum yields due to large contribution from non-radiative decay arising from carbon-carbon bond rotation.[9] However, these reasons could not fully account for the fluorescence enhancement of 5.4-times of **C6** in the presence of Van. As in the case for the squaraine dye-anthraquinone triad, another reason is likely due to an increase in the spatial separation between Cy5 and Fc, possibly caused by steric effects, upon Van binding to **C6** via the -D-Ala-D-Ala ligands, which reduces the hole-transfer efficiency between the two entities and recovers fluorescence.[3]

However, we thought that a fluorescence enhancement of 5.8-times at the maximum Van concentration tested, *i.e.* 16.5 μM, was unsatisfactory (Figure 3C). Since the hole-transfer efficiency is affected by the donor-acceptor (or dye-quencher) distance, the triads **C3** and **C9** were synthesized and investigations were carried out to examine if a shorter or longer linker between Cy5 and Fc would effect a larger fluorescence

enhancement factor (which translates to higher detection sensitivity) at the same concentration of Van.

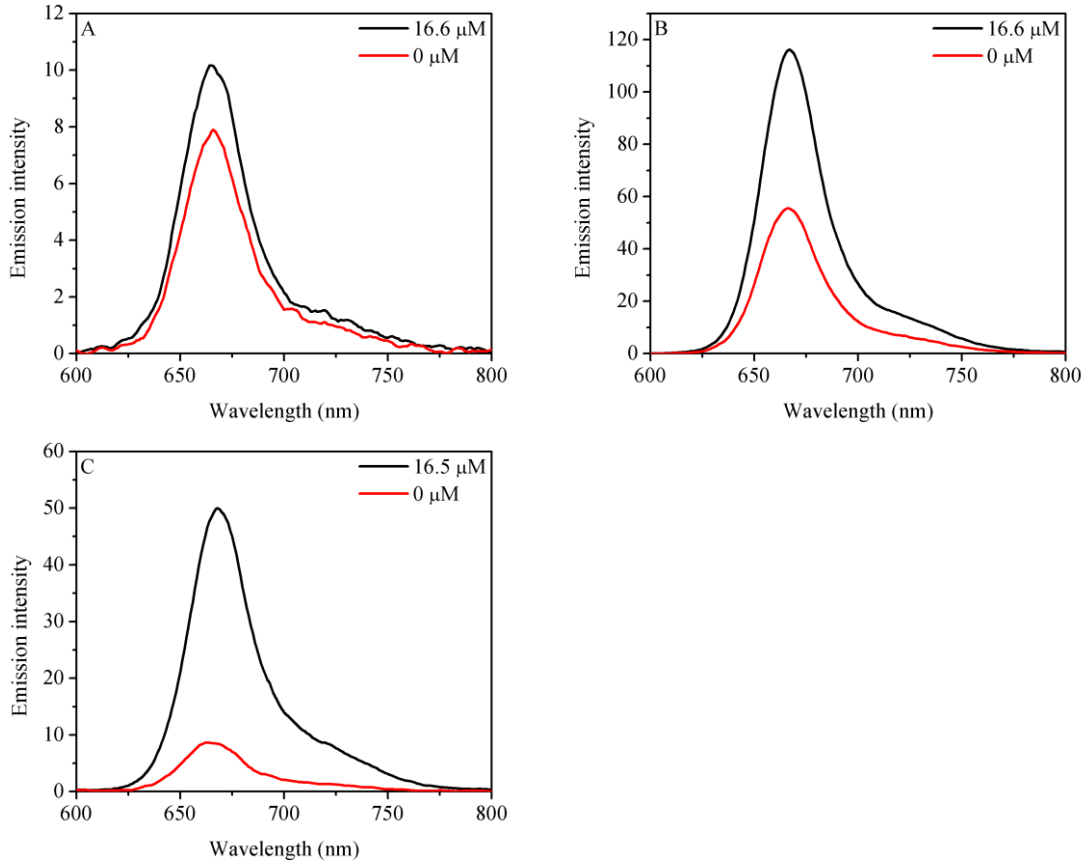

Figure 3. Fluorescence spectra of PBS solutions of (A) **C3**, (B) **C9** and (C) **C6** in the absence and presence of Van. Excitation wavelength λ_{ex} = 590 nm.

The synthesis of **C3** and **C9** has been discussed in section 3.3.1. Figure 3 shows the fluorescence spectra of **C3** and **C9** in PBS in the absence and presence of Van. The corresponding spectra for **C6** are also included for comparison (Figure 3C). Similar to **C6**, the fluorescence spectra of **C3** and **C9** displayed a slight shift of λ_{em} and an increase in emission intensity in the presence of ~17 µM of Van. For all three triads, the shift of λ_{em} was ~1-5 nm and is possibly due to the high affinity interaction between Van and the -D-Ala-D-Ala ligands (dissociation constant K_d ~10^{-6} M).[10] A similar spectral shift

was reported for biotinylated cyanine dyes upon binding to a high affinity ligand streptavidin (K_d for the biotin-streptavidin interaction is ~10^{-13} M).[11]

From Figures 3A and 3C, it can be seen that the fluorescence of **C3** and **C6** were quenched to a similar extent in the absence of Van. However, when Van was added, the emission intensity increased by 1.3-times and 5.8-times for **C3** and **C6**, respectively. We propose that, with a short 3-atom linker, after Van binds to the -D-Ala-D-Ala ligands of **C3**, Fc is still in close proximity to Cy5. As a result, there is still significant hole-transfer quenching and a low fluorescence recovery of 1.3-times in the presence of 16.6 μM of Van was obtained. When the length of the linker was increased to 6-atoms (*i.e.* **C6**), there is more flexibility for the Fc arm to swing further away from Cy5 upon Van binding. Consequently, the quenching effect is inhibited to a larger extent and a higher fluorescence recovery of 5.8-times was attained for **C6**.

However, further increase of the linker length to 9-atoms saw a drop in quenching efficiency (*i.e.* stronger fluorescence) in **C9** in the absence of Van (Figure 3B). Furthermore, in the presence of 16.6 μM of Van, only a small increment of 2.1-times in emission intensity was noted. These results suggest that when the linker length is too long, it is less likely for the Fc arm to swing close enough to Cy5 to effect efficient hole-transfer quenching. In addition, when Van is added, the distance between Cy5 and Fc in the bound complex does not change significantly, thereby yielding a small fluorescence enhancement factor. A similar observation was reported by Liu *et al.*, where an increase in the linker length between naphthalimide (fluorophore) and the nitrogen atom (quencher) on a piperazine ring resulted in poorer quenching and recovery of fluorescence intensity of the corresponding probe in the absence and presence of different concentrations of the human Ether-a-go-go-Related Gene (hERG) channel.[12]

To conclude, it appears that a 6-atom linker length is optimal, for which the corresponding triad **C6** gave the largest fluorescence enhancement factor of 5.8-times at ~17 μM of Van among the three triads investigated. However, the performance of this triad as a Van probe pales in comparison with the one discussed in Chapter 2. A possible reason could be due to the difference in polarity between the cationic cyanine dye Cy5 and zwitterionic squaraine dye Seta-640, where the former is less polar. The implication of this is higher quantum yields displayed by cyanine dyes in aqueous solutions due to a smaller contribution from non-radiative losses as compared to the more polar squaraine dyes[13] (*e.g.* quantum yields of Cy5 and Seta-640 in PBS are 0.27 and 0.13, respectively).[8] Following this line of reasoning, when bound to a hydrophobic molecule (*e.g.* protein) which inhibits non-radiative decay processes (to a certain extent), the resulting increase in quantum yield would be smaller for cyanine dyes compared to squaraine dyes.[13-15] Nonetheless, this study provides support for the use of the commercial squaraine dye Seta-640, which has a 6-atom linker, to construct the corresponding triad in Chapter 2.

3.4 Conclusion

In conclusion, a different electron donor-acceptor system consisting of the triad made up of Cy5 conjugated to two Fc moieties via Lys-D-Ala-D-Ala peptides was proposed for Van detection. This triad relies on a hole-transfer mechanism to quench its fluorescence in the absence of Van which was subsequently recovered in the presence of Van due to a disruption of the hole-transfer efficiency. In this study, the influence of the linker length between Cy5 and Fc on the hole-transfer quenching efficiency in the triad was also investigated. The results revealed that with a 6-atom linker, the triad **C6** gave the largest fluorescence enhancement factor of 5.8-times in the presence of ~17

μM of Van, for which a shorter 3-atom (*i.e.* **C3**) or longer 9-atom (*i.e.* **C9**) linker shows poorer performance due to either too close or too far spatial separation between Cy5 and Fc in the triad-Van bound complex.

3.5 References

1. Araki, Y.; Yasumura, Y.; Ito, O. *J. Phys. Chem. B* **2005**, *109* (19), 9843-9848.
2. Olshansky, J. H.; Ding, T. X.; Lee, Y. V.; Leone, S. R.; Alivisatos, A. P. *J. Am. Chem. Soc.* **2015,** *137* (49), 15567-75.
3. Wu, X.; Liu, F.; Wells, K. L.; Tan, S. L.; Webster, R. D.; Tan, H. S.; Zhang, D.; Xing, B.; Yeow, E. K. *Chemistry* **2015,** *21* (8), 3387-98.
4. Kandhadi, J.; Yeduru, V.; Bangal, P. R.; Giribabu, L. *Phys. Chem. Chem. Phys.* **2015,** *17* (40), 26607-20.
5. Melomedov, J.; Ochsmann, J. R.; Meister, M.; Laquai, F.; Heinze, K. *Eur. J. Inorg. Chem.* **2014,** *2014* (11), 1984-2001.
6. Sparano B. A.; Koide, K. *J. Am. Chem. Soc.* **2007**, *129*, 4785-4794.
7. Gustafson, T. P.; Cao, Q.; Achilefu, S.; Berezin, M. Y. *ChemPhysChem* **2012,** *13* (3), 716-23.
8. Shao, F.; Weissleder, R.; Hilderbrand, S. A. Monofunctional Carbocyanine Dyes for Bio- and Bioorthogonal Conjugation. *Bioconjugate Chem.* **2008**, *19*, 2487-2491.
9. Lee, H.; Berezin, M. Y.; Henary, M.; Strekowski, L.; Achilefu, S. *J. Photochem. Photobiol. A Chem.* **2008**, *200*, 438-444.
10. Xing, B.; Jiang, T.; Wu, X.; Liew, R.; Zhou, J.; Zhang, D.; Yeow, E. K. *Chemistry* **2011,** *17* (50), 14170-7.
11. Luschtinetz, F.; Dosche, C.; Kumke, M. U. *Bioconjug. Chem.* **2009**, *20*, 576-582.

12. Liu, Z.; Zhou, Y.; Du, L.; Li, M. *Analyst* **2015,** *140* (24), 8101-8.

13. Markova, L. I.; Terpetschnig, E. A.; Patsenker, L. D. *Dyes Pigm* **2013,** *99* (3), 561-570.

14. Povrozin, Y. A.; Kolosova, O. S.; Obukhova, O. M.; Tatarets, A. L.; Sidorov, V. L.; Terpetschnig, E. A.; Patsenker, L. D. *Bioconjug. Chem.* **2009**, *20*, 1807-1812.

15. Tatarets, A. L.; Fedyunyayeva, I. A.; Dyubko, T. S.; Povrozin, Y. A.; Doroshenko, A. O.; Terpetschnig, E. A.; Patsenker, L. D. *Anal. Chim. Acta* **2006,** *570* (2), 214-23.

Chapter 4 Development of a novel detection system for epinephrine based on FRET quenching of $NaYF_4$:Yb,Tm upconversion luminescence

Abstract: Epinephrine (EP), also known as adrenaline, is an important neurotransmitter regulating various physiological processes in the sympathetic nervous system. Abnormal EP concentrations in human fluids have been detected in the diagnosis of several health problems, hence rendering the quantitative analysis of this neurotransmitter of great significance. In recent years, increasing attention has been placed on development of detection methods employing nanomaterials due to the unique and tunable optical properties of such materials. Herein, we proposed a novel detection system based on the upconversion nanoparticle $NaYF_4$:Yb,Tm to detect EP via a fluorescence resonance energy transfer (FRET) mechanism. In the presence of EP, the emission peaks originating from Tm^{3+} transitions were quenched due to formation of a condensation product on the nanoparticle surface that absorbs in the same wavelength region.

4.1 Introduction

Epinephrine (EP), also known as adrenaline, is a catecholamine neurotransmitter which plays important physiological roles in the sympathetic nervous system (*e.g.* increasing blood pressure and blood sugar levels during fight-or-flight response).[1-2] The normal plasma concentrations of EP is in the range of 0.02-0.46 nM.[3] Abnormal EP concentrations have been associated with various adverse heart-related conditions such as myocardial infarction, arrhythmias and Takotsubo cardiomyopathy.[4] EP is also used as medication to treat a number of conditions including anaphylaxis, cardiac arrest, asthma attack and superficial bleeding.[2, 4] Therefore, the quantitative detection of the neurotransmitter in different human fluids and pharmaceutical formulations has important implications in the diagnosis of various health conditions and therapeutic interventions.

Various analytical tools have been developed for EP quantification in different media and these include high performance liquid chromatography (HPLC),[5-6] electrochemical detection,[7-13] capillary electrophoresis,[14] chemiluminescence,[15-16] fluorimetry,[17-18] spectrophotometry,[19] enzyme-based[20-22] and nanomaterials.[4, 23-29] However, these strategies suffer from one or more of the limitations such as tedious and time-consuming sample preparation and analysis procedures, insufficient sensitivity and/or selectivity for applications in real samples, and complicated and expensive instrumentation. Electrochemical detection is one of the most commonly used methods and a vast amount of literature has been dedicated to the development of modified electrode surfaces[7-13] to solve the problem of overlapping signals from co-existing and/or structurally similar species in complex media, and to achieve signal amplification.[9, 13] The latter is usually accomplished by modification of the electrode surface to enhance EP adsorption.[11] However, this was found to cause passivation and

fouling of electrode surface, which resulted in poor selectivity and sensitivity.[11, 13] Furthermore, the preparation of the modified electrodes can be expensive and challenging, and its stability is questionable considering the leaching of electron transfer mediators in the long term. There is also the issue of irreversible adsorption behaviour which requires renewal of electrode surface after each measurement, making it less suitable for routine analysis.[13]

Due to the unique and tunable optical properties of nanomaterials, its application in detection systems for various analytes has gained increasing popularity. For EP detection, several strategies using nanomaterials such as silver (Ag),[23-25] gold (Au)[4, 26-27] and carbon nanoparticles,[28] and graphene quantum dots (GQD)[29] have been proposed. Alam *et al.* developed a fast, sensitive and cost-effective approach based on the enhanced luminescence of terbium ion (Tb^{3+})-EP complexes in the presence of Ag nanoparticles (Ag NP) for EP sensing.[23] In their system, the lanthanide ion Tb^{3+} was used as the fluorophore, and the addition of Ag NP to pre-formed Tb^{3+}-EP complex was found to increase Tb^{3+} emission at 545 nm significantly (*ca.* ~6-times) compared to that of the Tb^{3+}-EP complex only. This was shown to be due to the enhanced absorption of Tb^{3+} due to increased electric field around the Ag NP (Figure 1). The luminescence intensity of the Tb^{3+}-EP-Ag NP system was linearly related to the concentration of EP for the range of 2.5-110 nM and a limit of detection (LOD) of 0.25 nM was obtained. Satisfactory recoveries ranging from 98-101% were achieved in pharmaceutical formulations, human serum and urine. However, the detection was carried out under an optimized pH of 9.0 which is above the biological pH of 7.0, and applications in human serum required an overnight deproteinization step which undesirably increases the analysis time.

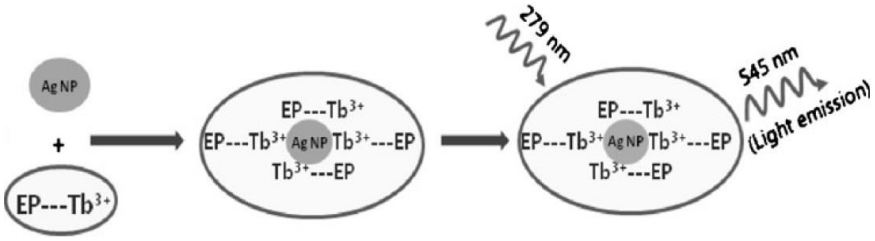

Figure 1. Schematic diagram showing the proposed detection mechanism of the Tb^{3+}-EP-Ag NP system. This figure is adopted from reference 23.

Two colorimetric sensors based on the different extent of deposition of silver nanoshell on gold nanorods (GNR)[26] or aggregation of aptamer-functionalized gold nanoparticles (Au NP)[4] in the presence of varying catecholamine concentrations were described in the literature. The former method makes use of the reducing ability of catecholamines to reduce silver ions (Ag^{+}) to Ag, which is deposited on the surface of GNR. The extent of Ag atom deposition depends on the reducing strength of the different catecholamines and their concentrations, which gave rise to a multicolour shift in absorption spectra of the resulting nanorods. This method was demonstrated to be able to produce unique colorimetric fingerprints for individual as well as mixtures of catecholamines in array platforms. The latter method was developed by Saraf *et al.* which makes use of the interaction between EP and a EP-binding aptamer functionalized on Au NP to cause charge destabilization and hence aggregation and colour change of the Au NP from red to blue. Their method was shown to exhibit high sensitivity toward EP with a determined LOD of 0.9 nM by spectrophotometry and 9 nM in a developed paper-based sensor. It is worth mentioning that the authors also did a study on the effect of size and morphology of the Au NP on the detection limit of the sensor. The results showed that 13 nm spherical Au NP gave the optimal detection limit and unsatisfactory performance was observed using larger spherical particles (e.g. 50 nm) or particles with

different morphologies (rods/urchins with sizes ~50 nm) due to greater negative charge and hence increased stability which reduces the aggregation behaviour of the particles.

Au NP have also been applied in surface-enhanced resonance Raman scattering (SERRS) sensing platforms to achieve trace detection of EP in serum.[27] In this method, Au NP were functionalized with nitrilotriacetic acid-iron (Fe-NTA) ligands which captured EP via metal-ligand coordination in less than 30 s in aqueous solution. Subsequently, cyclohexane was added to effect self-assembly of the particles into orderly arrays at the liquid/liquid interface due to reduced interfacial tension. This generated a 2D SERRS platform which was transferred to a silicon wafer from which enhanced Raman signal and sensitivity were attained (Figure 2). In a complex medium as serum, the ability of the Au NP to capture, transport and self-assemble EP provided signals with great contrast from background signals arising from various species such as amino acids. Consequently, sensitive detection of trace amounts of EP in the nM range could be performed at a characteristic Raman signal at 1482 cm^{-1}. The analysis time using this method was within 3 min and the results were highly reproducible. The authors did mention that additional signals should be monitored in samples where a mixture of catecholamines is expected. Furthermore, even though the particle surfaces can be easily regenerated for repeated EP sensing, the silicon wafers have to be completely cleaned from the particles in order for it to be reused, which can be challenging and was indicated to be out of the scope of the current study by the authors.

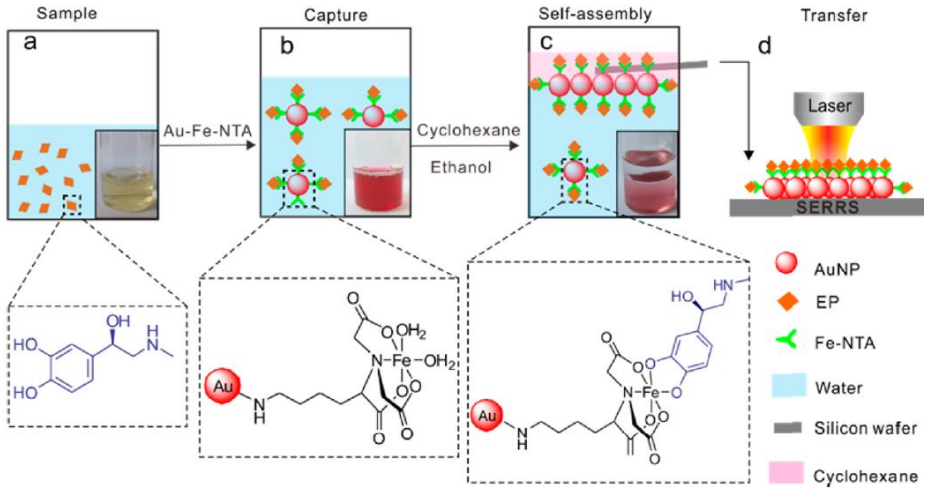

Figure 2. Schematic diagram showing the process of (b) EP capture and (c) self-assembly of Fe-NTA-functionalized Au NP to form a 2D SERRS platform which is (d) transferred to a silicon wafer for analysis. This figure is adopted from reference 27.

Apart from Ag and Au nanoparticles, carbon nanoparticles (CNP)[28] and GQD[29] have also been employed in the design of fluorescence-based detection systems for EP. For the former, the presence of EP was found to increase the fluorescence of CNP resulting from EP-induced aggregation of the particles, which blocked non-radiative decay processes and increased the rate of radiative electron-hole recombination, leading to fluorescence enhancement. Using this method, an extremely low LOD of 0.759 nM for the linear concentration range of 9.90-107 nM was attained, which provides sufficient sensitivity for monitoring of normal EP levels in urine samples. Furthermore, the addition of various compounds including norepinephrine (which bears high structural similarity to EP) did not cause significant change in the fluorescence intensity of the CNP in the presence of EP, thus demonstrating the good selectivity of the method toward EP. The latter method employing GQD was proposed by Wang *et al.* and the detection mechanism was based on the fluorescence quenching of the GQD by EP (known as adrenaline in the paper) upon excitation due to a photoinduced charge transfer

from GQD to EP, mediated by strong non-covalent interactions between the two species (Figure 3). This method offers a simple and label-free detection of EP, for which a LOD of 0.5 μM was determined for the linear concentration range of 1-200 μM. Applications in human serum were also demonstrated with satisfactory recoveries of 99.9-109%.

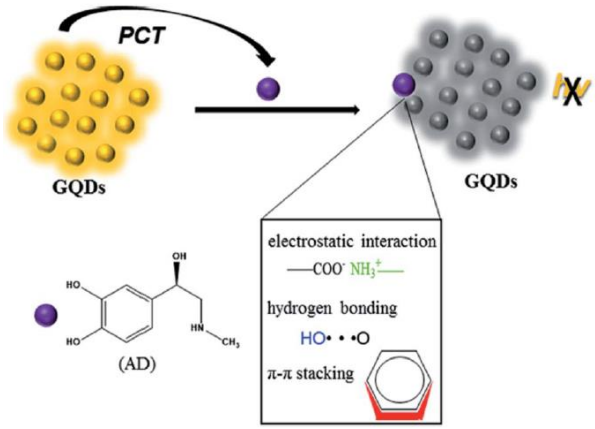

Figure 3. Schematic diagram showing the detection mechanism of GQD for EP. This figure is adopted from reference 29.

To the best of our knowledge, no work on the application of lanthanide-doped upconversion nanoparticles (UCNP) for EP detection has been reported. An important property of this nanomaterial is its photon upconversion ability, on top of excellent chemical and photo-stability and low toxicity. Herein, we proposed a novel detection system for EP based on o-phenylenediamine (OPD)-conjugated $NaYF_4$ doped with Yb/Tm (from here on referred to as $NaYF_4$:Yb,Tm). $NaYF_4$:Yb,Tm was prepared using a modified procedure[30] and coated with a silica layer to provide thiol functional groups to conjugate OPD. EP can undergo a condensation reaction with OPD in alkaline solution to form a product that absorbs in the wavelength region of 350-500 nm,[17] which overlaps with some of Tm^{3+} emissions (*e.g.* $^1D_2 \rightarrow {}^3H_6$ and $^1D_2 \rightarrow {}^3F_4$ transitions give emissions at 367 nm and 455 nm, respectively).[31] Therefore, we proposed that under a

set of optimized conditions, EP would react with the OPD conjugated on $NaYF_4$:Yb,Tm and form a condensation product that quenches some of Tm^{3+} emissions via fluorescence resonance energy transfer (FRET) upon excitation at 980 nm (Scheme 1). It is worth mentioning that the condensation reaction between EP and OPD can be accelerated by the addition of small amounts of acetone, and this method has been reported to yield fluorescence enhancement of the condensation product by 50-times, for which a detection limit of 9.3 nM was determined for the linear concentration range of 0.02-6 μM.[17] Although this method is simple and straightforward, we thought that EP detection on UCNP as an alternative sensing platform would provide opportunities for further development of the system in terms of single particle detection and regeneration of the particle surface for repeated measurements.

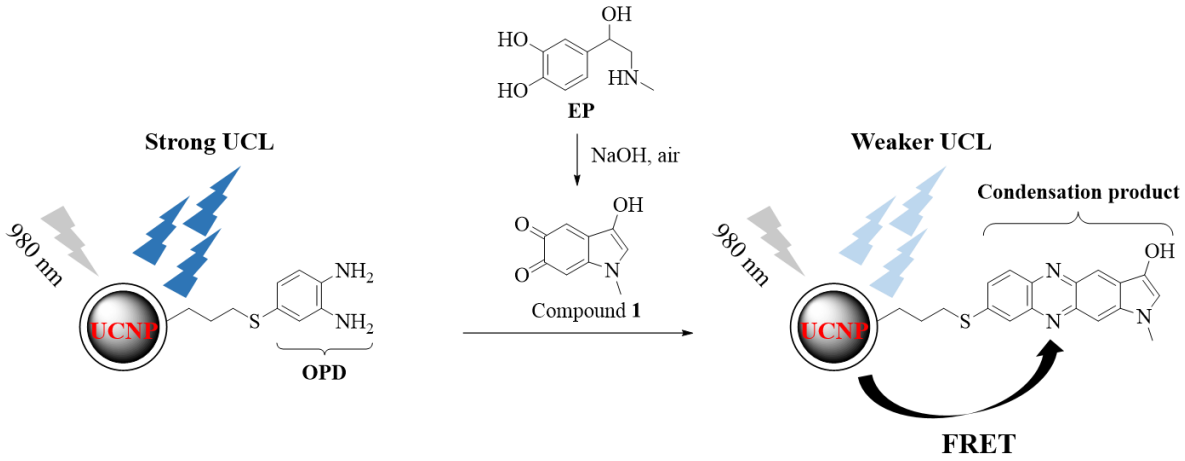

Scheme 1. A proposed mechanism for the quenching of upconversion luminescence (UCL) in the presence of EP. EP is first oxidized in air in an alkaline medium to form compound **1** which undergoes a condensation reaction with OPD to form a product that quenches Tm^{3+} emissions via FRET upon 980 nm excitation. The diagram is not drawn to scale.

4.2 Experimental

4.2.1 Materials

All chemicals and solvents (HPLC grade) were used as received. Unless otherwise stated, all chemicals were acquired from Sigma-Aldrich. $Y(CH_3CO_2)_3.xH_2O$, $Yb(CH_3CO_2)_3.4H_2O$, $Tm(CH_3CO_2)_3.xH_2O$, sodium hydroxide (NaOH) and aqueous ammonia (28%) were purchased from Sinopharm Chemical Reagent Co., Ltd. Oleic acid and glacial acetic acid were purchased from TCI Co., Ltd. and Schedelco Pte. Ltd., respectively. Deionized water was used in all experiments.

4.2.2 Synthesis

Oleate-capped UCNP (UCNP@OA). The synthesis was modified from a reported procedure.[30] To a 50 mL three-necked round-bottomed flask, 7 mL of methanol containing a total of 0.4 mmol of lanthanide precursors (molar ratio of Y/Yb/Tm = 79.5/20/0.5), 3 mL of oleic acid and 7 mL of 1-octadecene were added and mixed with stirring under nitrogen. The mixture was heated to 100 ℃ and reduced pressure was applied to remove methanol. The temperature of the solution was further increased to 150 ℃ to form lanthanide oleate complexes. After 1 h, the heating was stopped and the solution was cooled to room temperature. 6 mL of methanol containing 1 mmol of NaOH and 1.6 mmol of ammonium fluoride (NH_4F) was then added to the solution and the mixture was heated to 50 ℃ for 30 min before it was further heated to 100 ℃ and methanol removed under reduced pressure. After which, the mixture was heated to 290 ℃ via small temperature increments of 20-30 ℃/5 min and kept at this temperature for 2 h. The crude reaction mixture was then cooled to room temperature and ethanol was added to precipitate the nanoparticles. The nanoparticles were obtained by

centrifugation at 4000 rpm for 5 min, washed with ethanol and dispersed in 4 mL of cyclohexane.

Thiol (SH)-functionalized UCNP (UCNP@Si-SH). 15 mg of UCNP@OA, 1.5 mL of Igepal CO-520 and 12 mL of cyclohexane were mixed with stirring in a 25 mL round-bottomed flask for 5 min at 750 rpm at room temperature. The homogeneous clear solution obtained was sonicated for 5 min and stirred for another 5 min. 230 µL of aqueous ammonia (28%) was then added dropwise and the mixture was stirred for 30 min. Subsequently, tetraethyl orthosilicate (TEOS; 15 µL) diluted in cyclohexane (85 µL) was added dropwise and the mixture was stirred for 12 h. This was followed by the addition of (3-mercaptopropyl)trimethoxysilane (MPS; 3 µL) diluted in cyclohexane (27 µL) and the stirring was continued for another 9 h. The reaction was stopped by adding 20 mL of ethanol to the reaction mixture and the nanoparticles were collected by ultracentrifugation (A23-6x100 rotor, SORVALL LYNX 6000 centrifuge, Thermo Scientific) at 20000 rpm for 15 min at room temperature. The nanoparticles were then washed with ethanol/water (1:1, v/v) and ethanol, and finally dispersed in 2 mL of ethanol which was stored at 4 ℃ till the next reaction.

OPD-functionalized UCNP (UCNP@Si-OPD). 30 mg of UCNP@Si-SH was dispersed with sonication in 11 mL of anhydrous *N*,*N*-dimethylformamide (DMF) and stirred at 1000 rpm at room temperature. Appropriate amounts of an OPD stock (5 mg/mL; prepared before use) were added in 1 mL of DMF to the nanoparticles and the mixture was stirred for 3 h in the dark. The OPD-functionalized nanoparticles were collected by ultracentrifugation at 20000 rpm for 10 min at room temperature, and washed with DMF/water (1:1, v/v) and DMF. The obtained nanoparticles were dispersed in 500 µL of DMF and stored at 4 ℃.

4.2.3 Instrumentation

Transmission electron microscopy (TEM). TEM was performed on a JEOL-JEM-1400 equipment operating at a voltage of 100 kV. The nanoparticles were diluted with cyclohexane (for UCNP@OA) or ethanol (for UCNP@Si-SH) and 20 μL of the solution was dropcasted onto a carbon-coated copper grid (Beijing XXBR Technology Co., Ltd.). The TEM images were analyzed using ImageJ software.

Steady-state absorption and emission spectroscopy. Absorption spectra were recorded on a UV/Vis spectrometer (Cary 100, Varian). Emission spectra were recorded on a SEC2000 spectrometer (ALS Co., Ltd.) connected at 90 ° to the excitation laser (980 nm). The concentration of nanoparticles was 5 mg/mL.

4.2.4 Testing procedure for EP

For the preparation of EP stock solution, deionized water was deoxygenated with nitrogen gas for at least 1 h prior to use. 1 mM EP stock solution was prepared by first dissolving 1.832 mg of (-)-epinephrine in 0.1 mL of 1 M acetic acid. The volume was made up to 10 mL with the deoxygenated water.

The testing procedure for EP is as follows: 0.5 mL of water, an appropriate amount of the EP stock solution and 0.1 mL of 0.01 M NaOH were added sequentially and mixed using a micropipette in a 4 mL vial (no stir bar). The vial (without the cap) was placed in a warm water bath and the mixture was incubated at 30 ℃ for 5 min. Subsequently, 20 μL of acetone followed by an appropriate amount of UCNP@Si-OPD were added (with mixing after each addition) and the final volume of the mixture was made up to 2 mL with water. (For this step, the sequence of addition is very important.) The opening of the vial was covered with parafilm and the mixture was heated in boiling

water for 5 min. After which, the mixture was cooled in a water bath (tap water) for 5 min and the absorption and emission spectra of the resulting solution were recorded.

4.3 Results and discussion

4.3.1 Synthesis and TEM characterization of UCNP

Oleate-capped $NaYF_4$:Yb,Tm (20, 0.5 mol%) (UCNP@OA) was prepared using a modified procedure[30] to yield monodispersed nanoparticles with an average size of 26.65 ± 1.96 nm (obtained from a Gaussian fit of the particle size distribution) (Figure 4).

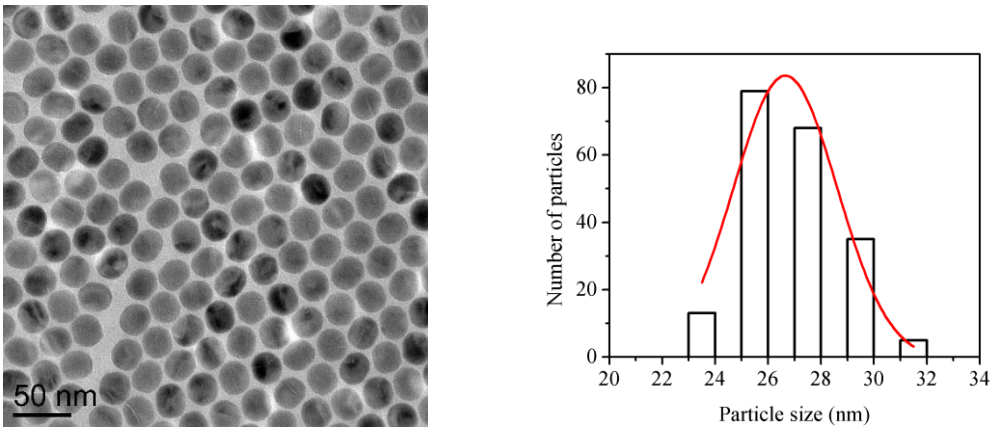

Figure 4. TEM image (right) and particle size distribution (left) of the prepared UCNP@OA. The particle size distribution was determined by counting 200 nanoparticles.

SH-functionalized UCNP (UCNP@Si-SH) was prepared by adding TEOS and MPS sequentially to UCNP@OA in a mixture of surfactant (*i.e.* Igepal CO-520), aqueous ammonia and cyclohexane using a reverse microemulsion method.[32] Briefly, the nanoparticles were first dispersed with sonication in a mixture of Igepal CO-520 and cyclohexane ("oil"). Aqueous ammonia was then added and the mixture was stirred for 30 min to form water-in-oil microemulsions, where single nanoparticle is encapsulated

in each microemulsion pool. Subsequent addition and diffusion of the silica precursors (*i.e.* TEOS and MPS) into this confined, aqueous media led to the hydrolysis and condensation of the precursors to form a silica layer expressing SH groups on the surface of the nanoparticle (Figure 5).

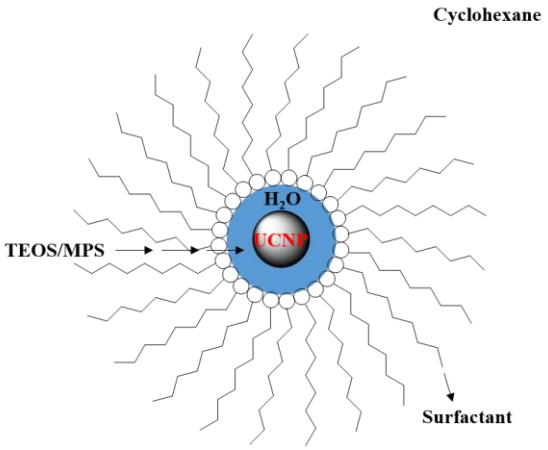

Figure 5. Schematic diagram showing the process of silica coating on UCNP in a water-in-oil microemulsion. The diagram, adapted from reference 32, is not drawn to scale.

A thin and uniform silica coating of single nanoparticle is highly desirable for an efficient FRET process, to which end, a set of optimized reaction conditions is required as the amount of reagents and reaction time are known to affect the thickness of the silica coating, coating of single or multiple core nanoparticle(s) as well as formation of undesired neat silica particles that do not contain a core nanoparticle.[32-36] Using a modified procedure,[37] the optimized reaction conditions as described under experimental section yielded UCNP@Si-SH (average size of 34.49 ± 2.03 nm) with a thin and uniform silica coating of ~4 nm (Figure 6). Although the thickness of the silica coating can be reduced to improve FRET efficiency (which is distance-dependent) by decreasing the amount of silica precursors, this was found (in separate experiments) to

yield nanoparticles that tend to be poorly coated. Therefore, we proceeded to use the nanoparticles with a silica coating of ~4 nm for the next step.

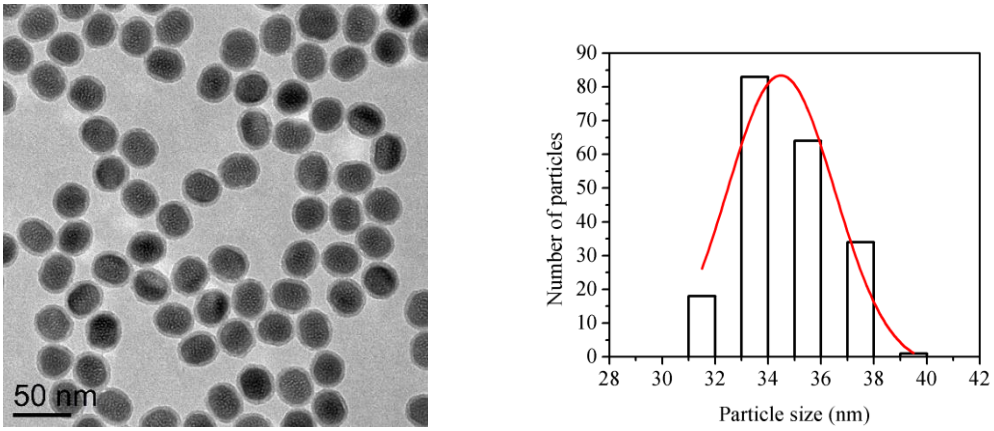

Figure 6. TEM image (right) and particle size distribution (left) of the prepared UCNP@Si-SH. The particle size distribution was determined by counting 200 nanoparticles.

The last step of synthesis involves conjugation of OPD to UCNP@Si-SH via the SH groups. The reaction was carried out in anhydrous DMF and in the dark as OPD easily oxidizes to form a dimer, 2,3-diaminophenazine, when exposed to oxygen and light.[38]

4.3.2 UV characterization of UCNP@Si-OPD

UV spectroscopy was also used to confirm the successful conjugation of OPD onto the nanoparticle surface. Figure 7A shows the absorption spectra of UCNP@Si-OPD when three different concentrations of 4-bromo-1,2-diaminobenzene were reacted with UCNP@Si-SH. The absorption peaks with maximum wavelengths (λ_{max}) around 270-273 nm are assigned to OPD on the nanoparticle surface, which represents a blue-shift of ~30 nm from that of free OPD in the same solvent, *i.e.* 304 nm (Figure 7B).

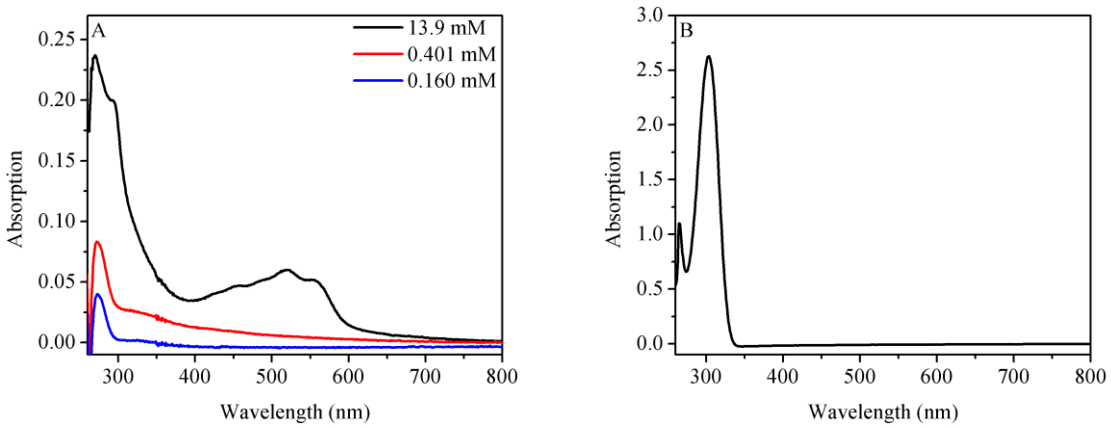

Figure 7. (A) Absorption spectra of UCNP@Si-OPD in DMF at three different reaction concentrations of 4-bromo-1,2-diaminobenzene. (B) Absorption spectrum of OPD in DMF. (The peaks in the 260-800 nm range are shown.)

Two reasons are suggested for this observation: first, the absorption spectrum of OPD is affected by the nature of the substituents at the para-position of the benzene ring. To conjugate OPD to the SH groups, a derivative of OPD, 4-bromo-1,2-diaminobenzene, was used (Figure 8). The absorption spectrum of this compound in DMF showed a λ_{max} at 314 nm (data not shown). In other words, having an electron-withdrawing substituent as the bromine atom causes a red-shift of the λ_{max} of OPD. In the final product, OPD is attached to the nanoparticle via a thioether bond (Figure 8). Contrary to the bromine atom, the thioether group acts as an electron-donating group. Thus, an opposite blue-shift of the λ_{max} of OPD is expected. The opposite effect of electron-withdrawing and -donating substituents was observed on the excitation spectra of para-substituted anilines.[39] Second, the absorption spectrum of OPD can also be affected by its surrounding electronic environment.[40] Compared to the free molecule, OPD attached to the nanoparticle surface is likely to be in close proximity to other functional groups such as OH and unreacted SH groups. Furthermore, the core nanoparticle also contains

electronegative fluoride ions.[40] Taken together, these factors could cause the electronic environment surrounding the OPD moiety to be significantly different from that of the free molecule in DMF, hence yielding different λ_{max}.

OPD 4-bromo-1,2-diaminobenzene OPD conjugated to nanoparticle surface

Figure 8. Chemical structures of OPD, 4-bromo-1,2-diaminobenzene and OPD conjugated to nanoparticle surface via thioether bond.

As mentioned previously, OPD can dimerize in air and light over time to form 2,3-diaminophenazine, which has a broad absorption band with maximum absorption at 430 nm.[41-43] When OPD is conjugated to the nanoparticle surface, it is more likely to come into close contact with neighbouring attached OPD, compared to the same concentration of free OPD in solution. As a result, there is a higher tendency for OPD dimerization to occur on UCNP@Si-OPD, especially if the concentration of attached OPD is high. Therefore, it is important to ensure that the concentration of OPD on UCNP@Si-OPD does not cause dimerization on the nanoparticle surface over time. To this end, different concentrations of 4-bromo-1,2-diaminobenzene were tested and the absorption spectra of the corresponding UCNP@Si-OPD is shown in Figure 7A. At a high reactant concentration of 13.9 mM, a broad absorption band at 400-600 nm was observed, which is likely due to the formation of 2,3-diaminophenazine or higher order polymers. Since a fresh UCNP@Si-OPD sample was tested, this indicates that the side reactions occurred during the reaction. The rate of dimerization is known to increase

with an increase of OPD concentration.[44] Accordingly, lower reactant concentrations were used, and satisfactory results were obtained with 0.401 mM and 0.160 mM of 4-bromo-1,2-diaminobenzene, where the corresponding absorption spectra of UCNP@Si-OPD showed absence of the 400-600 nm band (Figure 7A). Furthermore, the nanoparticles in DMF displayed stability when stored at 4 ℃ for at least 5 days. For subsequent reactions, a reactant concentration of 0.401 mM was used (the actual amount of OPD conjugated on UCNP@Si-OPD has not been determined).

4.3.3 Application of UCNP@Si-OPD to detect EP

The upconversion luminescence (UCL) spectra of UCNP@OA, UCNP@Si-SH and UCNP@Si-OPD upon 980 nm excitation were recorded in cyclohexane (for UCNP@OA) and DMF, and shown in Figure 9. The normalized spectra for all three UCNP displayed similar emission peaks, corresponding to different Tm^{3+} transitions which are consistent with other reports.[31, 45] The assignments are also included in Figure 9.

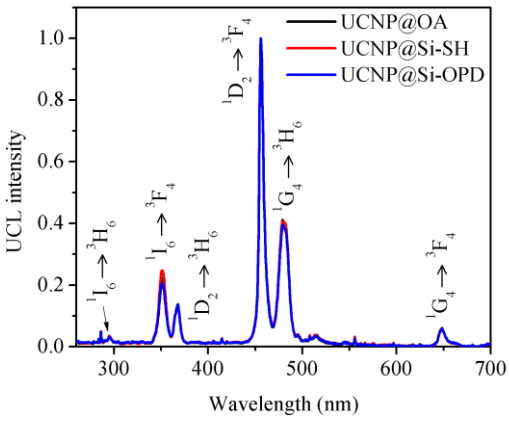

Figure 9. (Normalized) UCL spectra of UCNP@OA (in cyclohexane), UCNP@Si-SH and UCNP@Si-OPD (in DMF) upon 980 nm excitation. (The peaks in the 260-700 nm range are shown.)

The application of UCNP@Si-OPD to detect EP was investigated next. EP is known to undergo a condensation reaction with OPD to form a product that has a broad absorption band from 350-500 nm.[17] This wavelength region coincides with four of Tm^{3+} emission peaks, *i.e.* 351 nm ($^1I_6 \rightarrow {}^3F_4$), 368 nm ($^1D_2 \rightarrow {}^3H_6$), 456 nm ($^1D_2 \rightarrow {}^3F_4$) and 479 nm ($^1G_4 \rightarrow {}^3H_6$). Therefore, based on the spectral overlap, we attempted to develop a detection system for EP based on FRET quenching of Tm^{3+} emissions in the presence of EP upon 980 nm excitation. The experimental procedure was modified from a reported method.[17] Briefly, EP was first oxidized in air in an alkaline medium to form compound **1** (Scheme 1). Acetone followed by UCNP@Si-OPD were then added and the mixture was heated in boiling water. After 5 min, the mixture was cooled and the UCL spectrum of the solution excited at 980 nm was recorded. Figure 10A shows the UCL spectra of the nanoparticles in the absence and presence of 20 μM of EP. Clearly, the emission peaks of Tm^{3+} in the wavelength region of 300-500 nm were quenched in the presence of 20 μM of EP. The extent of quenching monitored at 456 nm was determined to be 1.3-times. (The shorter wavelengths, *i.e.* 351 nm and 368 nm, were not considered as it is close to the absorption of oxidized EP.)

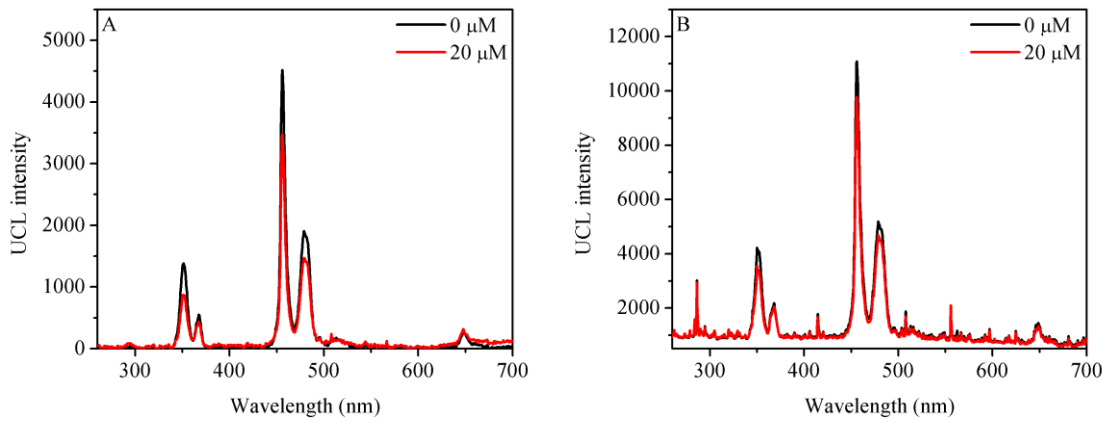

Figure 10. UCL spectra of (A) 1.25 mg/mL and (B) 2.50 mg/mL of nanoparticles in the absence and presence of 20 μM of EP upon 980 nm excitation. Note: The UCL spectra

for the latter were not corrected for background signal. (The peaks in the 260-700 nm range are shown.)

To increase the extent of quenching, separate experiments were carried out with increased concentration of EP or OPD (*i.e.* by increasing [UCNP@Si-OPD]). When the concentration of EP was increased to 100 μM, precipitation of white solid and gradual decrease in UCL intensity were observed. This indicates precipitation of the nanoparticles at higher EP concentration. The reason for this observation is unclear at the moment. When the concentration of UCNP@Si-OPD was increased from 1.25 mg/mL to 2.50 mg/mL, a cloudy suspension was obtained after cooling, but no visible precipitation was observed on standing. At a [UCNP@Si-OPD] of 2.50 mg/mL, the extent of quenching at 456 nm was determined to be 1.1-times (Figure 10B). A plausible reason for the cloudy appearance of the final solution might be due to reduced solubility of the nanoparticles at a higher concentration. Based on these results, it was concluded that 1.25 mg/mL of UCNP@Si-OPD is suitable for detection of EP, for which concentrations below 100 μM should be considered. To verify that the observed UCL quenching is due to formation of the condensation product, the above samples were centrifuged and the nanoparticles redispersed in DMF. A broad absorption band at 300-450 nm was observed (data not shown), confirming formation of the condensation product on the nanoparticle surface.

The above results showed the possibility of the prepared UCNP@Si-OPD to detect EP via a FRET mechanism. However, its performance is still far from satisfactory and requires further optimization. For example, the UCL quenching efficiency can be improved by increasing the amount of condensation product formed on the nanoparticle surface. This could be done by increasing the amount of OPD conjugated on UCNP@Si-

OPD by increasing the concentration of 4-bromo-1,2-diaminobenzene added to react with UCNP@Si-SH. Reactant concentrations that would not cause undesired side reactions can be considered, *i.e.* between 0.401 mM and 13.9 mM.

4.4 Conclusion

In conclusion, a novel detection system based on FRET quenching of Tm^{3+} emissions of OPD-functionalized $NaYF_4$:Yb,Tm in the presence of EP upon 980 nm excitation was proposed. Monodispersed core nanoparticles, *i.e.* UCNP@OA, were synthesized using a modified procedure and functionalized with thiol groups using a reverse microemulsion method. The latter yielded UCNP@Si-SH with a thin silica coating of ~4 nm. The final step of synthesis involved conjugation of OPD to UCNP@Si-SH to give UCNP@Si-OPD. The nanoparticles (UCNP@OA, UCNP@Si-SH and UCNP@Si-OPD) were characterized by TEM, UV and emission spectroscopy. UCNP@Si-OPD was applied to detect EP and preliminary results revealed quenching of UCL intensity of the nanoparticles by 1.3-times in the presence of 20 μM of EP. Though further work is needed to improve the quenching efficiency, these results point to the promising prospect of the prepared UCNP@Si-OPD as EP probes.

4.5 References

1. Peaston, R. T.; Weinkove, C. *Ann. Clin. Biochem.* **2004**, *41*, 17-38.
2. Karim-Nezhad, G.; Khorablou, Z. *Anal. Methods* **2017,** *9* (45), 6394-6402.
3. Soleymani, J. Advanced materials for optical sensing and biosensing of neurotransmitters. *Trends Analyt. Chem.* **2015,** *72*, 27-44.
4. Saraf, N.; Bosak, A.; Willenberg, A.; Das, S.; Willenberg, B. J.; Seal, S. *RSC Adv.* **2017,** *7* (77), 49133-49143.

5. Santos-Fandila, A.; Zafra-Gomez, A.; Barranco, A.; Navalon, A.; Rueda, R.; Ramirez, M. *Talanta* **2013,** *114*, 79-89.

6. Carrera, V.; Sabater, E.; Vilanova, E.; Sogorb, M. A. *J. Chromatogr. B Analyt. Technol. Biomed. Life Sci.* **2007,** *847* (2), 88-94.

7. Li, H.-H.; Wang, H.-H.; Li, W.-T.; Fang, X.-X.; Guo, X.-C.; Zhou, W.-H.; Cao, X.; Kou, D.-X.; Zhou, Z.-J.; Wu, S.-X. *Sens. Actuators B: Chem.* **2016,** *222*, 1127-1133.

8. Tadi, K. K.; Motghare, R. V.; Ganesh, V. *RSC Advances* **2015,** *5* (120), 99115-99124.

9. Atta, N. F.; El-Ads, E. H.; Ahmed, Y. M.; Galal, A. *Electrochimica Acta* **2016,** *199*, 319-331.

10. Dong, W.; Ren, Y.; Bai, Z.; Jiao, J.; Chen, Y.; Han, B.; Chen, Q. *J. Colloid Interface Sci.* **2018,** *512*, 812-818.

11. Ding, M.; Zhou, Y.; Liang, X.; Zou, H.; Wang, Z.; Wang, M.; Ma, J. *J. Electroanal. Chem.* **2016,** *763*, 25-31.

12. Mphuthi, N. G.; Adekunle, A. S.; Ebenso, E. E. *Sci. Rep.* **2016,** *6*, 26938.

13. Salimi, A.; Mamkhezri, H.; Hallaj, R. *Talanta* **2006,** *70* (4), 823-32.

14. Dong, Y.; Chen, H.; Chen, Y.; Hui, Y.; Chen, X.; Hu, Z. *J. Sep. Sci.* **2006,** *29* (13), 2049-2055.

15. Deftereos, N. T.; Calokerinos, A. C.; Efstathiou, C. E. *Analyst* **1993**, *118*, 627-632.

16. Du, J.; Shen, L.; Lu, J. *Anal. Chim. Acta* **2003,** *489* (2), 183-189.

17. Yang, J.; Zhang, G.; Wu, X.; Huang, F.; Lin, C.; Cao, X.; Sun, L.; Ding, Y. *Anal. Chim. Acta* **1998**, *363*, 105-110.

18. Yang, J.; Zhang, G.; Cao, X.; Sun, L.; Ding, Y. *Spectrochim. Acta A* **1997**, *53*, 1671-1676.

19. Sorouraddin, M. H.; Manzoori, J. L.; Kargarzadeh, E.; Haji Shabani, A. M. *J. Pharm. Biomed. Anal.* **1998**, *18*, 877-881.

20. Zhu, M.; Huang, X.; Li, J.; Shen, H. *Anal. Chim. Acta* **1997**, *357*, 261-267.

21. Poliakov, A. E.; Dumshakova, A. V.; Muginova, S. V.; Shekhovtsova, T. N. *Talanta* **2011,** *84* (3), 710-6.

22. Huang, H.; Gao, Y.; Shi, F.; Wang, G.; Shah, S. M.; Su, X. *Analyst* **2012,** *137* (6), 1481-6.

23. Alam, A.-M.; Kamruzzaman, M.; Lee, S. H.; Kim, Y. H.; Kim, S. Y.; Kim, G. M.; Jo, H. J.; Kim, S. H. *Microchimica Acta* **2011,** *176* (1-2), 153-161.

24. Siddiqui, M. R.; Rafiquee, M. Z. A.; Wabaidur, S. M.; Alothman, Z. A.; Ali, M. S.; Allohedan, H. A. *Anal. Sci.* **2015**, *31*, 437-443.

25. Hormozi Nezhad, M. R.; Tashkhourian, J.; Khodaveisi, J. *J. Iran. Chem. Soc.* **2010**, *7*, S83-S91.

26. Jafarinejad, S.; Ghazi-Khansari, M.; Ghasemi, F.; Sasanpour, P.; Hormozi-Nezhad, M. R. *Sci. Rep.* **2017,** *7* (1), 8266.

27. Zhou, B.; Li, X.; Tang, X.; Li, P.; Yang, L.; Liu, J. *ACS Appl. Mater. Interfaces* **2017,** *9* (8), 7772-7779.

28. Menon, S.; Jesny, S.; Sivasankaran, U.; Girish Kumar, K. *Anal. Sci.* **2016,** *32* (9), 999-1001.

29. Wang, M.; Li, Y.; Wang, L.; Su, X. *Anal. Methods* **2017,** *9* (30), 4434-4438.

30. Ai, X.; Ho, C. J.; Aw, J.; Attia, A. B.; Mu, J.; Wang, Y.; Wang, X.; Wang, Y.; Liu, X.; Chen, H.; Gao, M.; Chen, X.; Yeow, E. K.; Liu, G.; Olivo, M.; Xing, B. *Nat. Commun.* **2016,** *7*, 10432.

31. Wang, L.; Qin, W.; Liu, Z.; Zhao, D.; Qin, G.; Di, W.; He, C. *Opt. Express* **2012,** *20* (7), 7602-7.

32. Mader, H. S. Surface Modification of Silica Particles and Upconverting Particles Using Click Chemistry. Ph.D. Dissertation, University of Regensburg, Germany, 2010.

33. Johnson, N. J.; Sangeetha, N. M.; Boyer, J. C.; van Veggel, F. C. *Nanoscale* **2010,** *2* (5), 771-7.

34. Jana, N. R.; Earhart, C.; Ying, J. Y. *Chem. Mater.* **2007**, *19*, 5074-5082.

35. Yi, D. K.; Lee, S. S.; Papaefthymiou, G. C.; Ying, J. Y. *Chem. Mater.* **2006**, *18*, 614-619.

36. Kostiv, U.; Rajsiglová, L.; Luptáková, D.; Pluháček, T.; Vannucci, L.; Havlíček, V.; Engstová, H.; Jirák, D.; Šlouf, M.; Makovicky, P.; Sedláček, R.; Horák, D. *RSC Advances* **2017,** *7* (73), 45997-46006.

37. Gnanasammandhan, M. K.; Idris, N. M.; Bansal, A.; Huang, K.; Zhang, Y. *Nat. Protoc.* **2016,** *11* (4), 688-713.

38. o-Phenylenediamine [MAK Value Documentation, 1999]. *Occupational Toxicants* **1999**, *13*, 215-235.

39. Kwon, W.; Do, S.; Kim, J. H.; Seok Jeong, M.; Rhee, S. W. *Sci. Rep.* **2015,** *5*, 12604.

40. Taylor, J.; Litwinski, C.; Nyokong, T.; Antunes, E. *J. Fluoresc.* **2015,** *25* (3), 489-501.

41. Golla, E. D.; Ayres, G. H. *Talanta* **1973**, *20*, 199-210.

42. Wang, S.; Mosley, C.; Stewart, G.; Yu, H. *J. Photochem. Photobiol. A Chem.* **2008,** *197* (1), 34-39.

43. Zhou, P.; Liu, H.; Chen, S.; Lucia, L.; Zhan, H.; Fu, S. *Molbank* **2011,** *2011* (3).

44. Kim, M. C.; Lee, S. Y. *Nanoscale* **2015,** *7* (40), 17063-70.

45. Liu, J.; Bu, W.; Pan, L.; Shi, J. *Angew. Chem. Int. Ed. Engl.* **2013,** *52* (16), 4375-9.

Chapter 5 Summary and Outlook

5.1 Summary

Fluorescence-based techniques are highly sensitive and versatile analytical tools which can be tailored to detect various targets using different fluorescent materials and mechanisms. The choice of fluorescent material can include the traditional organic dyes or the uprising nanomaterials such as upconversion nanoparticles (UCNP), quantum dots, metal nanoparticles and so on. These materials can be employed alone or in combination to develop highly sensitive detection systems based on mechanisms involving charge transfer (*e.g.* photoinduced electron transfer (PET)) or energy transfer (*e.g.* fluorescence resonance energy transfer (FRET)). Often, the target(s) of detection include biologically relevant materials such as ions, small molecules, proteins and DNA. The rational design of suitable fluorescence-based detection systems for such targets enables monitoring of important physiological processes, disease states as well as elucidation of the pharmacokinetics and pharmacodynamics of various drugs in therapeutic drug monitoring practices; these are areas receiving increasing attention over the years. Also included in Chapter 1 is a comprehensive and detailed discussion on current methods reported to detect a first-line antibiotic vancomycin (Van) in different media.

In Chapters 2 and 3, two molecular PET-based probes were designed for Van detection. The first probe consists of a triad made up of a squaraine dye Seta-640 conjugated to two anthraquinone molecules via Lys-D-Ala-D-Ala peptides (Van-specific sequence) (Chapter 2). This probe was shown to detect Van with high sensitivity and selectivity in buffer and human serum. In the absence of Van, the fluorescence of the triad was quenched due to an energetically favourable electron transfer from the excited Seta-640 dye to anthraquinone. Upon addition of Van, the antibiotic binds with

high affinity to the triad (via the -D-Ala-D-Ala ligands) in a 2:1 stoichiometry and led to a significant fluorescence enhancement of 30-times. The detection mechanism, studied using time-resolved spectroscopy, revealed a minor contribution from polarity effects and a major contribution from inhibition of electron transfer arising from an increase in spatial distance between the Seta-640 dye and anthraquinone upon Van binding. The probe has detection limits of 7.00 nM and 96.9 nM in buffer and human serum, respectively, and its working range covers the clinically relevant range for Van. Furthermore, it displays high selectivity toward Van while being insensitive to other antibiotics and a degraded product of Van which bears high structural similarity to the antibiotic.

By varying the dye and quencher components, a second probe based on the triad consisting of a cyanine dye Cy5 conjugated to two ferrocene moieties via Lys-D-Ala-D-Ala peptides was proposed (Chapter 3). In the absence of Van, an energetically favourable hole transfer from the excited Cy5 to ferrocene resulted in fluorescence quenching of the triad; in contrast to the electron-transfer quenching mechanism of the previous probe. Upon the addition and binding of Van (to the triad), fluorescence recovery takes place via reduction of the hole-transfer efficiency caused by a lengthening of the distance between the dye and ferrocene; a similar recovery mechanism as the previous probe. Two other triads with a shorter or longer linker length between the cyanine dye and ferrocene were also prepared and the effect of linker length on the hole-transfer quenching efficiency in the triad was investigated. The results revealed an optimal linker length of six atoms, for which the corresponding triad **C6** gave the largest fluorescence enhancement factor of 5.8-times in the presence of ~17 μM of Van. Despite a poorer performance compared to the previous probe, this study

provides support for the use of the Seta-640 dye, which has a 6-atom linker, for the triad in Chapter 2.

In Chapter 4, a novel FRET-based probe utilizing UCNP as sensing material was proposed to detect an important neurotransmitter, epinephrine (EP). The probe consists of o-phenylenediamine (OPD)-conjugated $NaYF_4$:Yb,Tm. The nanoparticle was prepared by an Ostwald ripening process and coated with a silica shell expressing thiol groups to conjugate OPD. In the presence of EP, the neurotransmitter undergoes a condensation reaction with OPD on the nanoparticle surface to form a product that absorbs Tm^{3+} emissions. Some positive results were observed which point to the feasibility of such a system to detect EP, for which further optimization is needed to improve the quenching efficiency.

5.2 Outlook

Since we have already established an efficient (electron) donor-acceptor system involving the squaraine dye and anthraquinone in the triad presented in Chapter 2, the application of this system can be extended to include the detection of other macromolecular targets by changing the ligand. For example, the ligand can be changed to an azimilide molecule which can bind to the human Ether-a-go-go-Related Gene (hERG) potassium channel, which plays a critical role in regulating membrane potential of heart cells.[1]

Before the same could be done for the triad discussed in Chapter 3, the performance of the cyanine dye-ferrocene pair needs to be improved first and one way is to test other donor-acceptor combinations by changing either component in the final triad. For example, a Seta-640-ferrocene system could be tested. Using the Rehm-Weller equation in section 2.3.2, the Gibbs free energy for the hole-transfer from an excited

Seta-640 dye (*A*) to ferrocene (*D*) is calculated to be -0.728 eV (where $E_{red}(A)$ = -0.952 eV, $E_{ox}(D)$ = 0.250 eV [2] and E_{00} = 1.93 eV); indicating that the process is energetically favourable. Some factors to consider in the rational design of an efficient donor-acceptor system are the redox potentials of both components (which gives a hint of the feasibility of the hole-transfer process) and structure of the dye. The latter controls the dye properties such as its quantum yield in aqueous solutions. This could affect the extent of fluorescence enhancement in the presence of a target. As discussed in section 3.3 (Chapter 3), a possible reason for the poorer fluorescence enhancement observed for the cyanine dye-ferrocene triad compared to the squaraine dye-anthraquinone triad could be the difference in polarity between the two dyes, which is affected by their molecular structure.

For the EP probe discussed in Chapter 4, the upconversion luminescence (UCL) quenching efficiency can be improved by increasing the amount of condensation product formed on the nanoparticle surface. This might yield better detection sensitivity and a wider working range of the probe. A concurrent effort could be looking at ways to improve the quantum yield or upconversion efficiency of the core nanoparticle (*i.e.* $NaYF_4$:Yb,Tm) which would enhance Tm^{3+} emissions and hence energy transfer to the attached condensation product. One way is to reduce surface quenching effects by adding a shell layer to the core nanoparticle to construct core/shell structures consisting of either an active core/inert shell or active core/active shell.[3] (An inert shell layer means that it does not contain any absorbing or emitting lanthanide dopant.) Surface quenching effects are especially significant for UCNP due to its high surface-to-volume ratio which exposes the lanthanide dopants to deactivation by surface defects, capping ligands and solvent molecules that possess a high phonon energy.[3] An epitaxial growth of an inert shell layer on the core nanoparticle can address these problems by passivating the

surface defects and protecting the core from surrounding (usually capping) ligands and solvent molecules. For example, $NaYF_4$:Yb,Tm@$NaYF_4$ (core@shell) exhibited 23-times higher upconversion efficiency than $NaYF_4$:Yb,Tm. The shell layer can also be doped with Yb^{3+} ions to form an active shell where energy transfer can also take place from Yb^{3+} in the shell to Tm^{3+} in the core, thereby enhancing Tm^{3+} UCL. The UCL intensity of $NaYF_4$:Yb,Tm@$NaYbF_4$ was shown to be 5.3-times higher than $NaYF_4$:Yb,Tm@$NaYF_4$.[4] Last but not least, the optimized probe can also be developed to realize reversible EP detection on (immobilized) single nanoparticles.

5.3 References

1. Liu, Z.; Zhou, Y.; Du, L.; Li, M. *Analyst* **2015,** *140* (24), 8101-8.
2. Wu, X.; Liu, F.; Wells, K. L.; Tan, S. L.; Webster, R. D.; Tan, H. S.; Zhang, D.; Xing, B.; Yeow, E. K. *Chemistry* **2015,** *21* (8), 3387-98.
3. Chen, G.; Agren, H.; Ohulchanskyy, T. Y.; Prasad, P. N. *Chem. Soc. Rev.* **2015**, *44*, 1680-1713.
4. Qiu, H.; Yang, C.; Shao, W.; Damasco, J.; Wang, X.; Agren, H.; Prasad, P. N.; Chen, G. *Nanomaterials* **2014**, *4*, 55-68.

Publications

1. **Ng, S. M.**; Wu, X.; Khyasudeen, F.; Nowakowski, P. J.; Tan, H.-S.; Xing, B.; Yeow, E. K. L. *ACS Sens.* **2018**, *3*, 1156-1163.

2. Ng, Y. Y.; Tan, L.; **Ng, S. M.**; Chai, Y. T.; Ganguly, R.; Yeow, E.; Soo, H. S. Submitted to ACS Catalysis.